

VOLUME I TEXT

ORE DEPOSITIONAL PROCESSES IN THE FORMATION  
OF THE NAVAN ZINC/LEAD DEPOSIT,  
CO. MEATH, IRELAND.

IAIN KERR ANDERSON

A THESIS SUBMITTED FOR THE DEGREE OF  
DOCTOR OF PHILOSOPHY

STRATHCLYDE UNIVERSITY, GLASGOW

DEPT. OF APPLIED GEOLOGY

1990

## ABSTRACT

A comprehensive study of facies distributions, carbonate diagenesis and ore mineral textures and their relationships with host rocks in the Navan Zn/Pb deposit (69.9Mt @ 10.1% Zn, 2.6% Pb) was carried out in order to gain an understanding of the ore depositional processes. Underground mapping, core logging, and petrological examination of polished thin sections were aided by staining and cathodoluminescence techniques. Sulphur isotope analyses were carried out on the principal sulphide and sulphate minerals whose position in the paragenetic sequences was established by the textural study.

Facies variations in the late Courceyan shallow water Pale Beds carbonate sequence, dominated by calcarenites and micrites, are NNW-trending, and are attributed to the formation of major channels in the intertidal-subtidal environment.

Carbonate cementation in the Pale Beds calcarenites and micrites involved three stages of calcite cement and a late-stage ferroan dolomite. Selective dolomitization of detrital silt-rich calcarenites within the limestone sequence occurred in three stages. The earliest stage dolomite formed as a fine-grained diagenetic replacement, possibly pre-dating the calcite cement sequence, however the third stage was coeval with the late-stage dolomite in the limestones. In the western mine area towards the periphery of the main mineralization, massive, pervasive dolomitization of entire sections of the Pale Beds sequence also occurred in three stages and is regarded as being related to the mineralizing event.

A diversity of ore textures indicate that the majority of the sulphides in the Pale Beds were deposited by complex mineralizing processes involving continual replacement of, and open space infill within semi-lithified calcarenites and micrites, especially below the detrital silt-rich dolomites. Localization of sulphide deposition and the resulting stratiform/statabound nature of the ore are attributed to the presence of suitable traps within the compacting carbonate sequence, which formed stratigraphically below the early, diagenetic dolomite horizons.

Sulphur isotopes indicate that the bulk of the sulphur that combined with the metals was derived by bacteriogenic reduction of Lower Carboniferous sea water sulphate ( $\delta^{34}\text{S}_{\text{H}_2\text{S}} = -23.0$  to  $-14.5\text{‰}$ ). A far lesser component of hydrothermal sulphur ( $\delta^{34}\text{S}_{\text{H}_2\text{S}} \approx +18$  to  $+19\text{‰}$ ) was transported with the metals and derived from leaching of diagenetic pyrite in the Lower Palaeozoic pile below the deposit. Different ore textures reflect the

relative components of bacteriogenically-derived and hydrothermal sulphur. The presence of abundant dendritic and skeletal textures, stalactitic growths and fine-grained internal sulphide sediments are interpreted as the result of rapid sulphide precipitation when the ore fluids mixed with seawater containing abundant bacteriogenically-derived  $H_2S$  in a sub-seafloor environment. Paragenetically early sphalerite and coarse bladed galena textures incorporated a significant component of hydrothermal sulphur during crystal growth although the bacteriogenic component became dominant towards the end of precipitation of the bladed galena.

The dominant bacteriogenic sulphide supply must have been derived and continually replenished either from sulphate reduction in laterally equivalent lithologies rich in organic material, and/or from reduction in the shallow Lower Carboniferous sea and pore spaces in the top few metres of the sediment column above the mineralization.

Mineralization in the Pale Beds formed by mixing of two fluids at the site of ore deposition in a sub-seafloor, carbonate environment undergoing diagenesis. An ascending hydrothermal fluid carrying metals and some sulphur mixed with Lower Carboniferous seawater containing sulphate and  $H_2S$  formed by bacteriogenic sulphate reduction.

Exhumation of the mineralizing event in the Pale Beds in late Chadian times by submarine slumping and erosion resulted in local deposition of sedimentary to early diagenetic Fe-rich sulphides as complex breccias and massive Fe/Zn/Pb sulphides within a debris flow conglomerate.

The Navan deposit is regarded as syn-diagenetic in origin.

## CONTENTS

|                  |  | Page |
|------------------|--|------|
| <u>CHAPTER 1</u> | <u>INTRODUCTION</u>  | 1    |
| 1.1              | ZINC/LEAD DEPOSITS   | 1    |
| 1.1.1            | SEDEX Deposits   | 1    |
| 1.1.2            | MVT Deposits   | 5    |
| 1.1.3            | VMS Deposits   | 6    |
| 1.2              | IRISH DEPOSITS   | 6    |
| 1.3              | AIMS AND OBJECTIVES  | 8    |
| <u>CHAPTER 2</u> | <u>GENERAL GEOLOGY AND INTRODUCTION TO THE NAVAN DEPOSIT</u> | 10   |
| 2.1              | GENERAL GEOLOGY OF IRELAND                                   | 11   |
| 2.1.1            | Pre-Cambrian Basement  | 11   |
| 2.1.2            | Lower Palaeozoics  | 11   |
| 2.1.3            | Devonian (Old Red Sandstone Facies)                          | 12   |
| 2.1.4            | Lower Carboniferous  | 13   |
| 2.1.5            | Upper Carboniferous  | 16   |
| 2.1.6            | Permian, Mesozoic and Tertiary                               | 17   |
| 2.2              | TECTONISM AND STRUCTURE AFFECTING THE CARBONIFEROUS ROCKS    | 17   |
| 2.3              | INTRODUCTION TO THE NAVAN DEPOSIT                            | 19   |
| 2.4              | STRATIGRAPHIC AND STRUCTURAL SETTING OF THE NAVAN DEPOSIT    | 20   |
| 2.5              | INTRODUCTION TO THE MINERALIZATION                           | 25   |
| <u>CHAPTER 3</u> | <u>STRATIGRAPHY AND CARBONATE DEPOSITIONAL ENVIRONMENT</u>   | 27   |
| 3.1              | INTRODUCTION   | 27   |
| 3.2              | STRATIGRAPHY   | 28   |

|                  |  |    |
|------------------|--|----|
| 3.2.1            | Introduction   | 28 |
| 3.2.2            | Lower Palaeozoics  | 29 |
| 3.2.3            | Red Beds   | 29 |
| 3.2.4            | Laminated Beds   | 30 |
| 3.2.5            | Muddy Limestones   | 32 |
| 3.2.6            | Muddy Limestone Transition   | 34 |
| 3.2.7            | 5 Lens Interval and the Micrite Unit                                 | 34 |
| 3.2.8            | 4 Lens Interval  | 39 |
| 3.2.9            | 3 Lens Interval and the Micro-<br>conglomerates                      | 41 |
| 3.2.10           | 1 Lens Interval  | 44 |
| 3.2.11           | Upper Pale Beds  | 46 |
| 3.2.12           | Shaley Pales   | 47 |
| 3.2.13           | Argillaceous Bioclastic Calcarenites                                 | 48 |
| 3.2.14           | Waulsortian "Reef" Limestone   | 49 |
| 3.2.15           | The Erosion Surface and the Boulder<br>Conglomerate                  | 49 |
| 3.2.16           | Upper Dark Limestones  | 51 |
| 3.2.17           | Tertiary Intrusives  | 52 |
| 3.3              | LATERAL VARIATIONS IN THE STRATI-<br>GRAPHY ACROSS THE DEPOSIT       | 52 |
| 3.3.1            | Introduction   | 52 |
| 3.3.2            | Laminated Beds/Muddy Limestones                                      | 52 |
| 3.3.3            | The Micrite Unit and the Disappear-<br>ance of the Lower Dark Marker | 53 |
| 3.3.4            | 3 Lens Microconglomerates  | 58 |
| 3.4              | DEPOSITIONAL ENVIRONMENT   | 60 |
| 3.5              | CONCLUSIONS  | 63 |
| <u>CHAPTER 4</u> | <u>DIAGENESIS AND DOLOMITIZATION</u>                                 | 66 |
| 4.1              | INTRODUCTION   | 66 |

|                  |   |     |
|------------------|---|-----|
| 4.2              | CALCITE CEMENTS   | 66  |
| 4.3              | SILICIFICATION  | 70  |
| 4.4              | DOLOMITIZATION  | 70  |
| 4.4.1            | Introduction  | 70  |
| 4.4.2            | Detrital Silt-rich Dolomites  | 71  |
| 4.4.3            | Pervasive, Pitted Dolomites   | 73  |
| 4.4.4            | Partial Dolomitization  | 76  |
| 4.4.5            | Summary and Correlation of Dolomitization   | 79  |
| 4.5              | DOLOMITE FORMATION  | 82  |
| 4.5.1            | Early Replacement Dolomite in the Bedding-Parallel Silt-rich Horizons Prior to Mineralization | 82  |
| 4.5.2            | Late Cement (often saddle) Dolomite   | 85  |
| 4.6              | CONCLUSIONS   | 87  |
| <u>CHAPTER 5</u> | <u>ORE STYLES, TEXTURES AND RELATIONSHIPS</u>   | 89  |
| 5.1              | INTRODUCTION  | 89  |
| 5.2              | BEDDING-PARALLEL REPLACEMENT OF SEMI-LITHIFIED CARBONATE                                      | 90  |
| 5.2.1            | Description   | 90  |
| 5.2.2            | Disruption and Deformation  | 95  |
|                  | 5.2.2a Soft sediment  | 95  |
|                  | 5.2.2b Compactional   | 96  |
|                  | 5.2.2c Collapse   | 97  |
| 5.2.3            | Interpretation  | 97  |
| 5.3              | DIFFUSE, STRINGER REPLACEMENT VEINLETS  | 99  |
| 5.3.1            | Description   | 99  |
| 5.3.2            | Interpretation  | 102 |

|       |  |     |
|-------|--|-----|
| 5.4   | BEDDING-PARALLEL MASSIVE GALENA/<br>SPHALERITE/BARITE ORE HORIZONS   | 102 |
| 5.4.1 | Introduction   | 102 |
| 5.4.2 | Description  | 103 |
| 5.4.3 | Interpretation   | 106 |
| 5.4.4 | 2-5 Lens West  | 109 |
| 5.5   | BEDDING-PARALLEL INTERNAL SULPHIDE<br>DEPOSITION IN HIGH-GRADE ORE<br>HORIZONS                                   | 110 |
| 5.5.1 | Introduction and Morphology  | 110 |
| 5.5.2 | Evidence for Dissolution of the<br>Host Rock   | 111 |
| 5.5.3 | Internal Sulphide (sphalerite)<br>Deposition   | 113 |
| 5.5.4 | Complex, Chaotic Sulphide Clasts   | 114 |
| 5.5.5 | <u>In-situ</u> Solution Growths  | 116 |
|       | 5.5.5a Thin Section Petrography -<br>Introduction  | 116 |
|       | 5.5.5b Galena  | 116 |
|       | 5.5.5c "Stalactitic" Pyrite<br>Structures  | 118 |
|       | 5.5.5d Microscopic, Rhythmically<br>Banded, Crustiform Sphalerite<br>and Coeval Geopetal<br>Sphalerite Sediments | 120 |
|       | 5.5.5e Honeyblende Sphalerite  | 122 |
|       | 5.5.5f Late Barite and Calcite   | 123 |
| 5.5.6 | Bedding-Parallel and Cross-cutting<br>Mineralization in the Micrites   | 124 |
|       | 5.5.6a Laminated sphalerite/<br>argillite  | 125 |
|       | 5.5.6b Complex, Chaotic Clasts   | 127 |
|       | 5.5.6c <u>In-situ</u> Solution Growths   | 129 |
| 5.5.7 | Interpretation   | 130 |

|                  |  |     |
|------------------|--|-----|
| 5.6              | MASSIVE, CENTRAL 2-5 LENS-STYLE<br>MINERALIZATION                              | 134 |
| 5.6.1            | Introduction   | 134 |
| 5.6.2            | Description  | 135 |
| 5.6.3            | Interpretation   | 139 |
| 5.6.4            | Dolomitization   | 140 |
| 5.7              | BRECCIA STYLES OF MINERALIZATION   | 143 |
| 5.8              | CROSS-CUTTING VEINS  | 144 |
| 5.9              | LOW-GRADE DISSEMINATED SULPHIDES   | 145 |
| 5.10             | EXAMPLES OF THE RELATIONSHIPS<br>BETWEEN DIFFERENT STYLES OF<br>MINERALIZATION | 146 |
| 5.10.1           | 2-5 Lens Footwall Mineralization   | 146 |
| 5.10.2           | 2-4/2-3 Lenses   | 147 |
| 5.10.3           | 2-2 Lens   | 148 |
| 5.10.4           | 2-1 Lens   | 149 |
| 5.11             | DISTRIBUTION OF ORE IN THE PALE BEDS   | 150 |
| 5.11.1           | Lithological Control   | 150 |
| 5.11.2           | Structural Control   | 151 |
|                  | 5.11.2a The F3 Fault between Blocks<br>14 and 15                               | 151 |
|                  | 5.11.2b The F2 Fault between Blocks<br>6 and 7                                 | 152 |
|                  | 5.11.2c The F2 Fault in Block 2  | 152 |
| 5.12             | THE CONGLOMERATE GROUP ORE   | 154 |
| 5.12.1           | Introduction   | 154 |
| 5.12.2           | Description  | 154 |
| 5.12.3           | Interpretation   | 157 |
| 5.13             | CONCLUSIONS AND OBSERVATIONS   | 157 |
| <u>CHAPTER 6</u> | <u>SULPHUR ISOTOPES</u>  | 162 |

|        |   |     |
|--------|---|-----|
| 6.1    | INTRODUCTION  | 162 |
| 6.2    | POTENTIAL SULPHUR SOURCES   | 162 |
| 6.2.1  | Sulphur Transported with the Metals -<br>Hydrothermal Sulphur                                       | 163 |
| 6.2.1a | Potential sources of Hydro-<br>thermal Sulphur  | 164 |
| 6.2.1b | Factors Affecting Isotopic<br>Equilibrium Exchange in the<br>Ore Fluid and Minerals<br>Precipitated | 166 |
| 6.2.2  | Sulphur Supplied at the Site of Ore<br>Deposition   | 168 |
| 6.2.2a | Bacteriogenic Sulphate<br>Reduction   | 168 |
| 6.2.2b | Chemical or Abiological<br>Reduction  | 171 |
| 6.2.2c | Thermochemical Reduction of<br>Sulphate by Organic Matter   | 172 |
| 6.3    | SEAWATER SULPHATE   | 173 |
| 6.4    | PREVIOUS WORK ON THE DEPOSIT  | 173 |
| 6.5    | SUMMARY OF SULPHUR ISOTOPE RESULTS<br>FROM NAVAN  | 174 |
| 6.6    | INTERPRETATION  | 174 |
| 6.6.1  | Replacement of Carbonate Allochems  | 174 |
| 6.6.2  | Coarse Galena/Sphalerite  | 177 |
| 6.6.2a | Precipitation from Hydro-<br>thermal Sulphur Only   | 182 |
| 6.6.2b | Mixing of Hydrothermal and<br>Bacteriogenically-derived<br>Sulphur                                  | 184 |
| 6.6.3  | Bedding-parallel Massive Sulphides<br>Indicative of Open-space Deposition                           | 191 |
| 6.6.3a | Closed System Bacteriogenic<br>Reduction  | 192 |
| 6.6.3b | Precipitation from Hydro-<br>thermal Sulphur Only   | 193 |

|                  |  |     |
|------------------|--|-----|
| 6.6.3c           | Mixing of Isotopically Light<br>Bacteriogenic and Heavy<br>Hydrothermal Sulphur                  | 193 |
| 6.6.4            | 2-5 Lens West  | 194 |
| 6.6.5            | Vein Sulphides   | 195 |
| 6.6.6            | Pyrite in the Conglomerate Group Ore   | 196 |
| 6.6.7            | Barite (plus minor gypsum and<br>celestite)  | 198 |
| 6.7              | THE ORIGIN OF THE BACTERIOGENIC<br>SULPHIDE  | 203 |
| 6.8              | THE ORIGIN OF THE HYDROTHERMAL<br>SULPHUR  | 205 |
| 6.9              | DIAGENETIC PYRITE IN THE LOWER<br>PALAEOZOICS  | 209 |
| 6.10             | MINOR ZnS, PbS and CuFeS <sub>2</sub> VEINLETS<br>IN LOWER PALAEOZOIC ROCKS BELOW THE<br>DEPOSIT | 211 |
| 6.11             | LATERAL VARIATIONS IN THE SULPHUR<br>ISOTOPIC DATA   | 212 |
| 6.12             | COMPARISONS WITH OTHER IRISH DEPOSITS  | 213 |
| 6.12.1           | Tynagh   | 213 |
| 6.12.2           | Silvermines  | 214 |
| 6.12.3           | Tatestown  | 216 |
| 6.12.4           | Ballinalack  | 216 |
| 6.13             | SUMMARY  | 217 |
| <u>CHAPTER 7</u> | <u>CONCLUSIONS, DISCUSSION AND THE MODEL</u>   | 221 |
| 7.1              | CONCLUSIONS  | 221 |
| 7.1.1            | Host Rock Depositional Environment   | 221 |
| 7.1.2            | Carbonate Diagenesis   | 222 |
| 7.1.3            | Sulphide Deposition  | 223 |
| 7.1.4            | Relationship Between Faulting and<br>Mineralization  | 226 |
| 7.1.5            | Source(s) of the Sulphur   | 227 |

|       |  |     |
|-------|--|-----|
| 7.2   | EVIDENCE FOR THE TIMING OF SULPHIDE<br>EMPLACEMENT   | 228 |
| 7.3   | ORIGIN OF THE METALS   | 231 |
| 7.4   | DISCUSSION   | 233 |
| 7.4.1 | The Significance of Early Dolomitization at Navan, and Comparisons with Dolomitization in Other Irish Deposits | 233 |
| 7.4.2 | Dolomitization Related to the Creation of Open Spaces  | 236 |
| 7.4.3 | The Intersection of Two Trends at Navan  | 240 |
| 7.4.4 | The Reason for such Large Quantities of Ore at Navan   | 241 |
| 7.4.5 | Derivation of the Bacteriogenic Sulphur  | 242 |
| 7.5   | A COMPARISON WITH SEDEX AND MVT DEPOSITS AND STYLES OF MINERALIZATION  | 246 |
| 7.6   | THE MODEL  | 252 |
|       | <u>REFERENCES</u>  | 257 |
|       | <u>APPENDIX I STAINING TECHNIQUE AND CATHODOLUMINESCENCE</u>   | 280 |
|       | <u>APPENDIX II SULPHUR ISOTOPIC ANALYSES</u>   | 282 |
|       | <u>APPENDIX III ABBREVIATIONS FOR THE STYLES OF MINERALIZATION AND A LIST OF SULPHUR ISOTOPE RESULTS</u>       | 284 |

## ACKNOWLEDGEMENTS

I would like to thank the following people for their contribution to the contents of this thesis and invaluable assistance throughout the duration of my research.

I would like to thank Professor M.J. Russell at Strathclyde and Dr. J.H. Ashton at Tara Mines who jointly supervised the research. Professor Mike Russell gave me the opportunity to become involved in research on the Navan deposit and provided the stimulus for many of the ideas and theories essential in this study. Dr. John Ashton provided continual guidance at the mine, constantly invoking ideas and suggestions, particularly during the writing up over the past two and a half years.

I would also like to thank Dr. Adrian Boyce and Dr. Tony Fallick at the S.U.R.R.C. who introduced me to the techniques, applications and interpretation of sulphur isotopes and who also provided funding for two conferences attended during my research.

Numerous geologists and technical staff at Tara gave me assistance at the mine, in particular Adrian Black, who helped with the logging of diamond drill core and subsequent interpretation. Dermot Downing and Peter Powell greatly facilitated my time spent in the geology department at Tara. Coloured histograms of the isotopic data were kindly prepared by Frieda Baragwanath using the computerization system at the mine.

All the members of staff in the department of Applied Geology at Strathclyde are acknowledged for numerous discussions and advice, in particular Dr. Alan Hall who was continually consulted during the examination of polished thin sections. Murdoch MacCleod and Dougie Turner conducted X.R.D analyses and John Gilleece and Peter Wallace prepared numerous polished thin sections.

I would also like to thank Colin Andrew for many discussions and suggestions which extended my knowledge of base-metal depositional environments in Ireland outside the confines of the Navan deposit.

Colleagues in the office at Navan Resources assisted in the assembling of the final copies of the thesis.

The Natural Environmental Research Council provided funding for the research and additional financial support was kindly given by Tara Mines.

As a result of this research, I have been extremely fortunate to become acquainted with, and learned a great deal from, numerous geologists from academic institutions and the Irish mining and exploration industry.

## CHAPTER 1 INTRODUCTION

### 1.1 ZINC/LEAD DEPOSITS

Most of the world's zinc and lead is derived from sulphide deposits which have been loosely classified into three main groups:

1.1.1 Stratiform, sedimentary exhalative (SEDEX) ore deposits are characterized by conformable, syngenetic or early diagenetic replacement mineralization (Fe-sulphides, sphalerite and galena), occurring as discrete lenses in which thin sulphide layers and laminae (mm up to 30cm thick) are interlayered with barren or poorly mineralized sediments. These include some of the largest deposits in the world (Table 1.1): Mt. Isa, McArthur River (HYC), Broken Hill, Howards Pass, Sullivan, Red Dog, Meggen, Rammelsberg and Silvermines (Goodfellow and Jonasson, 1986; Gustafson and Williams, 1981; Hamilton et al., 1983; Lange et al., 1985; Large 1980, 1981a, 1983; Muir, 1983; Russell et al., 1981; Williams, 1978; Williams and Logan, 1986). The deposits are associated with sedimentary basins of varying magnitudes and are hosted by carbonaceous shales and siltstones (often dolomitic), sandstones, limestones and dolomites, cherts, and minor sedimentary breccias. Contemporaneous igneous activity is indicated by the presence of tuff horizons, for example McArthur River (Muir, 1983) and Rammelsberg (Large, 1986). The host rocks were deposited in a variety

of sedimentary environments from sabkha (McArthur River; Muir, 1979) and lacustrine (Mt Isa; Neudart and Russell, 1982) through to deep, marine basins (Howards Pass; Goodfellow and Jonasson, 1986).

The mineralization may extend through a stratigraphic interval of over 1000m (eg Mt. Isa) and there may be more than one stratiform orebody on the same stratigraphic level (eg Silvermines) (Large, 1983). The size of the deposits ranges up to 500Mt (Table 1.1).

The relative abundance of the base metals varies from 1:1, Zn:Pb at Mt. Isa and Sullivan, to 8:1 at Meggen, to deposits such as Howard's Pass which are almost monomineralic ZnS, and distinct zonations of the metals are observed (Large, 1980). The general trend is an increase in the Zn/Pb ratio laterally away from the centre towards the periphery of the ore zone (Large, 1983), with possibly an increase in the copper content in the stratigraphically higher, stratiform ore lenses (Russell et al., 1981). Manganese haloes in sediments at the same stratigraphic horizon around the orebody are observed at Tynagh (Russell, 1975), Silvermines (Gray and Russell, 1984) and Meggen (Gwosdz and Krebs, 1977).

Barite is frequently associated with base-metal deposition, often peripherally to the sulphides, eg Silvermines (Taylor and Andrew 1978), reflecting deposition in sulphatic seawater in a more oxidized environment (Large, 1981; Lydon, 1983).

Cross-cutting, stockwork mineralization stratigraphically below or adjacent to the stratiform mineralization, is usually interpreted as feeder zones to the stratiform ore, eg Silvermines (Taylor and Andrew, 1978) and Rammelsberg (Large, 1980). Alteration is often associated with the cross-cutting mineralization below a deposit. The two best-known examples are the silicification and associated copper mineralization in the "kneist" at Rammelsberg which cross-cuts the bedding in the footwall (Large, 1980), and the tourmalinization in a funnel-shaped zone that extends down to 450m below the massive sulphides at Sullivan (Ethier and Campbell 1977; Shaw and Hodgson, 1986). At Sullivan, alteration is also present in the hanging wall and consists of an albite and chlorite assemblage extending up to 125m above the sulphide zone.

An exhalative sedimentary origin, with the discharge of the mineralizing hydrothermal fluids and subsequent precipitation of the sulphides on the sea floor, has been proposed for the sulphide laminae (Finlow-bates, 1980; Goodfellow and Jonasson, 1986; Hamilton et al., 1983; Large, 1983; Lydon, 1983). Williams (1978) and Rye and Williams (1981), on the basis of textural and isotopic studies suggested that the stratiform sulphide deposition at McArthur River was produced diagenetically in the sediments, which were probably water-logged and only partially compacted. Neudart (1986) has proposed a similar diagenetic model for the stratiform Zn+Pb

mineralization at Mt Isa based on studies of the host rock depositional environment and relative timing of the mineralization.

The two most favoured models for the origin of the metals in these deposits are "hydrothermal convection" (Russell, 1978, 1983; Russell et al., 1981) and variants of "basinal brine expulsion", first applied to MVT deposits (Beales and Jackson, 1966; Badham, 1981; Lydon, 1983; Cathles and Smith, 1983; Sawkins, 1984). Russell's model involves hydrothermal convection of seawater and pore waters through the permeable crust, with the convection cells enlarging and deepening with time, and is corroborated by the results of recent drilling in the granites of Cornwall for geothermal energy (Pine and Batchelor, 1984). Basinal brine expulsion involves formation waters that derive metals from the enclosing host strata as the waters become warmer and more acidic during burial, and metals are released with the conversion of expandable clays to non-expandable clays and subsequently to micas during dehydration and diagenesis (Lydon, 1983). In this hypothesis, these metal-bearing fluids migrate and are expelled from the sediment column, often episodically (Cathles and Smith, 1983; Sawkins, 1984), with contemporaneous fault structures probably providing the plumbing system by which the metal-rich fluids reached the site of ore deposition.

1.1.2 Mississippi Valley Type (MVT) ore deposits are generally non-stratiform and characterized by their occurrence in limestones and dolomites, and by open-space sulphide precipitation in fractures and cavities. The best-known examples are the deposits occurring in the Tri-State, the Viburnum Trend in SE Missouri and the upper Mississippi Valley in North America, Pine Point in Canada, and the Alpine and Silesian deposits in Europe (various papers in Kisvarsanyi et al., 1983; Rhodes et al., 1984) (Table 1.1). The Zn:Pb ratios are highly variable, from 1:10 in SE Missouri to 10:1 in Central Tennessee (Sangster, 1983), although higher Zn:Pb ratios (> 3:1) are more typical of the deposits in general. The ores are generally characterized by a low concentration of copper although this metal is well represented in some mines in the Viburnum Trend.

The deposits are located at the periphery of major sedimentary basins rather than in basins as is the case for SEDEX deposits, and the origin of metal-bearing brines by basinal compaction and subsequent migration has been widely accepted to explain the deposits (Beales and Jackson, 1966). However this model cannot be applied to all the MVT districts (Ohle, 1980; Bethke, 1986).

A major problem in MVT deposits is the uncertainty of the timing of the mineralization due to the lack of methods for dating sulphide emplacement (Sangster, 1983).

1.1.3 Volcanogenic massive sulphide (VMS) deposits are generally zinc-copper-lead deposits, with varying metal ratios (Table 1.1), associated with basaltic and felsic and/or sedimentary rocks. These include the Noranda-type and Kuroko-type deposits with major presently producing examples being the Kidd Creek and Matsumine mines respectively (Franklin et al., 1981; Franklin, 1986; Ohmoto and Skinner, 1983; Tanimura et al., 1983), and those occurring in the Iberian pyrite belt, for example Neves Corvo (Carvalho, 1986). The deposits formed at or near the sea floor by precipitation of metals from uprising hydrothermal fluids (Franklin et al., 1981; Lydon, 1984a). The deposits are characterized by an overall higher copper content than either SEDEX or MVT deposits, and by the presence of distinct alteration assemblages associated with and generally underlying the mineralization. These alteration assemblages include chlorite, quartz-sericite-carbonate, and quartz-sericite-chlorite (Franklin et al., 1981; Date et al., 1983)

Present-day, sea floor deposits include those forming in the Red Sea and on the East Pacific Rise, by active "venting" of hydrothermal fluids (Pottorf and Barnes, 1983; Bischoff et al., 1983).

## 1.2 THE IRISH DEPOSITS

In Ireland, deposits with SEDEX, MVT and VMS characteristics occur, however it is the SEDEX and MVT

styles of mineralization that are of particular interest because of their strong association with Carboniferous limestones. The Irish deposits have never completely conformed to the SEDEX/MVT classification and therefore have certainly been regarded as problematical. Cavity-fill sulphides are evident in the Waulsortian limestones at Tynagh (Boast et al., 1981), sedimentary sulphides and bedded barite, with associated "feeder zones" are present at Silvermines (Taylor and Andrew, 1978), and breccia-hosted and cavity-fill sulphides are described from Kildare (Emo, 1986). A summary of the features of the ore geology of Zn+Pb deposits in the Central Irish Orefield is presented on Table 1.2.

The Navan deposit is the largest Zn+Pb orebody in Europe, and appears to have characteristics of both SEDEX and MVT deposits, in an area that has undergone only minor deformation and metamorphism since the Upper Palaeozoic. It therefore provides a unique opportunity of furthering our knowledge about these deposits, in a location which provides excellent timing constraints on the ore deposition and textural data on the styles of mineralization.

The Navan deposit has been studied and described by Andrew and Ashton (1982, 1985) and by Ashton et al. (1986). These authors suggest that the deposit formed by seafloor sulphide deposition as fine sedimentary laminations, with subsequent overprinting during the diagenesis of the host rocks by a complex variety of sub-

seafloor replacement styles and fracture-fill mineralization, and conclude that the deposit should be considered "... to be a variant of the sedimentary-exhalative type of base-metal orebody" (Andrew and Ashton, 1985). These conclusions provided the basis for a detailed study of features throughout the deposit which is presented in this thesis.

### 1.3 AIMS AND OBJECTIVES

The research was undertaken in an attempt to study and understand the processes involved in forming a large Zn/Pb deposit such as Navan. The aims and objectives of this study are:

- 1) to describe, classify and interpret the variety of textures and features within the sulphides,
- 2) to study the variations in the ore-hosting stratigraphy across the deposit and the relationships between the host rocks and mineralization, ie, the timing of diagenetic cements in the host rocks relative to the mineralization and the timing of dolomitization present within the sulphides and the host rocks,
- 3) to relate sulphur isotope data obtained from sulphides and sulphates to the paragenesis of ore deposition and the ultimate source(s) of the sulphur, and,

- 4) provide an insight into the depositional processes in the Navan orebody.

The approach to this research involved spending a total of one year at the mine studying the range of features accessible underground and supplementing this with detailed logging of drillcore from all areas of the mine. Combining this information with sulphide parageneses established from thin section petrography and utilizing sulphur isotope studies, is expected to help constrain the timing and process(s) involved in the formation of the deposit and other deposits with similar characteristics, and therefore will be of considerable use in the exploration for Zn+Pb deposits formed in tectonically active areas of carbonate sedimentation.

CHAPTER 2      GENERAL REGIONAL GEOLOGY AND AN  
INTRODUCTION TO THE NAVAN DEPOSIT

2.1 GENERAL GEOLOGY OF IRELAND

2.1.1 Pre-Cambrian basement

The Pre-Cambrian rocks in Ireland can be divided into two areas (Fig. 2.1):

1) Lewisian ( $\approx 1600\text{Ma}$ ) and Grenvillian ( $\approx 1000\text{Ma}$ ) gneisses and schists outcrop in Donegal and in the Ox Mountains, and represent the oldest rocks exposed in Ireland (Phillips and Sevastopulo, 1986). These are overlain by metamorphosed Dalradian sediments, comprising schists, quartzites and locally marbles, with lesser meta-volcanics and metabasic intrusions, outcropping in Connemara, Mayo and Donegal.

2) The Rosslare Complex in the Leinster Zone, is composed of amphibolite facies gneisses with lesser migmatites, which are  $> 540\text{Ma}$  in age (Phillips and Sevastopulo, 1986). North-west of the Rosslare Complex, the Cullerstown Formation is regarded as late Pre-Cambrian to Cambrian in age, and consists of quartzites and greywackes which have undergone lower greenschist-facies metamorphism (Max and Dhonau, 1974).

2.1.2 Lower Palaeozoics

The Lower Palaeozoic rocks dominantly outcrop in the E

and SE of the country, and are also found in the west in South Mayo, and in inliers in the Central Irish Plain (Fig. 2.1). The rocks are often cleaved, folded and metamorphosed to prehnite-pumpellyite facies (Oliver, 1978), and include greywackes, siltstones, shales, volcanics and major intrusives (Gardiner, 1974, 1978; Morris, 1983, 1987; Romano, 1980; Stillman, 1978). Ordovician felsic to andesitic volcanics formed in an island arc are most pronounced in the SE, in a linear belt extending from Arklow to Waterford, and are underlain by Lower Ordovician shales (Stillman and Williams, 1979).

In the Longford Down Inlier, the greywackes and shales are mainly Upper Ordovician to Silurian in age, whereas the inliers in the Central Plain are dominated by the Silurian.

In the Murrisk zone, 12km of Ordovician and Silurian sediments and volcanics accumulated in the South Mayo Trough (Anderton et al., 1979).

With the closing of the Iapetus Ocean in late Ordovician (Hutton and Murphy, 1987) or early Silurian times (Stone et al., 1987), late Caledonian deformation, low-grade regional metamorphism and associated plutonism occurred. Tectonism produced sinistral shear zones, strike-slip faults, and upright, polyphase folds (Phillips et al., 1976; Phillips and Sevastopulo, 1986). The general trend or grain of the Caledonian structures is NE to ENE. The

plutonism associated with this deformation resulted in the emplacement of granites around 400Ma, including the Leinster, Galway and Donegal granites (Brindley, 1973; O'Connor and Bruick, 1978).

### 2.1.3 Devonian (Old Red Sandstone Facies)

Early Devonian sedimentation (non-marine) was restricted to fault-controlled basins in the Murrisk Zone, now outcropping in the Curlew Mountains (Gardiner and MacCarthy, 1981). Subsequent Middle Devonian deposition of thick continental sediments was concentrated in the Dingle-Shannon Basin, now outcropping on the Dingle Peninsula (Fig. 2.1). The rocks include alluvial fan and flood plain sediments derived from the then upstanding Caledonian mountains. Sediments in the Dingle Basin were deformed in the late Devonian (Acadian).

The ENE-trending Munster Basin formed as a post-orogenic depositional site prior to the late Devonian (Gardiner and MacCarthy, 1981), and the earliest part of the late Devonian succession is confined to this fault-controlled basin (Phillips and Sevastopulo, 1986). The sediments reach a maximum thickness of 6km in the axial zone, and consist of mudstones and sandstones with thick pebble conglomerates of alluvial fan origin in the east. The direction of sediment transport in rivers was to the south, with flow to the west in the basin itself. Pyroclastics and mafic to felsic volcanics were extruded

and deposited in the north-west of the Munster Basin in mid-late Devonian times.

In the latest Devonian times, deposition of the Old Red Sandstone migrated into the Midlands with deposition of 100m-1km of sediment (Sevastopulo, 1979). Subsidence rates increased in the South Munster Basin at this time. The basins were infilled and replaced by coastal plains in late Devonian to early Carboniferous (Strunian), and the first signs of marine transgression, spreading westwards, are expressed as deltaic deposits (Kinsdale Delta) south of Cork City (Gardiner, 1975a). However the major transgression occurred in the Lower to Middle Courceyan with the top of the Old Red Sandstone marking a change from fluviatile to marine conditions. In most places the top of the ORS facies is Lower Courceyan in age (MacDermott and Sevastopulo, 1972).

#### 2.1.4 Lower Carboniferous

During the early Courceyan (*spictatus* and *inornatus*-*Siphondella* conodont biozones; Varker and Sevastopulo, 1985), the sea transgressed northwards rapidly from what is now the Celtic Sea, with two main periods of incursion. The overall result of this was a change from deposition of thin carbonate and clastic sands to tidal flat deposits as the rate of deposition exceeded the rate of subsidence, and finally to carbonate muds (Fig. 2.2). Thicker accumulations of deltaic muds and sands, up to

800m, occurred in the still rapidly subsiding South Munster Basin (Sevastopulo 1979).

In the latter part of the Courceyan (*P. communis carina* and *Sc. anchoralis* conodont biozones; Varker and Sevastopulo, 1985) a variety of carbonate lithologies were deposited on the well-developed carbonate shelf north of the South Munster Basin (Fig. 2.2). In the south, deposition of argillaceous limestones up to 250m thick (Ballysteen Limestones) gave way to Waulsortian carbonate mudbanks, firstly in the Cork area (MacDermott and Sevastopulo, 1972; Sevastopulo, 1979; Philcox, 1984). The Waulsortian mudbanks reached their greatest thickness and extent towards the very end of the Courceyan, up to 750m thick in the Shannon area and extending up to 200km across the depositional strike. The Waulsortian limestones formed as knolls and sheets in water depths of around 200-300m in the marginally sub-photic zone, by in situ accretion of carbonate muds trapped by organisms (Lees, 1961; Lees and Miller, 1985). Further north, calcareous sandstones are overlain by inter-tidal micrites which pass up into more open marine limestones and shales (Philcox, 1984; Sevastopulo, 1979). In the Central Irish Midlands, the Courceyan stage is dominated by the Navan Group and Argillaceous Bioclastic Calcarenite Group carbonate sediments, with the Navan Group covering around 8200km<sup>2</sup> of the east Central Midlands and attaining a maximum thickness of around 400m at Navan (Andrew, 1986a; Philcox, 1984). The Navan Group

consists of a thin terrigenous base that passes up through tidal, laminated muds and sands into a sequence dominated by shallow marine micrite, oolitic and bioclastic calcarenites and calcareous sands (Andrew, 1986a; Andrew and Ashton, 1985; Philcox, 1984). The uppermost section of the Navan Group consists of muddy, bioclastic limestones and siltstones. The ABC Group consists of a sequence of argillaceous, bioclastic (crinoid and bryozoa-dominated) calcarenites and thin skeletal shales, with Waulsortian mudbanks forming up to 50% of the Group in places.

A diagrammatic section through the Courceyan from SW to NE is illustrated in Figure 2.3.

The transgression continued during the Chadian, with the development of marine conditions over large areas of the north and north-west of Ireland, depositing bioclastic shelf limestones (Sevastopulo, 1979). The Waulsortian facies disappeared during the Chadian (Lees, 1961; Sevastopulo, 1979), associated with subsidence rates relatively greater than sedimentation, and cherty limestones of basinal facies were deposited in deep-water (>500m) basins (Sevastopulo, 1979; Philcox, 1984). In places, eg the North Dublin Shelf, deposition of shelf facies oolitic limestones and micrites was the result of local regression.

The earliest volcanic activity in the Carboniferous occurred in County Limerick during the late Courceyan to

Chadian, with the eruption of submarine alkali basalts and eventual subaerial build-up of volcanic ashes (Strogen, 1973, 1977).

Prior to the Arundian, a major episode of tectonic instability and faulting on steep slopes of the carbonate shelves or ramps, resulted in submarine slumping/erosion and debris flow deposition, for example the Rush Conglomerate and the Boulder Conglomerate at Navan.

During the Arundian many shelf areas that existed in the Chadian were replaced by basinal facies, often turbiditic limestones, frequently termed "Calp". Throughout the remainder of the Lower Carboniferous, well-bedded limestones and shales were deposited in the Central and NW Irish Midlands. The thickest carbonate successions in the NW (up to 2200m; Sheridan, 1972) accumulated during the Chadian to Brigantian in the actively subsiding North West Basin, bounded by the Ox Mountains Horst and the North West Platform.

#### 2.1.5 Upper Carboniferous

The Upper Carboniferous rocks are most extensively exposed in the Clare-South Limerick Basin in Munster and in scattered remnant outliers in the Midlands, and comprise Namurian deltaic deposits, including coal measures, as well as Westphalian sediments (Fig. 2.1). These silts and sands were derived from the W, NW and SW and the thickest successions were deposited in actively

subsiding basins (Sevastopulo, 1981).

#### 2.1.6 Permian, Mesozoic and Tertiary

Permian and Mesozoic sediments are restricted to the NE of the country and to small grabens in Kingscourt and Wexford (Phillips and Sevastopulo, 1986). Tertiary deposition was dominated by extensive eruptions of plateau and flood basalts in the NE of the country, with coeval basic dyke intrusions.

### 2.2 TECTONISM AND STRUCTURE AFFECTING THE CARBONIFEROUS ROCKS

Tectonic activity during the late Devonian to early Carboniferous is evident as a structural control to the northern margin of the Munster Basin. Here, faulting produced scarps which subsequently controlled alluvial fan deposition (Phillips and Sevastopulo, 1986).

Waulsortian limestones deposited in 250-350m of water in late Courceyan times implies differential rates of subsidence resulting from active faulting at that time (Boyce et al., 1983). In the Chadian, submarine debris flows observed at Silvermines and Navan were features produced essentially by instability resulting from syn-sedimentary faulting (Boyce et al., 1983; Ashton et al., 1986).

However, the majority of the structures in the

Carboniferous rocks are the result of the late Carboniferous to Permian tectonic event. The terms Variscan, Armorican or Hercynian have been used to describe this deformation and the structures produced have been studied and described extensively (Gill, 1962; Collier, 1984; Cooper et al., 1984; Sanderson, 1984). The most intense folding occurred in the south with the formation of large-scale, upright folds with wavelengths and amplitudes of several kms and trending ENE, with superimposed minor folds (Fig. 2.4). A spaced cleavage is characteristically associated with this folding. Gill (1962) termed this southern region zone 3 of the three zones he delineated in Ireland (Fig. 2.4). The folding is cut by extensive faulting in this region, with normal, strike-slip and thrust faults evident (Collier, 1984). The displacement on the larger faults may be up to 5km. The northern limit or boundary of this zone, often termed the "Hercynian Front", marks a topographic change (ORs mountains to the south and low-lying Carboniferous to the north) more than a change in tectonic style, as cleavage, folding and thrusting are all present some distance to the north of this boundary (Sevastopulo, 1981; Phillips and Sevastopulo, 1986).

Gill's zone 2, occupying most of the Central and Eastern Irish Midlands, is characterized by a transition between gentle folding in zone 1, the NW Midlands, and the tight folding in zone 3 (Fig. 2.4). In zone 2 the cleavage is less pervasive than zone 3 with the southern area

characterized by intense normal faulting and close folding, with more gentle folding in the north. These northern gentle folds have an ENE to NE Caledonian trend. In zone 1, north and north-west of the Longford Down Inlier, the pattern is one of faulted blocks with NE-trending faults (Fig. 2.4). Any folding is gentle and as in zone 2 the general Hercynian trend is the same as that of the Caledonian structure.

### 2.3 INTRODUCTION TO THE NAVAN DEPOSIT

The Navan orebody was discovered in 1970 by Tara Exploration and Development Company Ltd, following shallow soil geochemistry carried out over the previous year (O'Brien and Romer, 1971; Libby et al., 1985). A distinct geochemical anomaly was detected on the north side of the River Blackwater, with peak values of 5000ppm Zn and 2000ppm Pb. The first diamond drillhole was completed in November 1970 and intersected 12m of 8.5% combined Zn+Pb, and a major drilling program was subsequently initiated (Libby et al., 1985). Underground development began in 1973 and ore reserves at that time including that on the north side of the River Blackwater, which was made unavailable to Tara by the actions of third parties, were 69.9mt grading 10.1% Zn and 2.6% Pb.

The mine has been in production since 1977 and is presently owned by Outokumpu Oy, with an annual production of 2.6mt of ore. A variety of mining methods

are employed involving open stoping, pillar mining and backfilling (Libby et al., 1985).

#### 2.4 STRATIGRAPHIC AND STRUCTURAL SETTING OF THE NAVAN DEPOSIT

The Navan deposit is hosted in gently dipping, Lower Carboniferous limestones situated on a faulted SW edge of the Longford Down Inlier (Fig. 2.5). The Lower Carboniferous carbonate succession in the Navan area is dominated by Courceyan-Arundian limestones with the bulk of the deposit hosted in the Courceyan section of the stratigraphy (Fig. 2.6). The Courceyan succession in the Navan area consists of the Navan and Argillaceous Bioclastic Calcarenite (ABC) Groups (Andrew 1986a), with the deposit itself hosted in the Pale Beds succession in the Navan Group (Fig. 2.6). The Pale Beds also host various styles of Zn/Pb mineralization at Tatestown, Keel, Moyvoughly, Oldcastle and numerous other minor showings (Fig. 2.7) (Various papers in "Geology and Genesis of Mineral Deposits in Ireland", Andrew et al. (eds), 1986). The Pale Beds consist of a variable thickness of inter-tidal micrites at the base, passing up into oolites, silty calcarenites and calcsiltites, with a distinct increase in the sand content in the top 50m. The Pale Beds are thickest in the Navan area (up to 200m thick), in contrast to 100-120m in the rest of the NE Midlands. They are overlain by silty and muddy, bioclastic limestones and shales termed the Shaley Pales

(Philcox, 1984).

The ABC Group is generally about 300m thick and comprises argillaceous, bioclastic shales and limestones. Waulsortian "Reef" limestone knolls are developed to varying degrees in the uppermost ABC and are up to 250m thick. At the margins of the Waulsortian mudbanks, knoll-forms grade laterally into "flank-bank" crinoidal calcirudites and "off-bank" facies dominated by argillaceous limestones (Lees, 1961; Lees and Miller, 1985; Andrew, 1986a).

The ABC Group is overlain by > 1000m of well-bedded calc-turbidites of the Middle Limestone Group (MLG) of Arundian age, termed the Upper Dark Limestones (UDL) or "Calp".

In the Navan mine area a submarine erosion/slump surface of pre-Arundian age cuts deeply into the ABC and Navan Groups, removing up to 700m of the stratigraphic section including parts of the ore-hosting succession (Andrew and Ashton, 1985). The term erosion/slump is used throughout this thesis because although it is evident that large sections of the stratigraphy have been removed, it is probable that some form of slumping was responsible rather than simple erosion. The presence of, and evidence from the erosion surface and overlying Boulder Conglomerate provide overwhelming constraints on the timing of at least some of the mineralization in the Pale Beds (Chapters 3 and 5). South of Navan, more than 800m

of the Courceyan stratigraphic section have been removed and in places the erosion surface cuts into the underlying Lower Palaeozoics (drillhole EP17; C.J. Andrew, pers comm) and the Boulder Conglomerate/UDL rest unconformably on the Lower Palaeozoic rocks (Tara drilling).

General trends within the Pale Beds over the Irish Midlands have been recognised (Philcox, 1984; Navan Resource plc Company Reports) (Fig. 2.8). From Navan westwards to Ballinalack and Granard, the Pale Beds are typified by a lower member dominated by birdseye micrites up to 100m thick. These micrites are typically overlain by up to 45m of pale grey calcareous sandstones (the Upper Pale Beds), which feather out to the S and SE. These sandstones are present as a few 3-4m thick units in the Upper Pale Beds in the Navan area, but are better developed throughout the rest of the North Midlands. Further to the west towards Strokestown and Roscommon, sandstones and siltstones come to dominate the Pale Beds, which here are dominated by clastic and evaporite-bearing sabkha sediments. Typically the Pale Beds consist of oolitic and pelletal calcarenites towards their southern facies boundary (approximately from Moynure-Cloghran-Rosenallis-Monasterevin, Fig. 2.7).

The general structure in the Navan area is dominated by a complex SW-plunging anticline which is cut by NE and ENE-trending faults, and locally N-S faults (Fig. 2.5). The Lower Carboniferous beds in the mine area generally dip

at 20-25 degrees to the SW. Lower Palaeozoic low-grade metamorphosed shales and volcanics are exposed in the core of the anticline and include a chloritized/sericitized syenite intrusion.

Geophysical anomalies around the deposit can be related to the Caledonian geology: magnetic anomalies over known outcrops of Ordovician volcanics, positive gravity/non-magnetic anomalies probably reflecting a denser, uplifted Pre-Cambrian to Cambrian basement, and a negative gravity anomaly lying 15km SE of the mine thought by some workers to represent a late Caledonian granite, the so-called Kentstown pluton (Coller et al., 1986). The deposit lies at the junction of an E-W and a NE-SW-trending magnetic anomaly.

The main faults in the Navan area (Figs. 2.5 and 2.9) are the Randlestown and the A-C-D Fault complex (Andrew and Ashton, 1982,1985; Ashton et al., 1986).

Detail of the structure within the deposit is shown in Figures 2.9 and 2.10. There are two main fault systems or trends in the mine area (Andrew and Ashton 1982,1985; Ashton et al., 1986):

- 1) The earliest faulting was ENE-trending. The two largest faults are the B and the T Faults (Figs. 2.9 and 2.10). Both are normal faults with a listric profile. The throw on the B Fault averages 50-60m, but the throw on the T Fault is much greater with the downthrown side

displaced by about 200m at its north-eastern end. Both faults are unmineralized. The B Fault separates Zones 1 and 2 in the mine and is truncated by the erosional surface. The T Fault downthrows the erosion surface by up to 50m. Associated with this displacement of the erosion surface by the T Fault is a thickening of the overlying Boulder Conglomerate on the downthrown side (<5m on north, >15m on downthrown south); evidence regarded by Andrew and Ashton (1985) as showing the fault to have been active contemporaneously with the deposition of the Boulder Conglomerate. Parallel and sub-parallel to these two faults are a series of faults in Zone 1, the main representatives being the F-1, F-2, F-3 and F-26 Faults (Fig. 2.9). Displacements are all normal in the order of 10-20m. As with the B and T Faults, these are unmineralized.

2) NE-trending faults cut the Courceyan and Arundian rocks and include the A and C Faults. The A Fault is a reverse, dextral fault with a vertical displacement of up to 50-60m (Figs. 2.9 and 2.10). Complex NNW-trending folds which decrease in intensity away from the faults occur in the well-bedded Upper Dark Limestones and display a sense of dextral rotation approaching the faults (Phillips et al., 1983). The C Fault complex has an apparent normal displacement of approximately 150m.

Within the deposit and regionally developed in the NE Midlands, are NNW-trending joints and calcite veins. The largest of these are up to one metre across and often

vuggy. These are extensional features (NE-SW extension) and there is a dominance of sinistral shear (Coller et al., 1986). The calcite veins cut the mineralization and are regarded as Hercynian or later in age (Andrew and Ashton, 1982). Rare examples occur where fractures and calcite veins of similar orientation cut a Tertiary dolerite indicating that at least some of the fracturing occurred post-Tertiary.

## 2.5 INTRODUCTION TO THE MINERALIZATION

The mineralization is essentially confined to the basal 150m of the Pale Beds, with the orebody comprising several tabular, massive sulphide horizons. Marker beds in the stratigraphy are used to divide the ore into five lenses (Figs. 2.6, 2.10 and 2.11). The term "lenses" is used because of the generally depressive effect on the ore grades by the marker beds, and they are also partly defined for stratigraphic convenience. These lenses are termed 5 Lens to 1 Lens passing from the stratigraphically lowest mineralization in the Pale Beds, upwards (Figs. 2.10 and 2.11). The deposit is further divided into three zones by the B and A Faults (Fig. 2.10), with the ore being thickest in the up-dip area of 2 Zone (up to 80m of >5% Zn+Pb). The basal lens in Zone 1 for example, is termed 1-5 Lens. Pyrite/marcasite-rich mineralization in the Boulder Conglomerate is termed the Conglomerate Group Ore (CGO), and comprises <3% of the total tonnage in the deposit (Ashton et al., 1986). It

occurs in the SE side of Zone 2 and particularly in Zone 3 and is coincident with a palaeotopographic low in the erosion surface.

The ore is most laterally extensive in the 5 Lens and mineralization in the 4,3,2 and 1 Lenses is generally confined to Zone 2. Truncation of the Pale Beds and the mineralization by the erosion surface means that the original, eastern up-dip extent of the deposit is unknown. The ore in the Pale Beds dominantly occurs in bedding-parallel, stratiform, massive sulphide horizons, although local, cross-cutting contacts with the host rock are evident in places. A variety of textural styles are present indicating processes of replacement and open-space deposition of the sulphides. Other forms of mineralization include high-angle, cross-cutting veins and minor breccia styles. The mineralization in the CGO differs in that well-laminated pyrite with lesser sphalerite, often exhibiting soft-sediment deformation fabrics, represents syn-sedimentary to early diagenetic deposition.

CHAPTER 3    STRATIGRAPHY AND CARBONATE DEPOSITIONAL  
ENVIRONMENT

3.1    INTRODUCTION

The Lower Carboniferous succession at Navan (Courceyan to Arundian in age, Fig. 2.6) unconformably overlies Lower Palaeozoic, low-grade (prehnite-pumpellyite facies) metasediments, volcanics and intrusives (Andrew and Ashton, 1982, 1985; Ashton et al., 1986). The carbonate succession consists of shallow marine carbonates deposited on a transgressive margin, which grade up into calc-turbidites. The rock-types are highly variable and represent changing depositional environments in time and space. The orebody is largely hosted in the Courceyan section of the stratigraphy, in the "Pale Beds" (Philcox, 1980). Philcox (1980) worked out the stratigraphy from the initial drilling in the mine area, however the area presently considered is much larger with more data available both from underground and surface drilling, enabling the detailed facies changes to be examined. Twenty eight surface drillholes and over one hundred underground holes were logged at Navan, and thirty four thin sections were prepared from selected core samples from these holes.

This chapter examines the stratigraphy of the host rocks in detail including several strong facies variations which were discovered across the mine area. There is a

distinct change in the stratigraphy from the central mine area out towards the west across a NW/NNW trend, and two stratigraphic columns representative of the western and central mine areas have been compiled from detailed logging of drill core (Fig. 3.1). These are combined with cross-sections across the mine to establish the environment of sedimentation and its controls in the Navan area.

The carbonate terminology used throughout the thesis is a combination of that used for core and thin section descriptions. The carbonate lithologies observed in core are subdivided into micrite or calcilutite (<0.32mm), calcsiltite (0.32-0.62mm), calcarenite (0.62-2mm), calcirudite or microconglomerate (>2mm) and dolomite. Dunham's classification (1962) is used in the thin section petrography.

## 3.2 STRATIGRAPHY

### 3.2.1 Introduction

Representative surface drill holes were selected as type sections for the western and central (or eastern) mine areas respectively (N910 and N314), augmented by observations from other holes in each area, to give a complete stratigraphic section (Fig. 3.1). There are major differences between the two areas, with holes to the west being typical of the Pale Beds succession

outside the Navan deposit.

### 3.2.2 Lower Palaeozoics

Lower Palaeozoic rocks have been intersected in a small number of holes and consist of a variety of intercalated shales, greywackes and volcanics, which are strongly folded and sheared. They are Ordovician in age (Romano, 1980). Green tuffaceous horizons are well-developed in some holes and are interbedded with sediments. Syenite intrusives also occur in some holes, with baked contacts within the adjacent sediments. The syenite is usually altered, with abundant chlorite and sericite developed. Minor chalcopryrite occurs in quartz/carbonate veins which brecciate the syenite.

A "deep" weathering in the top 8 to 10 metres directly below the Lower Carboniferous unconformity resulted in intense hematisation and represents a continental weathering prior to the deposition of the basal Carboniferous Red Beds.

### 3.2.3 Red Beds (RB) (<50m thick)

The Basal Carboniferous lithologies are made up of conglomerates, sandstones and shales of a fluvial origin, with no obvious differences between the central and western areas. A Lower Courceyan age has been ascertained from miospores in the Red Beds at Moate

(Keegan, 1981). The rocks exhibit a characteristic red colouration due to hematite cements.

Clasts in the conglomerates are well-rounded and poorly sorted, and are a polymict assemblage of Lower Palaeozoic pebbles. Caliche nodules are visible in many holes. The onset of marine deposition occurs as a rapid transition into the overlying Laminated Beds, often marked by a thin, green reduction zone usually less than 0.5m thick.

#### 3.2.4 Laminated Beds (LB) (30-45m thick)

The Laminated Beds are divided into 7 units (CA to CG from top to base; Philcox, 1980) composed of calcsiltites, sandstones and argillites, and are the equivalent of the Mixed Beds of the eastern Irish Midlands. Philcox's CA unit is what is now termed the Muddy Limestones (Andrew and Ashton, 1982). There is a broad upward trend of increasing carbonate content in the Laminated Beds (Fig. 3.1).

The lowermost unit, the CG, is the thickest (up to 22m) and consists of finely interbedded/laminated sandstones and argillites. As a general feature, the lower sections are dominated by argillite and the upper are sandstone-rich. Soft-sediment deformation structures are abundant throughout the unit and are best expressed as ball and flow/sedimentary boudinage structures, caused by differential compaction of the thin shales around the sandstones and resulting in an almost nodular texture.

Slump, and ball and pillow structures are observed and small-scale, syn-sedimentary faulting, slumping and erosion may be seen locally (Plate 3.1). Some horizons at the top of the unit are bioturbated and the layering becomes less obvious, however as a general rule the layering is preserved throughout. Shelly layers dominated by small brachiopods occur near the middle of the CG, but are difficult to correlate from hole to hole. These probably represent accumulation of biodebris in small depressions, perhaps small channels.

The CG unit grades over 3 metres into a massive, pale grey sandstone termed the CF unit. This sandstone is non-calcareous and is up to 4 metres thick. Cross-bedding is developed, especially towards the base. The sandstone is absent from some holes and is replaced by CG-type material. This is interpreted in terms of lensoid-type deposition, perhaps the result of the sand body being deposited as bars or alternatively channel sands.

The CF sandstone is overlain by a variable, 7 metre thick CE unit containing the first main carbonate horizon, a 2-3m calcsiltite, the top of which is marked by a widespread, 10cm thick oncolitic layer. The rest of the unit consists of flaser-bedded argillites and sandstones with muddy calcsiltites at the top.

Above the CE, the CD unit is a distinctive pale grey calcsiltite with mud laminae in the basal sections and

mud flakes orientated parallel to bedding throughout.

A rapid transition exists between the CD and the overlying CC argillite or mudstone. In this transition, nodules of "cauliflower" chalcedony are commonly developed. These range in size from 2cm to around 10cm in diameter. Gypsum has been found within the quartz indicating that this was originally an evaporitic horizon which has subsequently undergone diagenetic silicification (Chowns and Elkins, 1974; Gustafason pers comm, in Andrew and Ashton, 1985). The CC unit itself is a 3 metre thick dark, laminated argillite with occasional thin micritic horizons.

The uppermost member of the Laminated Beds is the CB unit, composed of laterally variable, interbedded, pale, calcareous sandstones and argillites with local sandy calcarenites.

The upper units of the Laminated Beds are often cut out by an erosional feature in the western mine area which has removed the CB, CC, CD and part of the CE unit at its maximum down-cutting (considered in detail in Section 3.3.2).

### 3.2.5 Muddy Limestones (ML)

West (10-25m thick)

The Laminated Beds are overlain both conformably and non-conformably by a varied group of microconglomerates or

calcirudites and dark bioclastic argillites, commonly 10-15m thick but attaining a thickness of 25m in places, and termed the Muddy Limestones. The lower sections are dominated by the microconglomerates or calcirudites (Plate 3.2). These are poorly sorted and consist of biodebris, micritic clasts and grit-size quartz fragments. The biodebris is coarse and is made up of crinoids and brachiopods. Intraclasts of micritic material up to 1.5cm in diameter are observed, although no micrites of this stratigraphic level are known in the area. The maximum development of the microconglomerate (18m thick) occurs overlying the erosional feature in the LB (Fig. 3.1). Here, angular clasts of the underlying LB occasionally up to 4cm in diameter are found in the basal microconglomerate and the Muddy Limestones penetrate into cracks and fractures in the top 10cm of the LB below. In some holes, the bottom 2 or 3m of the Muddy Limestones are composed of a dark muddy calcsiltite in place of the microconglomerate.

The upper sections of the ML contain black argillites, often well-layered and fissile, which are up to 6m thick. Corals, crinoids and fenestellid bryozoa are found throughout. The dark argillite can be traced into the central mine area towards the east, however the microconglomerates thin out (Figs. 3.3-3.4).

East (8 to 12m thick)

The Muddy Limestones are thinner here and composed almost

entirely of calcsiltites and dark argillites. Towards the base, there is a thin, discontinuous (0.2-0.5m) horizon similar to the microconglomerate in the west termed the Limestone Conglomerate (LCG) by Philcox (1980). This is regarded as the lateral equivalent or extension of the thicker units in the west.

### 3.2.6 Muddy Limestone Transition (MLT) (0-10m thick).

The Muddy Limestones grade into the Micrite Unit through the Muddy Limestone Transition (MLT). The transition is considered as a part of the Micrite Unit and is 5-10m thick. It consists of micritic lithologies, locally silty, interbedded with calcsiltites. Thin, dark argillite horizons are found throughout this section. A characteristic feature is the presence of in-situ Syringopora colonies which are up to a metre in width in underground headings.

### 3.2.7 5 Lens Interval and the Micrite Unit (ML-LDM or LDQ)

The term "Micrite Unit" (MU) applies to the interval between the top of the Muddy Limestones (ie including the MLT) and the top-most micrite horizon encountered in 5 Lens. In the west this usually comprises the entire 5 Lens interval but in the east the micrites are more poorly developed.

West (35 to 65m thick)

The MU is dominated by micrites although other lithologies including silty/sandy dolomites, calcarenites and shale bands are present (Fig. 3.1).

The basal 15m is characterized by well-developed, light grey, stylolitic micrites with interbeds of fine-grained, buff dolomites (Fig. 3.1, Plate 3.3). The micrites are generally composed of pelletal wackestones and grainstones, with a siliciclastic component of less than 1-2%. Calcispheres are common and may comprise up to 2% of the rock (Plate 3.4), indicating low energy environment of deposition (R. Anderton, pers comm). This interpretation is supported by the micritic nature of the rocks themselves. Fenestral porosity (up to 8-10% of the rock) is infilled by generations of calcite cement, as are locally developed birdseyes (Plate 3.4). The general sequence is of a fringing bladed calcite followed by a coarser, blocky calcite infill.

Stylolites contain concentrations of organic material and are deflected around the fenestral pores, post-dating them. Birdseyes may contain pale sphalerite crystals which post-date the early bladed calcite. In one core sample, pyrite was observed as a geopetal infill within the birdseye. These relationships between sulphide and micrite imply that the disseminated mineralization in these samples occurred syn-diagenetically, before primary porosity was infilled by diagenetic cements.

Oncolites are common in the basal 1-3m of the micrites, and are suggestive of an inter-tidal environment with moderate circulation in a shallow, standing body of water (Longacre and Stoudt, 1982). They occur at the base of the micrites over the entire mine area. In some areas, horizons of intraclasts up to 2cm in diameter are also found in the basal 5 or 6m of the micrites.

The dolomite horizons in this part of the stratigraphy are about 0.1 to 1.5 metres thick. They are thickly bedded and homogeneous. Individual horizons are generally semi-continuous (Fig. 3.2). Contacts between dolomite and underlying micrite are sharp, whereas those between dolomite and overlying micrite are more gradational. A 6-12m thick dolomite occurs 18-20m above the base of the micrites (Plate 3.5). It is pale grey to buff in colour, fine-grained and is thick to massively bedded. This horizon is easily identifiable in all holes and is useful as a marker when correlating faulted holes. In thin section this lithology contains 70-80% dolomite, 10% calcite, and 10-20% detrital quartz and feldspar (abundant microcline). The dolomite is developed as interlocking, idioblastic to hypidioblastic crystals, which range from 40 to 100 $\mu$ m in size (Plate 3.6). The siliclastic component in the dolomites is volumetrically greater than in any of the micrites, and is silt to fine sand-size. The quartz and feldspars are sub-angular to sub-rounded and are corroded at the margins where in contact with the dolomite. There are no original fabrics

preserved in the rock. In places a coarser dolomite (up to 350 $\mu$ m across) is found in isolated "pockets" and these areas are quartz-free (Plate 3.6). This dolomite is interpreted as the result of dolomitization of an original carbonate that contained a significant siliclastic (detrital silt) component. Dolomitization resulted in a volume reduction within the rock that produced small pockets which were infilled by a later stage coarser dolomite, and these dolomites are now massive with no remnant porosity.

The upper parts of this dolomite unit are often dominated by bioclastic calcarenites containing 5-10% silt, which have a gradational contact with the dolomite below and the overlying micrites (Fig. 3.1). In some areas (eg, Block 17) the calcarenites contain sparry, crinoid-rich horizons, and it is only the bottom 1 or 2 metres that has been dolomitized to any degree. In such cases, where the dolomite is limited in its vertical development, there is a corresponding increase in the thickness of the overlying calcarenites. These factors suggest that the dolomites form by dolomitization from the base upwards of an originally silt-rich calcarenite layer in the micrites.

The upper sections of the Micrite Unit are characterized by light grey micrites, with well-developed birdseyes throughout. Occasional pale, oolitic horizons occur within the micrites and these are partially dolomitized. A characteristic feature in this part of the stratigraphy

is the presence of up to 6 or 7 black/green shale bands which are 5-10cm thick and are interbedded with the micrites. The shales are dominated by detrital quartz and feldspar and only contain minor carbonate.

The base of the Lower Dark Marker Equivalent (LDQ) marks the top of the 5 Lens interval and the micrites may extend right up to this contact, however it is common to find a pale, bioclastic/oolitic calcarenite in the top 3-4 metres. The LDQ is a dull, silty dolomite with small mud flakes aligned parallel to the bedding.

East (30-40m thick)

The micrites are usually 2 to 4m thick (developed above the MLT) though range from 0 to 10m in thickness. Birdseyes are common in most sections studied. In some holes minor, thin micrite horizons are occasionally present 10 to 12m above this, but they rapidly die out laterally (Fig. 3.3).

The 5 Lens is characterized by fine grained oolitic calcarenites and pale dolomites, with a 4 to 5m thick dolomite near the base which may be equivalent to the main dolomite horizon in the west (Fig. 3.1). The base of the Lower Dark Marker (LDM), absent in the west, marks the top of the 5 Lens (Figs. 2.6 and 3.1). The LDM is divided into a dark argillaceous siltstone base (Plate 3.7) up to 5 or 6m thick at maximum (LDM siltstone) and an overlying dull, sandy dolomitic unit (LDM sandstone).

The siltstone is best developed and the sandstone is impersistent.

Ten metres below the LDM is the base of a 3-5m thick muddy, dolomitic calcsiltite termed the Bottom Dark Marker (BDM). This marker is not always developed and pinches out in some areas. It is particularly well-developed in Blocks 1 and 2 in 1 Zone and in 2 Zone Upper. The interval between the BDM and the LDM is dominated by coarse, light grey, bioclastic calcarenites and calcirudites (bioclastic and oolitic grainstones), which have a sharp contact with the base of the LDM. Brachiopods and echinoderms are the main skeletal components and the rocks are medium to well-sorted. These are regarded as high-energy, shallow-water deposits (Bathurst, 1975) and the allochems are frequently abraded.

#### 3.2.8 4 Lens Interval (LDM/LDQ-LSM)

West (18 to 20m thick)

Overlying the micrites is a section of the stratigraphy characterized by three dull, medium to thickly bedded dolomitic lithologies, separated by lighter grey oolitic calcarenites containing scattered brachiopod debris (Fig. 3.1). The dolomites are used as marker horizons and include the Lower Dark Marker Equivalent (already described), the Sub Lower Sandstone (SLS), and the Lower Sandstone Marker (LSM). They are all similar in

appearance, but the LSM has a greater silt/sand content. The SLS contains small, dark mud flakes parallel to bedding similar to the LDQ. These markers are 2.5 to 4m thick. The basal contacts between the darker dolomites and the underlying lighter calcarenites are sharp. The LDQ lies on the micrites or oolites and in both cases the contact is knife-edge, often cross-cutting at a low-angle. This contact is possibly erosional. The LSM and the SLS can be traced back into the central mine area. The most variable unit is the LDQ, which becomes less well-defined moving towards the central mine area.

The LSM typically consists of 60-70% dolomite, 18-20% quartz, 10-15% feldspar and 4-5% calcite (Plate 3.8). The dolomite occurs as interlocking, hypidiotopic to xenotopic crystals which are 20 to 250µm in size, similar to those in the 5 lens dolomites. The detrital material is medium to fine sand-size. Under cathodoluminescence the quartz grains exhibit a violet luminescence, typical of an igneous source (Miller, 1985). Pressure solution contacts are found between the dolomite and the quartz grains which implies that the dolomitization took place during the diagenesis of the host rock, ie prior to diagenetic pressure solution events and the total lithification of the rock. Calcite is found within the dolomitized rock and represents remnants of the original carbonate. The SLS and LDQ are similar to the LSM in thin section, except that they contain less detrital material.

The abundance of feldspar and the sub-rounded to sub-

angular nature of the detrital component suggests an immature quartz/feldspar input.

East (22 to 25m thick)

This interval consists of light grey calcarenites, usually oolitic, and buff-coloured, silty dolomites (LDM sandstone and the SLS). Between the base of the LSM and the SLS, the calcarenites contain 3 or 4 distinct brachiopod-dominated bands, which are used as a marker (BM1). A second brachiopod marker, (BM2) is located 10 to 12m above the base of the LDM and contains abundant, disarticulated brachiopod shells scattered over a 1-2m interval. This horizon can be traced into a single band of brachiopod debris at the top of the LDQ passing out into the western mine area (Fig. 3.3).

### 3.2.9 3 Lens Interval (LSM-NOD) and the microconglomerates

West (27-35m thick)

Above the LSM is a 12 to 20m thick unit consisting of thick beds of a coarse microconglomerate/rudite, interdigitated with laminated to thinly-bedded, dark, silty argillites (Fig. 3.1). The coarse lithologies include fossil-rich horizons, dominated by brachiopod and crinoid debris, intraclast or pelletal calcirudites and bioclastic sandstones/microconglomerates (Plates 3.9a-b). Graded bedding has been observed in some holes.

The silty argillaceous horizons vary in thickness from a few centimetres up to 3 metres, with the majority around 0.5 to 1.5m thick. Individual horizons cannot be correlated with any confidence and there is a strong variation in the development of the argillites from one hole to another. The carbonate content is low and these lithologies are dominated by terrigenous input, although some contain abundant fenestellid and crinoidal debris.

The basal 8-10m of the unit is dominated by the microconglomerates, and the contact between this and the LSM below is sharp. The LSM may only be 1 to 2m thick below the microconglomerates and the contact is interpreted as an erosional surface (Section 3.3.4).

In thin section a variety of bioclasts are observed in the microconglomerates including: brachiopods, echinoderms, algae, bryozoa and ostracods. The brachiopod shells are up to 1cm in length and although disarticulated, they are not fragmented; they are well-preserved with pseudopunctate forms common. Ostracods are intact and provide a primary, intra-skeletal pore space. In general the biodebris shows only minor rounding or abrasion. The detrital component consists of quartz and feldspar grains up to 3mm in diameter. The quartz is generally of igneous origin (violet luminescence; Miller, 1985), although polycrystalline, metamorphic grains are also observed. Pellets and micritic intraclasts are also common, with the latter implying that the micrites in the 5 Lens interval were being eroded in the vicinity.

The top of this unit is a silty argillite and above it is a distinct, light grey, oolitic calcarenite (packstone/grainstone). This is 3 metres thick and is one of the best-developed oolitic limestones in the entire stratigraphy, with ooliths clearly visible in hand specimen.

The Nodular Marker (NOD) lies directly above the oolites and can be traced across the entire mine area with little change in appearance (Plate 3.10). The NOD is 8-12m thick. The basal contact is sharp and marks a change in the depositional environment from clean oolitic grainstones into dark, silt-rich, packstone-wackestones, with an abundance of echinoderm debris. Numerous muddy wisps give it the so-called "nodular" texture and in section can be seen to be the result of pressure solution. Occasional intraclasts are composed of bioclastic grainstones. A fine-grained dolomitization of the matrix (dolomite forming around 1-2% of the rock) is observed in all sections studied and crinoid ossicles occasionally have dolomitized cores.

East (40-45m thick)

There are no microconglomerates developed at all and this observation combined with the increase in thickness for this interval implies that a major facies change exists between the two areas in this section of the stratigraphy (Fig. 3.1). The LSM is thicker here with a gradational upper contact. The interval above is made up of a

monotonous sequence of oolitic calcarenites (packstones to grainstones), with minor dolomitic, sand-rich horizons. Towards the top, 10m below the base of the Nodular Marker, there is a distinct horizon of a fine-grained, muddy dolomite about 3m thick. This horizon is persistent in all holes studied throughout the central mine area. There may be a similar type of lithology discontinuously developed 3 to 5m below this. The top 3 or 4m of the 3 Lens interval is characterized by pale grey, "clean", oolitic limestones similar to those directly below the NOD in the west.

The Nodular Marker is also substantially thinner in the east averaging 4 to 6m.

### 3.2.10 1 Lens Interval (NOD-UDM)

(55-65m thick in the west, 48-55m thick in the east)

The top of the 1 Lens interval is the Upper Dark Marker (UDM), which is made up of 2 or 3 bands of black, fissile argillite (each between 0.5 and 0.8m thick) separated by a muddy calcsiltite. The entire thickness of the UDM is 2 to 2.5m. The section between the UDM and NOD is comprised of two main lithological units:

A lower unit is comprised of medium to light-grey, "banded", coarse, bioclastic calcarenites (grainstones) which are thickly bedded and dominate the 1 Lens interval for 25 to 30m above the top of the NOD. The calcarenites

are frequently oolitic and the banding is a result of horizons dominated by oolites in a calcarenite with fewer oolites and more biodebris. The siliciclastic content in these rocks is less than 5%.

A feature of this section of the stratigraphy in the west is often an intensive dolomitization resulting in a sacharoidal texture to the rock, which is pitted and locally vuggy (Plate 3.11). The vugs are up to 2cm in diameter and often contain well-developed dolomite rhombs on the margins and honeyblende sphalerite crystals. In some holes in the west this type of dolomitization occurs throughout the Pale Beds stratigraphy, however it is in this interval that it is most intensive and persistent.

An upper unit is comprised of dark, silty, fine-grained calcarenites and calcsiltites often containing muddy wisps and not dissimilar in parts to the NOD. Biodebris is scattered throughout and consists of echinoderms and brachiopods. Approximately 20 to 22m below the UDM at the base of the upper unit, there is a 2 to 3m thick horizon which is characterized by an increase in the amount of muddy wisps and is packed with small echinoderm fragments. This is termed the Sub Dark Marker (SDM). The basal contact is usually sharp with coarse calcarenites below continuing down to the NOD.

In the upper unit, a concentration of finger bryozoa up to 1.2m thick, the Lower Bryozoa Marker (LBY), is a pervasive marker horizon 14-16m below the UDM. The

bryozoa are hosted in a silty calcsiltite and again there is a sharp break at the base into pale, clean, oolitic calcarenites.

A thin black shale band (< 10cm thick) occurs 1.5m above the LBY, and is observed in all holes. In 2 Zone in the main mine area, this shale marks the hangingwall of the uppermost mineralization in 2-1 Lens.

### 3.2.11 Upper Pale Beds (45 to 55m thick)

The Upper Pale Beds above the UDM are up to 55m thick (in the west) and characterized by a high sand content (up to 75% in parts). The lithologies vary from coarse, pale sandstones through to sand-rich calcarenites and are thick to massively bedded. The most distinct horizon is a pale, calcareous or dolomitic sandstone which occurs 14 to 15m above the UDM and is termed the Upper Sandstone Marker (USM). This sandstone is 4 to 5m thick and is cross-bedded (Plate 3.12). Soft-sediment fluidization or liquefaction structures are observed. Thin sections show that it is made up of 50-60% quartz, 30-40% feldspar and 10% calcite. Other less well-developed sandstones are found in this part of the stratigraphy although these are thinner and discontinuous and probably lensoidal. The remainder of the Upper Pale Beds consist of sandy calcarenites and locally oolitic lithologies.

A pervasive dolomitization similar to that described in the lower unit of the 1 Lens interval in the west has

been noted in many holes in the western mine area in general but appears to be absent in the east.

### 3.2.12 Shaley Pales (SP) (up to 110m thick)

Overlying the Pale Beds succession is a highly varied sequence of muddy calcarenites, calcsiltites and shale or argillite horizons, with lesser amounts of sandstones. These are termed the Shaley Pales (Philcox, 1980) and may be up to 110m thick; however they are almost always incomplete, cut out at the main erosion surface, and pervasively faulted, and correlation between adjacent holes is only possible using sections of the sequence as opposed to individual horizons (for a detailed description see Philcox 1984). Philcox (1980, 1984) defined the base of the Shaley Pales as the first argillite horizon greater than 0.5m thick and divided the overlying lithologies into the Lower, Middle and Upper Shaley Pales (LSP, MSP and USP respectively).

The Lower Shaley Pales are typified by cyclic units consisting of a pale sandstone base, a muddy or silty calcarenite in the middle with local argillite layers and a black argillite on top which often exhibits a banded or striped appearance (Philcox, 1984). Each unit is approximately 8m thick. Biodebris is confined to the middle section of each unit. Bioturbation is common in the silty calcarenites and is a characteristic feature of this part of the LSP.

The Middle Shaley Pales are dominated by dark, fossiliferous argillites and muddy calcarenites, with fenestellid bryozoa, brachiopods and crinoids. A marker horizon termed the Upper Bryozoa Marker (UBY) occurs about 7m above the base of the MSP and is characterized by an abundance of encrusting-type bryozoa over a 0.2 to 0.3m interval. The top of the MSP is usually marked by a discontinuous, pale, micaceous, quartzitic sandstone; however in places this passes laterally into a sandy bioclastic calcarenite (A. Black, pers comm) .

The Upper Shaley Pales are characterized by silty calcarenites interbedded with unfossiliferous argillites.

Dolomitization of parts of the LSP and MSP results in a buff colouration to the core.

### 3.2.13 Argillaceous Bioclastic Calcarenites (ABC)

(60-250m thick)

The Shaley Pales grade up through a dark argillite at the top into a monotonous sequence of muddy calcarenites with concentrations of dark argillaceous seams, which give the rock a pseudo-nodular texture in places. The calcarenites are characterized by coarse, packed crinoidal debris with individual fragments up to 2cm in length.

### 3.2.14 Waulsortian "Reef" Limestone (WRL)

(up to 200m thick)

The "Reef" Limestone (mudbank) is part of the ABC Group previously described (Fig. 2.6) and is only developed in holes to the north-west of the main mine area. It is composed of light grey micritic limestones with characteristic development of stromatactis and is similar in appearance to the better-developed, thicker Waulsortian mudbanks elsewhere in the Midlands (Lees, 1961; Philcox, 1984). Part of the "Reef" succession comprises a distinctly coarser, sparry, crinoidal calcirudite called the "Ardracchan Limestone", and is equivalent to the Waulsortian, crinoidal facies of Lees (1961).

### 3.2.15 The Erosion surface and the Boulder Conglomerate (BC)

The stratigraphic section previously described is truncated by a pre-Arundian erosional/slump surface which cuts down to the SSE, removing up to 700m of the Pale Beds, Shaley Pales, ABC and Waulsortian "Reef" in the south-east of the mine (2 Zone East). The slope on the unconformity is irregular; however an average NW-SE gradient across the mine area of approximately 400m of section removed/kilometre has been estimated by Philcox (in press). There is no evidence of alteration, weathering or karstification below the unconformity, or

oxidation associated with the unconformity. It is overlain by a variable thickness of Boulder Conglomerate.

#### West (0-10m thick)

The conglomerate consists of a variety of poorly sorted clasts and blocks of "Reef" limestones, ABC, Shaley Pales and Pale Beds, in a dark, argillaceous matrix. The matrix often contains large crinoids similar to those found in the ABC.

#### East (0-45m thick)

The erosion surface cuts further into the stratigraphy as far down as 5 Lens in parts of 2 and 3 Zone (Fig. 3.1), and the Boulder Conglomerate is substantially thicker than in the west. Angular blocks of Waulsortian mudbank >5m in diameter have been observed in underground headings and for this reason it is difficult in some surface holes in the west to establish whether the Waulsortian mudbank is in-situ or present as very large blocks in the Boulder Conglomerate. Clasts of the Pale Beds are more common in the east and the conglomerate often contains mineralized lenses. This mineralization takes the form of massive and breccia sulphides which are dominantly pyritic but in places contain massive Zn+Pb mineralization, and termed the Conglomerate Group Ore (CGO) (Chapter 5). Laminated pyrite is commonly observed and rare clasts of underlying Pale Beds mineralization indicate that at least some of the ore emplacement in the

Pale Beds was pre-erosion and submarine slumping.

### 3.2.16 Upper Dark Limestones (>1000m thick)

The BC grades up into the overlying Upper Dark Limestones which are made up of interbedded calcarenites and argillites (Plate 3.13). The bed thickness varies from 2-3m to less than 0.5m. The proportion of limestone to argillite is also strongly variable. The upper sections of the UDL contain up to 45% argillite and there is a gradual decrease to less than 5% in places around 10-20m above the base. The argillite content in the basal 10 to 15m of the UDL comprises >40% of the unit. The beds are markedly thinner at the base and this section of the UDL is termed the Thinly Bedded Unit (TBU). The TBU is best developed over topographic lows in the erosion surface/BC. Thin framboidal pyrite laminae are frequently developed throughout the TBU and occur for >50m above the base within dark argillites in the UDL.

Very rare oolitic horizons and "pods" occur in the UDL and often have a leached appearance and are very friable.

Silicification in the form of thin, pale grey, cherty horizons is found in the lower parts of the UDL, although neither these or the oolites can be correlated as markers. Philcox (1980) identified the A-A and A-C shale markers in the UDL and more recent stratigraphic correlation by Philcox (1989) has shown that these markers and several concretionary mudstone horizons he

identified onlap the erosion surface/BC progressively from SE to NW.

### 3.2.17 Tertiary Intrusives

North-south trending Tertiary basalt sills ( $\approx$  2m thick) transgress the carbonate sequence and dip towards the west.

## 3.3 LATERAL VARIATIONS IN THE STRATIGRAPHY ACROSS THE DEPOSIT

### 3.3.1 Introduction

Detailed logging of drillcore by the author and Tara geologists has enabled the construction of cross-sections illustrating the facies and thickness changes across the deposit.

The major facies variations occur along NNW-SSE and NW-SE trends with little or no discernible variation from NW to SE. These are illustrated in Figures 3.3-3.6.

### 3.3.2 Laminated Beds/Muddy Limestones

An erosional feature exists in the Laminated Beds in the western mine area which has a N-S trend and cuts steeply into the LB, as far down as the CE unit (Figs. 3.3-3.5). Without further drilling to the west it is difficult to

ascertain whether this is an erosional slope or a channel feature. At its maximum incision, the erosion surface has removed up to 15m of the LB. This occurred over a horizontal distance of approximately 100m. Tidal channels are common in the tidal flat environment and are up to 15m deep in modern examples (Shinn, 1983). The width of such channels varies from around 50 to >100m. The erosional feature in the Laminated Beds may therefore be a form of tidal channel. The overlying Muddy Limestones reach a maximum thickness of 28m directly above the maximum erosion in the LB and contain rip-up clasts of the underlying material. Here the ML contains up to 18m of microconglomerates and these die out into the central mine area (Figs. 3.3-3.5).

### 3.3.3 The Micrite Unit and the disappearance of the Lower Dark Marker

The most obvious variation across the mine is a thinning of the micrites towards the east (Figs. 3.3-3.6). The isopach contours run NW to SE where the thinning is most pronounced (Andrew/Ashton, 1982 and Fig. 3.6), however there are other effects superimposed on this and the overall thinning/thickening of the micrites is due to two factors:

- 1) The micrites become inter-digitated with calcarenites and lesser dolomites at the top of the unit, passing from the west into the central mine area, and then the upper

horizons die out completely (Figs. 3.3, 3.4 and 3.6). This rapid transition results in the micrites thinning from greater than 40m to less than 20m over a lateral distance of about 45 to 50m and this thinning is NW-trending (Fig. 3.6). Further east, the micrites vary in thickness from 10-12m to less than 3 or 4m. In this region the micrites are substituted by fine-grained oolitic limestones (locally dolomites) and coarse, thick bioclastic calcirudites below the LDM, and they represent higher energy deposition than the low energy micrites. The oolitic limestones can be regarded as prograding into the micrites Fig. 3.4).

2) Using the base of the LSM as a datum line, there is a thickening of the interval from the base of the LSM to the top of the ML towards the west, from 52-55m to 65-70m. The micrites thicken correspondingly (Figs. 3.3, 3.4 and 3.6). The region of major thickening occurs in a NNE-SSW trend and is in the same area (not coincident however) as the erosional feature in the Laminated Beds. Thus the latter may have exerted some control on the thickness of the micrite deposited. NE-SW trending "belts" of thinned micrite in the west (Fig. 3.6) are attributed to faulting even although only apparently unfaulted holes were used in the contouring. Similar trending faults in the main mine area can be extended into these "belts".

The LDM is absent from the western mine area and from compilations of data from drillcore it may be seen to die

out along a line running NNW-SSE, which is roughly parallel to the thickening of the micrites (Fig. 3.5). The siltstone unit of the LDM is 5 to 6m thick in the eastern area (Fig. 3.5) and thins to less than one metre towards the west, before dying out completely. The detrital silt-rich LDM deposited on top of coarse, bioclastic calcarenites and calcirudites would suggest that it is the result of some form of terrigenous incursion into the system and Andrew and Ashton (1985) proposed a deltaic origin for the LDM. The LDM was correlated with a dolomitic horizon in the western mine area termed the LDQ by mine geologists, but it has become apparent that the LDQ is stratigraphically slightly higher in the succession (Figs. 3.1, 3.3 and 3.4). However, the basal section of the LDQ can be correlated with the sandy/silty dolomite above the LDM siltstone, the LDM sandstone (Figs. 3.3 and 3.4).

The BDM is often best-developed where the LDM disappears and is present as a 5m thick siltstone which thins rapidly both eastwards and westwards. The trend of the maximum development of this horizon is the same as in the LDM, ie NNW-SSE (Fig. 3.5).

Two possibilities are considered to explain the lateral variations in the micrites: a) a tidal channel (Fig. 3.7), and b) a gentle palaeoslope towards the west (Fig. 3.8).

a) Contouring of the thickness of the Micrite Unit by

Andrew and Ashton (1985) showed that the micrites thicken eastwards from the central mine area in a NNW-SSE trend. This is supported by the presence of up to 70m of micrites in holes drilled in Slane, around 15-18km east of Navan (see also Fig. 2.8). Andrew and Ashton (1985) explained the thinning of the micrites in a simplified model, in terms of a tidal channel cutting down into the micrites. They cited the presence of high-energy coarse bioclastic, sparry calcarenites and a deltaic incursion in the form of the LDM as further evidence for a channel. This seems an attractive explanation for the variations observed, and is consistent with the rapid thinning of the micrites. However the inter-fingering of the micrites as they die out would suggest that the tidal channel migrated to a certain extent as the carbonate sediments accumulated (Fig. 3.7). The upper sections of the micrites in the west contain 5 or 6 dark, black/green shale bands up to 5-10cm thick (Figs. 3.1, 3.3 and 3.4). These shales are approximately stratigraphically equivalent to the LDM and BDM in the central mine area and are dominated by terrigenous material and are interpreted as more distal equivalents to the LDM and BDM which are dominated by silt-size, detrital input, and represent the finer grained material transported and settling out of suspension (Fig. 3.7). The same sort of transition is observed in many present day deltas.

b) A gentle palaeoslope towards the west is an alternative model, however is less attractive. The

increase in the thickness of the interval between the top of the ML and the base of the LDQ would suggest that thicker sediments accumulated towards the west, possibly as a result of a gentle slope in that direction (Fig. 3.8). The low-energy depositional environment of the micrites as opposed to higher energy oolites in the central mine area, could also be explained by slightly deeper water towards the west. Within the basal micrites logged in Blocks 18 and 19 horizons containing an abundance of micritic intraclasts up to 2cm in diameter are found. These are interpreted as rip-up clasts from the central mine region which are transported and re-deposited down-slope towards the west. However, the abundance of birdseyes in the micrites are a feature characteristic of inter-tidal deposits, and oolitic and bioclastic calcarenites are more typical of subtidal carbonate deposition, i.e. the opposite of that expected from a gentle slope towards the west (Fig. 3.8). The fact that >30-40m of micrites are developed at the base of the Pale Beds throughout most of the eastern Central Irish Midlands and are often succeeded by oolitic limestones (various papers in Andrew et al., 1986) would imply that the micrites represent a slightly shallower water depositional environment than the oolites at the onset of the transgression, and not slightly deeper.

The former model is favoured to explain the lateral variations in the Micrite Unit.

### 3.3.4 3 Lens microconglomerates

There is clearly a major change in the depositional environment towards the west between the base of the LSM and the NOD in the form of microconglomerates/calcirudites inter-digitated with dark, silty argillites (Figs. 3.3, 3.4 and 3.9). The limit of the development of the microconglomerate (<3m thick) occurs in a trend almost N-S (Fig. 3.5). The variation in the 3 Lens interval is interpreted as the result of an erosional event (possibly similar to that observed in the Laminated Beds) prior to the deposition of the Nodular Marker, cutting down and removing oolitic calcarenites towards the west, and the resultant deposition of coarse microconglomerates on top of this surface. The grading within individual units in the microconglomerates suggests that they were laid down as pulses or several events rather than one event. The lines of evidence for this erosional feature possibly in the form of a channel such as in the Laminated Beds, are:

- 1) thickness variations in the stratigraphy and a thickening of the Nodular Marker as a result of infilling of a low-angle erosional feature (Figs. 3.4 and 3.9),
- 2) a sharp erosional contact between the microconglomerates and the LSM in the west (Fig. 3.9),
- 3) an onlapping effect between the microconglomerates

and the calcarenites (Figs. 3.4 and 3.9). In the west, the microconglomerates lie directly on the LSM. Passing eastwards, they are developed about 5 to 8m above the LSM as a single 3 to 5m intersection, being replaced by calcarenites, and in the central mine area this part of the succession is dominated by oolitic calcarenites with local sand-rich horizons. The dark, silty bands in the west grade laterally into muddy/silty calcsiltites separated by oolitic layers. There is a marked change in the dip of the beds in underground headings between the calcarenites and the overlying microconglomerates, with beds dipping more steeply in the latter (Fig. 3.9),

- 4) fragments of mineralization in intraclasts in the microconglomerate (Fig. 3.9),
- 5) micrite clasts within the microconglomerate indicate erosion of the micrites in the vicinity. Microconglomerates directly overlie an erosional surface at the top of the micrites at Tatestown (Andrew and Poustie, 1986) and therefore the micrite clasts may have been derived from this area, ie NW of Navan. A NW derivation is consistent with the facies trends at Navan and the channel feature may have extended along this trend from Navan to Tatestown, with transport of material from NW-SE.

### 3.4 DEPOSITIONAL ENVIRONMENT

The Lower Carboniferous lithologies from the Laminated Beds up through to the Upper Dark Limestones represent a general deepening in the water depth during carbonate deposition (Fig. 3.10)

The nature of the Laminated Beds suggests spring or storm tide deposition in a tidal flat environment (Shinn, 1983) and are the result of the onset of a marine transgression. This transgression also resulted in an increase in the carbonate content passing up through the LB succession from sandstones and muds, to calcsiltites. The preservation of the layering, only locally disturbed and homogenised by bioturbation, indicates a supratidal environment where burrowing organisms would have difficulty enduring fluctuating salinities and exposure (Shinn, 1983). The presence of a replaced evaporite horizon corroborates the shallow, supratidal nature of the environment of deposition. The overlying muddy limestones containing abundant corals and brachiopods are the first main carbonate sediments, possibly represent a slight increase in the water depth. Thick microconglomerates in the western mine area were deposited in a tidal channel which incised into the underlying Laminated Beds.

The beginning of the Pale Beds succession is dominated by micrites, with oncolites and in situ Syringopora colonies at the base suggesting a supratidal environment, moving

up into more supratidal-intertidal birdseye micrites. The micrites, containing abundant calcispheres, are likely to represent deposition in a low energy regime (R. Anderton, pers comm). There is a significant clastic input in many horizons in the form of silt and fine sand, often present in lithologies which were subsequently dolomitized. In the central mine area, the micrites are substantially thinner than in the west and give way to overlying oolitic and coarse, bioclastic limestones, indicative of a higher energy regime.

The remainder of the Pale Beds are dominated by a variety of oolitic and bioclastic calcarenites and calcsiltites best interpreted in terms of a subtidal/bank margin environment of deposition (Bathurst, 1975; Halley et al., 1983; Shinn, 1983). Silt-rich carbonates in the Pale Beds, usually dolomitic, contain abundant feldspar as sub-rounded to sub-angular grains, which imply proximity to the detrital source. The nature of this source is uncertain, however the presence of significant amounts of K-feldspar points to the syenite intrusives and keratophyric volcanic breccias to the NE of the deposit as a possibility. Tidal channel deposition again resulted in thick microconglomerates in the western mine area.

There is a marked increase in the detrital content of the rocks in the Upper Pale Beds, with sandstones and sandy limestones, perhaps corresponding to greater uplift rates in adjacent land masses. The sand-rich horizons in the

Upper Pale Beds (and in the LB) appear to be lensoid in nature and were probably deposited as some form of bar.

There is evidence that tidal channels controlled not only the deposition of coarse microconglomerates in the western mine area in the Muddy Limestones and the Pale Beds, but also gave rise to a marked thinning of the Pale Beds micrites in the central mine area.

A major change in the depositional environment marks the onset of the Shaley Pales and ABC, with an abundance of argillite in a deeper water environment.

The overlying Waulsortian "Reef" limestones are characteristic of deep water, carbonate deposition and indicate water depths approaching 300m (Lees and Miller, 1985; Miller, 1986). The Boulder Conglomerate was deposited as a submarine, debris flow (Boyce et al., 1983) and was the result of instability, probably associated with extensional syn-depositional faulting (Ashton et al., 1986) which led to a deeper water environment. The succeeding thick Upper Dark Limestones were laid down as well-bedded, calc-turbidites, and represent carbonate slope deposition, by modern analogue, probably in water depths greater than 500m (McIlreath and James, 1984).

The change in depositional environment passing up the Lower Carboniferous succession may be explained by a marine transgression in the Courceyan and the deposition of shallow water carbonates (Pale Beds), with an

evolution of the carbonate bank from a ramp to slope through the Courceyan to the Arundian similar to that described by Gawthorpe (1986) for the Dinantian carbonates in the Bowland basin. In the Bowland Basin, the carbonate facies and facies associations in the Courceyan to early Arundian indicate two distinct depositional environments, with evolution from a carbonate ramp involving deposition of bioclastic wackestones and packstones with lesser mudstones in a shallow marine environment (75-100m below sea level), to mudstones, calcarenites and debris-flow breccias and conglomerates deposited on a carbonate slope.

### 3.5 CONCLUSIONS

1. The Lower Carboniferous limestones in the Navan mine area represent shallow water deposition in the Courceyan carbonates including the ore-hosting lithologies, which grade up into deeper water argillites, Chadian age Waulsortian limestones and Arundian calc-turbidites. In the main mine area much of the upper sections in the stratigraphy are cut out by an erosional surface with the deposition of a debris flow conglomerate on top. The Pale Beds hosting the mineralization were deposited in a shallow marine environment which varied from supratidal to subtidal/bank margin, dominated by micrites and oolitic/bioclastic packstones to grainstones but including important dolomites.

2. Dolomitic horizons are marked by a distinctly higher detrital silt content than the surrounding limestones.
3. The lithologies vary across the mine area and there are major differences in the stratigraphic sections between the western and central mine areas. These can be summarized as:-

Western

Central

- |   |   |
|---|---|
| <p>a. Overall thickness of the 1 Lens interval is 50-60m and reaching 65-70m in the far west.</p>                     | <p>Constant thickness of around 48-55m.</p>                     |
| <p>b. Microconglomerates in the 3 Lens interval, deposited on an erosional surface/channel towards the west.</p>      | <p>Oolitic sections.</p>  |
| <p>c. LDM is absent, however there are shale bands in the micrites at approximately the same stratigraphic level.</p> | <p>LDM with up to 6m of siltstone at the top of the 5 Lens.</p> |
| <p>d. Thick micrites, usually greater than 45m, and in places greater than 60m.</p>                                   | <p>Thin micrites, often less than 2 or 3m.</p>                  |

e. An erosional feature (channel) cutting into the Laminated Beds, with thick Muddy Limestones containing microconglomerates deposited on top.

Laminated Beds succession complete.

4. Major facies variations trend NNW-SSE and can largely be explained by a depositional environment in which tidal channels were active.

## CHAPTER 4    DIAGENESIS AND DOLOMITIZATION

### 4.1    INTRODUCTION

An outline of the diagenetic stages within the Pale Beds is presented (Figure 4.1) and is based on thin sections of micrites and dolomites in the Micrite Unit, and calcarenites, dolomites and microconglomerates, including the main marker horizons, in the rest of the Pale Beds stratigraphy. Staining techniques and cathodoluminescence (see appendix) were used as an aid in the identification of the different diagenetic stages.

### 4.2    CALCITE CEMENTS

Using stained thin sections, the oolitic and bioclastic packstones to grainstones including the microconglomerates or calcirudites show a sequence of cements which begin with a bladed calcite rim which is followed by a more blocky calcite which becomes more ferroan with time (Figs. 4.2-4.3; Plate 4.1a). The last stage of infill cement is a ferroan dolomite, usually zoned, and comprises 5-6% of the rock (Plates 4.1a-b). The calcite cements are precipitated in the pore space surrounding the allochems but are also deposited within brachiopod shells where the original fibrous shell structure has been dissolved out; the shell being preserved as a micritic rim with calcite growing in towards the centre. Ostracod shells have particularly

well-developed calcite cements precipitated in the primary intraskeletal void and fenestellid bryozoa chambers exhibit a similar feature. The proportion of bladed to blocky calcite varies and in some cases the original pore space may be entirely filled by bladed crystals.

Using cathodoluminescence (CL), the calcite cements show a more complex pattern of deposition (Figs 4.2-4.3; Plates 4.2b, 4.3b, 4.4b, 4.5b, 4.6b and 4.7b). The cements are best developed on the margins of shell debris and oolites. Four diagenetic stages have been identified under CL (Stages a-d). The bladed calcite crystals seen in normal, transmitted light are composed of Stage a) and early generations of Stage b) (see below). The outer zones in Stage b) correspond to parts of the blocky calcite seen in transmitted light, which also includes Stage c) (see below) (Figs. 4.2-4.3).

Stage a) dark to non-luminescent calcite cement forms small, meniscus-style rims fringing ooliths, larger bladed crystals fringing shell fragments and is best developed as large crystals in the first generation of syntaxial overgrowths on echinoderm fragments (Figs. 4.2-4.3; Plates 4.2b, 4.3b, 4.4b, 4.5b, 4.6b and 4.7b). In some cases the bladed crystals grade into a granular or mosaic-type crystal growth at the base of the crystal exhibiting the same luminescence. Where the overgrowths on the echinoderm debris are well-developed the same generation rims on the ooliths are almost absent,

implying that this early cement was preferentially precipitated on the echinoids in these areas. The birdseyes in the micrites have a dark-non luminescent calcite as the first generation of cement which possibly corresponds to this stage (Plates 4.7a-b).

Stage b) dull to bright yellow luminescent calcite is deposited as zoned crystal growths on the earlier rimming cement around the allochems and as subsequent overgrowths on the echinoid debris (Figs. 4.2-4.3; Plates 4.2b, 4.3b, 4.4b, 4.5b, 4.6b and 4.7b ). In the latter case it forms as the "contouring overgrowths" described by Walkden and Berry (1984). The zoned calcite grows as large crystals into the pore space. The zoning varies throughout the stratigraphy and correlation of individual zones or sequences of zones would require a more detailed study of the different lithologies and the cements. As a general rule however, the later zones exhibit brighter luminescence with the outermost zone always bright yellow luminescent.

Stage c) medium yellow luminescent calcite represents the last stage of calcite deposition and often infills the remaining porosity. It is precipitated as blocky crystals and exhibits little or no zoning (Figs 4.2-4.3; Plates 4.4b, 4.5b, 4.6b and 4.7b). In places however, there is a final stage of cementation in the form of ferroan dolomite.

Stage d), where present, occurs as well-developed rhombs

of non-luminescent ferroan dolomite precipitated as a final cement infilling remnant porosity left after c) above (Fig. 4.3). The lack of luminescence is consistent with the ferroan nature of the dolomite.

There are therefore 3 stages of calcite cement, with dark to non-luminescence in the earliest stage and brighter luminescence in the later stages. Luminescence in carbonates is controlled by the presence of manganese and iron ( $Mn^{2+}/Fe^{2+}$  ratio; Frank et al., 1982) with the  $Mn^{2+}$  as the activator and  $Fe^{2+}$  as the inhibitor of luminescence (Long and Agrell, 1965; Sommer, 1972). The pattern of luminescence observed would therefore suggest that the  $Mn^{2+}/Fe^{2+}$  ratio increased with time during deposition of the calcite cements.

These cements show a similar evolution in luminescence to that representing marine cements precipitated from marine pore waters in the shallow burial environment (Miller, 1986). The change in luminescence in the calcite cements from essentially a dark to non-luminescent calcite to a dull-bright zoned calcite and finally a medium-dull luminescent calcite, can be explained in terms of a change in the redox state of the cementing fluids from the oxidation zone down through to the sulphate-reduction zone (Frank et al., 1982; Miller, 1986). Within the oxidation zone, the manganese ions are present as  $Mn^{3+}$  and  $Mn^{4+}$  which cannot be incorporated into the calcite lattice (Miller, 1986) and therefore the low manganese content of the calcite would produce little or no

luminescence. A change to more reducing conditions (sulphate-reduction zone) would convert  $Mn^{4+} \rightarrow Mn^{2+}$  and any  $Fe^{2+}$  would possibly be incorporated into pyrite, thus a high  $Mn^{2+}/Fe^{2+}$  ratio would result in a brighter luminescence. The zoning within the Stage 2) calcite cement may reflect fluctuations in the Eh conditions during precipitation.

### 4.3 SILICIFICATION

Silicification occurs as authigenic quartz overgrowths on detrital quartz grains. The original grain boundaries are marked by inclusion trails of calcite within the quartz and in places the authigenic overgrowths contain numerous inclusion trails (Plates 4.8a-b). Where found adjacent to a carbonate cement, the inclusions in the quartz are not in optical continuity with the surrounding cement, implying that the inclusions probably represent original carbonate allochems, ie they are vestigial. Overgrowths have been replaced locally by small dolomite rhombs, indicating that silicification is pre-dolomitization in age.

### 4.4 DOLOMITIZATION

#### 4.4.1 Introduction

Dolomitic lithologies are present in the stratigraphy (Chapter 3, Sections 3.2.7, 3.2.8 and 3.2.10) and it is

apparent in drillcore that there are two types of dolomite. The first is typified by the LSM, SLS and several horizons in the 5 Lens interval, and occurs as bedding-parallel, pale-dull dolomite (usually 2-4m thick) with little or no internal structure observed. These dolomitic horizons are characterized by a higher detrital silt content than typical calcarenites in the stratigraphy (Chapter 3, Sections 3.2.7-3.2.8). The second type of dolomite is a more pervasive form of buff-coloured dolomite which may be up to 50m thick in core, often has a distinctly pitted or vuggy appearance and is generally confined to sections of the 3 to 1 Lens intervals in the western mine area (Chapter 3, Section 3.2.10). It is not in close proximity with economic mineralization (Chapter 3, Section 3.2.10). In places this latter dolomitization is confined by muddy or silty horizons.

#### 4.4.2 Detrital silt-rich dolomites

The silt-rich dolomites which are characteristic of the Micrite Unit and many of the marker beds are dominated by ferroan dolomite, though the Fe-content varies. Using cathodoluminescence, a series of dolomitizing events or stages can be established which shows the complex nature of dolomitization that produced the present lithology.

Unfortunately, due to the overall darkness of the luminescence, the majority of the dolomite stages could

not be photographed under cathodoluminescence.

Stage 1) the earliest dolomite has a dull brown/red luminescence and is a mosaic dolomite. The rhombs have dissolved or corroded edges. This stage often comprises up to 55% of the rock. It has an inclusion-rich, cloudy appearance and is slightly ferroan. It formed by replacement of the original carbonate.

Stage 2) highly ferroan, dark to non-luminescent dolomite which is common in veins cutting Stage 1) (Stage 1 is never found in veins) and occurs as rims around Stage 1) rhomb "cores". The rhombs in the veins are up to 2mm in size. Sphalerite, barite, and occasionally galena, occur in these veins and pre-date the dolomite (Plates 4.9a-b).

Stage 3) dark/bright red luminescent dolomite. Usually there are 2 dark zones separated by a bright red one. This is precipitated in veins which cut both Stages 1) and 2) and is also preferentially deposited in small pockets or vugs within the matrix material as a cement (Plates 4.9a-b). This stage corresponds to Stage d) which post-dates the calcite cements.

Stage 4) late-stage, bright yellow, blotchy luminescent calcite, which is closely correlated with Stage 3) and is found following the same veins and dissolving the dolomite (Plates 4.9a-b). This stage is also deposited in the vugs that contain the last stage of dolomite deposition.

It is important to understand that the "matrix" dolomite in these rocks is affected by all the stages and events that occur and it is only by looking at relationships between the matrix and veins or fractures that we can build up a sequence of events. It is evident that the dolomitization did not occur as a single event. There is an early dolomite which pre-dates sulphides which tend to be concentrated in fractures containing Stage 2), ferroan dolomite. These sulphide-bearing fractures are clearly cut by fractures containing Stages 3) and 4) cements.

#### 4.4.3 Pervasive, pitted dolomites

A comparison with holes that are undolomitized suggests that this style of dolomite resulted from dolomitization of typical oolitic and bioclastic calcarenites as opposed to the selective dolomitization of detrital silt-rich horizons. Both the allochems and the matrix of the original limestones are converted to dolomite, although the lithology often preserves its original fabric (often oolitic or pelletal). There are 4 main diagenetic stages within these rocks which are illustrated in Plates 4.10a-b, 4.11a-b, 4.12a-b, 4.13a-c and 4.14a-b:

Stage A) slightly ferroan, medium to dull brown/red luminescent dolomite (Plates 4.10b and 4.11b).

Stage B) bright orange/yellow to orange/red luminescent, often zoned dolomite deposited around Stage A) (Plates

4.10b and 4.11b).

Stages A) and B) replace both the allochems and the cement, however the allochems and cements exhibit different styles of replacement. Pelletal structures and shell fragments are replaced by a granular-style of dolomitization dominated by A), with Stage B) deposited as a fine rim around the granules (Plates 4.10b and 4.11b). Dolomitization of the matrix cements on the other hand is in the form of well-developed rhombs which do not have a centrifical style of growth (Plates 4.10b and 4.11b), implying that they are a replacement rather than a cement (J. Miller, pers comm). The rhombs are cored by Stage A) and have a zoned rim of Stage B). This difference in texture of the dolomite is due to the original texture in the rock, with the finer-grained carbonate in the pellets and shell fragments replaced by granular dolomite and the coarser cements replaced by coarser rhombs.

Some of the original allochems are replaced by the rhombs implying that they contained sparry calcite.

This bright luminescent dolomite has not been seen elsewhere. The bright orange/yellow zone has undergone neomorphism and there are numerous, minute rhombs which exhibit a very bright red luminescence giving a new texture. Stage A) may correspond in part to Stage 1) in the silty dolomites as it exhibits an approximately similar luminescence, although Stage A) is slightly

brighter.

Stage C) coarse, ferroan dolomite deposited as a cement, which is dark luminescent with one or two distinct bright red zones (Plates 4.11b and 4.12b). In transmitted light, stained sections have zones which are non-ferroan and which correspond to the bright red luminescence. This dolomite is deposited in small spaces left after Stages A) and B), but is best developed in larger vugs up to 2cm across, where it is precipitated on the margins and may form crystals up to 2 or 3mm in length (Plates 4.12a-b). In these vugs, crystals of honeyblende sphalerite are deposited prior to Stage C) dolomite. Stage C) is correlatable with Stage 3) in the silty dolomites.

Stage D) late-stage, bright luminescent, blotchy calcite infills the remaining secondary pore space (Plate 4.12b). This stage correlates with Stage 4) in the silt-rich dolomites.

Sulphides are restricted to the precipitation on the edges of small vugs developed after Stages A) and B), and infilled by Stages C) and D), ie there is pre and post-ore dolomite. However, the sulphides are honeyblende sphalerite with occasional pyrite, which represent the last stage of sulphide mineralization in many cases in the deposit (Chapter 5) and therefore it is uncertain whether the pre-sulphide replacement dolomite in fact pre-dates all the mineralization or is just a late-stage event, pre-dating the honeyblende.

Some of the pitted dolomites, with up to 15-18% secondary porosity at present, appear to have two stages of dolomite. In stained thin sections it can be seen that there are Fe-poor areas of dolomite which have ghost textures of original ooliths, and are surrounded by larger rhombs of ferroan dolomite, with no relict textures evident (Plates 4.13a and c). Under CL, the early Fe-poor dolomite exhibits bright orange/red luminescence as expected and the ferroan dolomite rhombs are dark luminescent (Plate 4.13b). It would therefore appear that the early dolomite replaced the original oolitic limestone, resulting in a reduction in the volume of the rock, and later Fe-dolomite precipitated in the secondary pore space generated. The dolomite in these rocks may possibly correlate with Stage C).

One feature noted is the presence of well-developed authigenic quartz overgrowths on detrital grains. Inclusions within the quartz overgrowths are medium-bright yellow luminescent calcite implying that the silicification pre-dated the dolomitization (Plate 4.14b).

Stylolites present in the dolomites post-date the dolomite and cut through the rhombs.

#### 4.4.4 Partial dolomitization

Parts of the limestone succession in the 5 and 4 Lens intervals dominated by oolitic and bioclastic

calcarenites, have been partially replaced and cemented by dark-non luminescent dolomite with stages equivalent to the two styles previously described (Sections 4.4.2-4.4.3). Three examples of partially dolomitized lithologies were examined under CL and each example exhibits a different diagenetic sequence. All 3 examples were essentially bioclastic calcarenites and there is no apparent reason for the different diagenetic sequences.

#### Example 1

- a) Allochems cemented by calcite,
- b) Neomorphism of the allochems by a medium-dull luminescent calcite which can be traced in microfractures which cut the allochems and the cement. This results in a uniform luminescence and is correlated with calcite cement Stage 3),
- c) Dolomitization of the matrix by a ferroan, dark luminescent dolomite, with small vugs infilled with later dark/bright red luminescent cement. The dark luminescent dolomite is fine-grained although it still forms well-developed rhombs, and occurs as a replacement of calcite cement. The allochems show only slight signs of dolomite replacement. This dolomite has obliterated any texture in the cement, although traces of original calcite are present within the dolomite. The dolomite is encroaching on the allochems but has been arrested. The dolomite

correlates with Stages 2) and 3) in the silty dolomites and partly with Stage B) in the coarse, vuggy dolomites

Quartz grains have non-luminescent silica overgrowths which are displacive into neomorphic calcite, with no corrosion by the calcite.

### Example 2

- a) Allochems cemented by calcite,
- b) Dolomitization of the matrix as above in Example 2 above,
- c) Late-stage neomorphism of the allochems by a bright luminescent calcite, which cuts the dolomite and dissolves it. Micro-fractures in the detrital quartz have been sealed by the dolomite. The neomorphic calcite correlates with Stages 4) and D) in previous dolomites (Plates 4.15a-b).

### Example 3

- a) Allochems cemented by calcite,
- b) Allochems dolomitized (particularly well-developed in fenestellid bryozoa) or partly dolomitized by a dark luminescent dolomite, possibly due to their having a higher Mg-content in the initial calcite. This dolomite is thought to correlate with Stages 2) and 3),

c) Neomorphism of the original calcite cement by uniform, bright yellow luminescent calcite.

#### 4.4.5 Summary and correlation of dolomitization

There are two main styles of dolomite, each with with three main dolomitizing stages and a later calcite infill, with the later stages common to both styles (Fig. 4.1):

In detrital silt-rich dolomites, the earliest dolomite precipitated (Stage 1, dull luminescent) formed by replacement of original calcite and is very fine-grained. The later stages of dolomitization (Stages 2 and 3) are cements which are highly ferroan and commonly zoned. There is often a major dissolution/corrosion of Stage 1) prior to subsequent generations. Any sulphides were deposited during Stage 2).

In the more pervasive dolomites, the earliest stages of dolomitization also formed as replacements (Stages A and B), however the relationship between Stages A) and B), and Stage 1) in the silt-rich dolomites are uncertain. Late generations of dolomite (Stage C) are highly ferroan and are of cogenetic with Stage 3). These later dolomites often exhibit saddle-type crystals. Honeyblende sphalerite was deposited in vugs prior to Stage C), ie there is pre and post-sulphide dolomite, however due to the lack of ore grade sulphides in these rocks it is impossible to say whether the replacement dolomite

(Stages A and B) formed prior to all the mineralization or just the late-stage honeyblende. Coarse honeyblende sphalerite also occurs in NW-trending calcite joints interpreted as Hercynian in age (Andrew and Ashton, 1982), which clearly post-date the mineralization. The honeyblende in the veins is thought to be the result of remobilization of previously deposited sphalerite and this may also apply to the honeyblende in these vugs. The timing of the early replacement dolomitization in the western mine area away from the economic mineralization, although pre-dating the honeyblende, is therefore uncertain. However, there are two possibilities:

- 1) The vertically extensive dolomite replacement restricted to the western mine area, and that in the bedding-parallel, silt-rich horizons throughout the mine area, occurred synchronously. If the honeyblende sphalerite in the vugs which post-date the replacement is regarded as synchronous with that in the massive sulphides, then contemporaneous dolomite replacement could not be ruled out. Relationships between the massive dolomite replacement in the western area and the selective, bedding-parallel replacement in the main mine area, would suggest that the dolomitizing fluids arose in the west, replacing entire sections of the stratigraphy, and migrated along silt-rich, bedding-parallel beds of enhanced permeability towards the central mine area. If the massive replacement dolomitization in the western mine area was coeval with the early replacement in the

silty horizons in the central mine area, then this may explain why the deposit dies out towards the west, as the dolomitization of large sections of the stratigraphy would result in them becoming less permeable and thereby unsuitable for ore deposition.

2) The massive dolomite replacement of entire sections of the stratigraphy in the western mine area dominated by oolitic and bioclastic grainstones occurred at different time (later) than the pre-mineralization dolomite replacement in the silty horizons, and was possibly genetically related to the mineralization. This interpretation is supported by the presence of a similar style of massive dolomitization to that observed at Navan in Pale Beds-hosted prospects in the general vicinity of the Navan mine (for example, the mineralization at Clonabreeny, Moyvoughly and Sion Hill), and implies a genetic association between mineralization and the dolomitization. Ore-grade mineralization is absent from the pervasively dolomitized rocks in the western mine area. At Sion Hill, "... the mineralization is best developed in undolomitized rocks, and the more intense the dolomitization, the less chance that the rocks are mineralized..." (Geological Survey of Ireland, Open Files). Massive, replacive, ferroan dolomite is observed at Moyvoughly, where there are "...significant ore deposits above and below the dolomites, but only small amounts actually within them..." (Danielli, 1983).

The latter interpretation is favoured with the pervasive

early replacement dolomitization in the western mine area being related to the mineralizing event and therefore post-dating the pre-mineralization dolomitization of the silt-rich horizons.

#### 4.5. DOLOMITE FORMATION

The formation of bedding-parallel dolomitic horizons like those in the Micrite Unit and in the 4 Lens interval, was of prime importance in localizing high-grade sulphides (Chapters 5 and 7), with Stage 1) dolomite precipitated prior to the mineralization (Section 4.4.2). The processes and problems of dolomitization throughout the world have been the subject of much speculation and debate and are not fully understood (Hardie, 1987). The following section is not primarily concerned with the origin of dolomites, but is an attempt to assess the features observed at Navan in relation to the mineralization.

##### 4.5.1 Early replacement dolomite in the bedding-parallel, silt-rich horizons prior to the mineralization (Stage 1)

The Stage 1) dolomite described in Section 4.4.2 is interpreted as being precipitated as replacement of detrital silt-rich calcarenites prior to the mineralization.

Dolomite formation can occur without difficulty at elevated temperature, i.e. 100°C, as opposed to its reluctance to form at say 25°C (Hardie, 1987). When dealing with an environment of hydrothermal ore deposition, elevated temperatures are to be expected. At temperatures greater than 60°C, most natural sub-surface waters become potential dolomitizing fluids (Hardie, 1987).

Models for early diagenetic dolomite formation have centred on two main processes; variations on the mixing or dorga model of Badiozami (1973), and the sabkha model based on studies of Holocene dolomites (Butler, 1969). Hardie (1987) has pointed out serious weaknesses in both of these models.

A deep burial diagenetic model whereby compaction of sediments during burial results in the expulsion of pore water, has been proposed by Mattes and Mountjoy (1980). The clay minerals in shale sequences undergo mineralogical changes during increased burial and compaction that can result in release of water and magnesium, which migrate and become available for dolomitization. At Navan, the carbonate sediments were semi-lithified in many cases during mineralization (Chapter 5), and had not undergone deep burial prior to dolomitization. Although there are shale sequences within the vicinity (Sheridan, 1972), these are younger than the host rocks at Navan and are unlikely to have provided the requirements for dolomitization.

Rosen et al. (1986) proposed a model of shallow burial origin for the dolomitization in carbonate-rich horizons in siliclastic sediments of Miocene age in Virginia. These ferroan dolomites are formed without deep burial or compaction. The origin of the dolomitizing fluid is marine seawater, which is influenced by sulphate-reducing bacteria, with later meteoric overprinting due to uplift. The bacteria reduce the sulphate to sulphide, thus lowering the sulphate concentration in the seawater. Baker and Kastner (1981) demonstrated experimentally that sulphate ions inhibit dolomite formation, using the Holocene Abu Dhabi sabkha dolomite and low-sulphate groundwater brines as support for their experimental observations. Hardie (1987) has pointed out that many modern sedimentary dolomites are forming from brines with sulphate concentrations up to 70 times that of seawater and casts doubt over the validity of the Baker-Kastner model.

A shallow burial origin for dolomite has also been invoked by Burns and Baker (1987). They calculated that the maximum depth for dolomitization in the Miocene Monterey Formation of California of rocks containing 10-20% dolomite, was within the uppermost few metres of the sediment column.

Hird et al. (1987) recognised three distinct types of dolomite in Dinantian limestones in SE Wales, with the earliest dolomite (3-15 $\mu$ m in diameter) formed by replacement during early diagenesis. Late dolomite veins

formed during deep burial and contain coarse saddle crystals up to 2mm in diameter.

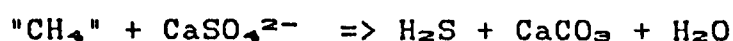
Another possibility is that the dolomite is hydrothermal in origin and related to the mineralization. The elevated temperatures associated with the hydrothermal activity would overcome one of the main barriers to dolomite formation. Dolomites that are regarded as being related to hydrothermal ore deposition, for example in MVT deposits (Radke and Mathis, 1980), are generally coarse, saddle-type crystals and not the fine-grained dolomitization observed at Navan.

The nature of dolomite formed diagenetically in the shallow burial environment is consistent with the early dolomite at Navan (Stage 1) in that early diagenetic dolomite is fine-grained, generally between 5 and 150  $\mu\text{m}$  in diameter, and forms by replacement of the original carbonate.

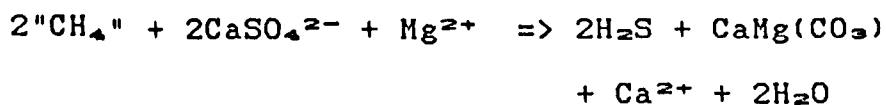
#### 4.5.2 Late cement (often saddle) dolomite (Stages 3 and C)

Late generations of dolomite are coarser and often form as saddle-type crystals (particularly Stage C), especially where precipitated in vugs in the rock. At this point it is worth considering the features and interpretation of the coarse, white, sparry, saddle dolomites which are so commonly associated as gangue with many of the epigenetic MVT deposits in carbonate rocks.

Fluid inclusion studies indicate temperatures of 60-150°C and salinities of 2-6 times normal seawater for the formation of the saddle dolomites in MVT deposits (Radke and Mathis, 1980). Evaporites are commonly associated with these dolomites and where evaporites are not presently observed, there is strong evidence for their former presence in the form of collapse breccias attributed to evaporite dissolution (Beales, 1975; Beales and Hardy, 1980). Traces of residual bitumen are commonly found and are probably best-developed in the Pine Point deposit (Macqueen, 1986; Macqueen and Powell, 1983). These features have led many authors to conclude that the dolomite formation was associated with sulphide deposition, as a by-product of low temperature (60-150°C) chemical sulphate reduction by some form of organic material producing the required H<sub>2</sub>S (Beales and Hardy, 1980; Macqueen and Powell 1983; Powell and Macqueen, 1984). This can be expressed by:



In the presence of aqueous magnesium this becomes



Machel (1987) has advocated the formation of saddle dolomite in a Devonian reef in Alberta by thermochemical sulphate reduction and chemical compaction at

temperatures in excess of 110°C during deep burial. Although there are no sulphides present, this again illustrates a requirement of elevated temperatures for the formation of saddle dolomite.

The late stages of dolomite at Navan, which generally post-date the sulphides and in places form saddle-type crystals may therefore be associated with the mineralization, which would have provided the increased temperatures necessary for their formation. The process of chemical reduction by organic matter is addressed in a later section on sulphur isotope studies, however it is noted at this stage, that there is little or no bitumen or hydrocarbon observed in the host rocks in the deposit. It would therefore appear that these dolomites were not formed by interaction between hydrocarbons and sulphate as in many MVT deposits (eg Pine Point). A more probable origin is that proposed by Russell (1983) to explain the late dolomite/copper association seen in deposits such as Tynagh and Mt. Isa, where Mg-rich fluids represent the waning stage of the ore fluid during hydrothermal convection.

#### 4.6 CONCLUSIONS

The diagenetic history of the ore-hosting succession involved initial cementation of the limestones by a sequence of calcite cements. Dolomitization of bedding-parallel, silt-rich horizons occurred by initial

diagenetic replacement possibly during and at least in part following the original calcite cement sequence, and occurred prior to the mineralization. However, the last stage dolomite cement is regarded as being related to the mineralizing event.

Complex, pervasive dolomitization of entire sections of the stratigraphy in the western mine area (dominantly in the 3 to 1 Lens intervals) formed by initial replacement and later cements. Although the last stage cement can be correlated with the that in the bedding-parallel dolomites, the earlier replacements in the two styles of dolomite do not readily correlate. The early replacement throughout sections of the stratigraphy in the western mine area is therefore interpreted as being related to the mineralizing event.

5.1    INTRODUCTION

In this chapter, the geometry, texture and mineralogy of the sulphides observed underground and in core/handspecimen are combined with detailed petrographic examination of the various forms of mineralization, so that the processes of ore deposition might be understood. This is essential as a foundation for the sulphur isotope study. There are eight main styles of mineralization in the Pale beds, which are (not necessarily in order of formation):

- 1) Replacement of semi-lithified carbonate by sphalerite (Section 5.2)
- 2) Diffuse, sphalerite/galena bedding-parallel, stringer veinlets (Section 5.3)
- 3) Bedding-parallel, massive galena/sphalerite/barite formed by infilling of small inter-connected cavities and replacement around these cavities (Section 5.4)
- 4) Deposition of bedding-parallel, high-grade, cavity fill sulphides (although in the micrites, cross-cutting, anastomosing mineralization exhibiting similar textures is common) (Section 5.5)
- 5) Massive sphalerite and galena fracture-infill and replacement in (central) 2-5 Lens (Section 5.6)

- 6) Breccia style mineralization (Section 5.7)
- 7) Cross-cutting veins (Section 5.8)
- 8) Disseminated sulphides (Section 5.9)

The Conglomerate Group Ore (CGO) within the Boulder Conglomerate is dealt with separately near the end of the chapter (Section 5.12). Each style of mineralization in the Pale Beds is examined individually, but they are all inter-related and represent the superimposition of continual processes which led to formation of the mineralized section. Samples were collected from all styles of mineralization and sulphide/host rock contacts. Over 120 underground headings and 100 drillholes were examined, and 70 large, polished thin sections (6cm x 4cm) were prepared. The areas studied underground are tabulated in Table 5.1 and illustrated diagrammatically on Fig. 5.1. All the lenses have been studied and exhibit many features in common. However, certain aspects of the mineralisation are confined to distinct parts of the succession and these are dealt with separately.

## 5.2 REPLACEMENT OF "SEMI-LITHIFIED" CARBONATE

### 5.2.1 Description

This style of mineralization is observed throughout the deposit although it tends to be concentrated in calcarenites rather than the micrites. The mineralization

was studied in detail in 2-1 Lens (204-206W, 1345 level and 222W, 1315 level), 2-2 Lens (W20S-W40S, 1285 level) and 2-3 Lens (240N, 1375 level). It consists of layered sphalerite-rich sulphides which exhibit a bedding-parallel fabric (Figs. 5.2-5.3; Plates 5.1-5.3). These layers may form sulphide intersections up to 2 metres thick but are often found as a few 1-5cm thick bands within host limestones (Fig. 5.2). The upper parts of 2-1 Lens for example, are dominated by this style. The mineralization is frequently laterally discontinuous and is often disrupted by features including pull-apart brecciation and slumping structures (Plate 5.2). For this reason, although a horizon in which this texture is evident may be traced for distances of up to ten metres or more, individual layers often cannot be continually traced over distances greater than 1-2m. The layers are generally pale brown; many have a darker brown/orange margin either at the top or bottom of the layer (Plate 5.3). Sulphide/host contacts vary from sharp to diffuse. An obvious feature is the dominance of sphalerite and occasionally pyrite over galena.

A layered fabric is observed where sphalerite is precipitated as a replacement on the top and bottom of a bedding-parallel structure (Fig. 5.4). Fluids moving horizontally replaced the carbonate in a symmetrical fashion both upwards and downwards from a permeable layer, possibly formed during early carbonate diagenesis. These sphalerite layers exhibit the change from a dark

brown/orange colour to lighter brown traversing away from the margins into the host material. After replacement, the sphalerite often became detached from the host lithology as bands and was then replaced by new generations of ZnS formed in a similar manner. The resulting bands of sphalerite are disrupted and often have a buckled or compressed appearance, possibly indicating that they were in a semi-lithified state (Plate 5.4).

Evidence for the processes involved and the timing of this replacement is found in thin sections prepared from both massive horizons and lower grade, more isolated layers. This reveals that much of the sphalerite is made up of fine grains but that it also occurs as replaced carbonate debris (allochems), for which the term "sphaleritized allochems" will be used throughout the text. The sphalerite pseudomorphs and preserves the original carbonate structure in biodebris, although the degree of preservation varies (Plates 5.5a-c). Oolites and pellets are also commonly replaced, but internal structure, ie radial or concentric fabric, is not clearly retained (Plate 5.5a). Algal borings were found in one small area within sphaleritized pellets, which implies that some diagenetic processes had occurred in the carbonate before ZnS precipitation and replacement.

This layered sulphide is therefore interpreted as the result of very delicate sub-seafloor replacement. Evidence for the early timing of some of this replacement

can be seen in one section where replaced oolites have a rimming-style sphalerite coating and a later, blocky sphalerite infill (Plate 5.5a). The rimming sphalerite appears to occur as a primary cement prior to development of any carbonate cement, rather than as a replacement fabric, although it could be argued that if the ZnS pseudomorphs the allochems so well then the cements could also have been perfectly pseudomorphed. However, the blocky sphalerite was deposited as an open space growth and implies that the replacement occurred prior to all the calcite cements. Also, in unreplaced bioclastic carbonates directly above or below the sulphide the allochems often show an open-packed relationship and do not exhibit abundant pressure solution contacts (Plate 5.5d). The sphaleritized allochems however are much more closely packed and pressure solution contacts are commonly observed (Plate 5.5c). This is consistent with replacement of semi-consolidated, uncompacted carbonate debris as opposed to lithified rock, as replacement of a cemented rock be expected to produced open-packed sphalerite allochems.

Replaced oolites occur in the layers which have a darker sphalerite base and become paler upwards. It is evident in thin section that the darker colouration is due to the fact that the allochems are totally replaced and there are subsequent rimming sphalerite cements around the edge of the layers, whereas the lighter colouration is due to partial replacement with no rimming cements evident. This

is a form of gradational replacement front resulting from solutions moving/percolating through the sediment and sphaleritizing the bioclasts in-situ. In some instances there is overprinting of later sphalerite and occasionally galena on this style, and the original texture becomes obscured by new generations, taking the form of a granular texture nucleating on the replaced allochems (Plates 5.6a-b). The granular texture is developed to varying degrees, even on a centimetre scale, with some areas of minor superimposition containing only a few scattered "granules" and others where the original texture is almost completely obliterated.

In places the sulphide consists of granular sphalerite within which randomly scattered detrital quartz grains are present. This is thought to represent replacement of a carbonate without biodebris.

Although there is considerable replacement, many textures and fabrics within these sulphides suggest that some sulphide precipitation occurred within small, originally horizontal bedding-parallel veins after the sphalerite replacement. These are tabular, usually only a few centimetres to a few tens of centimetres in length, and layers of host rock may contain several isolated bedding-parallel veins (Plate 5.7). The maximum thickness of these structures where seen in entirety is approximately 5-6cm and they are commonly 20-30cm apart. In many cases sulphides deposited within these vein structures are disrupted.

They are infilled by three main styles of sulphide: finely laminated sphalerite and pyrite sediment, colloform and stalactitic pyrite growths, and galena crystals with later pyrite replacement (Figs. 5.5a-b; Plate 5.8).

In all cases, a blocky calcite/dolomite with occasional barite is the last stage of infill. The calcite and dolomite are the same generation as the last stage calcite and dolomite in the host rocks (Chapter 4, Sections 4.2 and 4.4) The sulphides are strongly disrupted and brecciated along with the replacement sphalerite, and the result is a complex assortment of poorly sorted clasts of sulphide, usually 2-3 cm in size, but ranging down to only a few millimetres across.

#### 5.2.2 Disruption and deformation

Disruption textures in the sulphides were mainly developed in-situ and can be classified as soft-sediment deformation, compaction, and collapse features.

##### 5.2.2a Soft-sediment

Soft-sediment, pull-apart structures are common within sulphide layers enclosed in calcarenites, indicating that the host material was semi-consolidated after the mineralization (Fig. 5.6; Plate 5.2). In drill core, sphalerite-rich sulphides are slumped into the host

material, resulting in local deformation of the host rocks.

#### 5.2.2b Compactional

The layering in the more massive sulphide horizons enclosing an unreplaced block of host limestone is often parallel to the margins of the block (Figs. 5.7-5.8). This is the result of modification of the original layering during compaction, whereby the sulphides and the unreplaced carbonate had differing rheologies. The sulphide was disrupted around the carbonate which compacted more rapidly, and resulted in a boudinage-effect within the sulphides and disruption of the layers (Fig. 5.8). Although there is a general layering in the sulphide, it is disrupted and brecciated into a complex assemblage of clasts. Importantly, the host rocks are more massive and show little disruption. It is clear that these clasts are the result of in-situ brecciation of the layering. Contacts between sulphides and enclosed clasts of host rock can vary dramatically over tens of centimetres, from very sharp to diffuse, where the sulphide "grades" into the host rock as a few isolated, disrupted fragments of mineralization. (Figs. 5.7-5.8).

Sulphide layers are linked by crosscutting veins that also have replacement textures. These veins have a buckled appearance due to compaction during lithification of the carbonate sequence, again illustrating the early

timing of sulphide deposition (Fig. 5.9).

### 5.2.2c Collapse

It is evident in many of the samples studied that the sphalerite precipitated on the upper surface of a narrow, bedding-parallel cavity has subsequently become detached from the surface, probably due to its density and the presence of open space below, and collapsed as layers and clasts into the original bedding-parallel structure (Fig. 5.10). The disrupted clasts often have small geopetal sphalerite sediments subsequently precipitated on their top surfaces (Plate 5.9).

### 5.2.3 Intrepretation

There is a close association between processes of bedding-parallel replacement, and open-space, vein-type deposition of sulphides in a semi-lithified carbonate, initiated with the formation of permeable horizons parallel to bedding which were exploited by the mineralizing solutions and presumably enlarged. The layer-parallel mineralization formed by a combination of 3 processes:

- 1) Prior to the mineralization, diagenetic porosity formed in the sediment enhancing the permeability. The origin of these open spaces is uncertain but many major sulphide horizons occur at the contact between underlying

limestones and overlying silty dolomitic lithologies. Differences between the two lithologies, such as state of lithification, may have been sufficient to initiate the formation of small spaces, which were exploited by the ore fluids. For example, there may have been early dolomitization (Section 4.4.2; Stage 1) of narrow, centimetre-scale, silt-rich horizons within the calcarenites, increasing the competency of these horizons and then acting as a "crust" below which small spaces could be created. The actual process of space formation may then be similar to that advocated for the origin of some stromatactis cavities (Bathurst, 1982; Wallace, 1987).

2) The rate of dissolution of the limestone was greater than the rate of sulphide precipitation and this resulted in formation of secondary spaces.

3) During and after replacement by sphalerite, small-scale contacts between host material above and underlying sulphide were areas where space may have been created due to density contrast.

The replacement of allochems by sphalerite must be the result of a delicate, gradual dissolution/replacement rather than a total dissolution of the host rock. This is interpreted as a form of diffusional/precipitation front with a thin film replacement, involving the reactions:





The conditions of the ore fluid at this time would have been less reactive than those which would for instance, dissolve and obliterate the original textures.

The sphalerite selectively replaced calcite allochems and so layers with an abundance of allochems would have been preferentially replaced. Prior to sulphide deposition, where there were horizons containing abundant carbonate debris within more siliclastic, detrital layers, selective replacement resulted in bedding-parallel mineralization. Unreplaced material adjacent to the sulphide is silty and contains small dolomite rhombs between detrital quartz grains. The contact between this and the sulphide is sharp and is locally marked by a thin concentration of dark, organic-rich seams, which may have provided boundary surfaces between which the ore fluids passed along and precipitated sphalerite by replacement. Minor amounts of ZnS do occur as inter-particle disseminations between the quartz grains implying that some fluid permeated into this material and was not entirely restricted to carbonate layers.

### 5.3 DIFFUSE, LAYERED ZnS, STRINGER REPLACEMENT VEINLETS

#### 5.3.1 Description

This type of mineralization is dominated by ZnS and

consists of bedding-parallel, but locally cross-cutting, diffuse "stringer" sulphides (Fig. 5.11). The principal difference between this style and the previous one is that the stringer mineralization is developed within silty, dolomitic rocks instead of calcarenites. This style was studied in detail in 2-3 Lens (252/253 accesses, 1315 level) where it occurs directly above a massive sulphide horizon (Plate 5.10). The sulphide can be up to 0.5 metres thick but dominantly forms thin, diffuse layers less than 2-3cm thick.

Thin sections of narrow, diffuse bands and more massive areas show a complex sequence of sulphide deposition, dolomitization and disruption. Irregular galena/sphalerite veinlets are surrounded by a halo of fine-grained sphalerite penetrating into the host rock (Plates 5.11a-b). The sphalerite around the veinlets has a granular texture with minor replaced biodebris. The veinlets themselves consist of a typical assemblage of dendritic galena, rhythmically banded sphalerite and a later generation of coarse honeyblende and barite rosettes which in places exhibit geopetal features (Plate 5.11b) (see Section 5.5.5). The veinlets are very irregular, thicken and thin dramatically, and are unlike normal brittle fractures. The galena is entirely concentrated in these structures and is absent from the surrounding host rock. It appears that the galena grew within the veinlet along with sphalerite, but much of the zinc diffused or permeated out into the host rock.

The dolomite is present as well-developed rhombs (up to 120  $\mu\text{m}$  in diameter), however is poorly developed directly around the veinlets where the sphalerite is dominant. Passing 1 to 2cm outwards into the host rock, the dolomitization is extensive and overprints the ZnS. Authigenic quartz overgrowths are particularly well-developed on detrital quartz grains adjacent to the veinlets and are progressively less well-developed passing further outwards into the host rock. The presence of numerous inclusions of sphalerite within the dolomite crystals, which are concentrated in the outer areas of the rhombs, is the result of dolomite precipitation before and after deposition of the sphalerite (Plate 5.11c). Using cathodoluminescence, three distinct stages of dolomite precipitation are observed (Fig. 5.12a). These stages; dull luminescent, dark-non luminescent, and dark with bright red zone luminescent, correlate with those found in the dolomites described in Chapter 4 (Section 4.4.2; Stages 1,2 and 3) and it is clear that there was dolomitization both pre- and post-ore deposition. Sphalerite inclusions are also developed within the quartz overgrowths indicating that silicification post-dated the mineralization. The relationships between sphalerite, dolomite and quartz are illustrated in Fig. 5.12b.

Where this style of mineralization is most extensively developed, there are two different mineral assemblages: dolomite-quartz-sphalerite-barite, and sphalerite-

dolomite-quartz. In the former the sphalerite is granular and in the latter it occurs as replacement of biodebris. The sphalerite-rich material often occurs as angular clasts in a matrix of dolomite, quartz, sphalerite and barite (Plate 5.12). This is an in-situ brecciation probably due to differences in the degree of consolidation between the two assemblages.

### 5.3.2 Interpretation

This style of mineralization was deposited in calcarenites which had been partly dolomitized prior to the mineralization. Dolomitization had not obliterated the original allochems and they were partly preserved by the later sphalerite. Sphalerite was precipitated by replacement around narrow veinlets with galena and sphalerite deposited within the veinlets. There is evidence for late dolomitization and silicification after the sphalerite deposition.

## 5.4 BEDDING-PARALLEL MASSIVE GALENA/SPHALERITE/BARITE

### 5.4.1 Introduction

More massive replacement mineralization than previously described and one of the distinctive textures in the deposit, consists of coarse contorted galena bands and aggregates associated with a sphalerite/barite assemblage. The sulphides occur in bedding-parallel

horizons less than 1.5m thick. Some of the best examples of this style of mineralization are found in 2-2 Lens (W20S-W40S, 1285 level) and much of this section is based on samples from this lens (Fig. 5.13; Plates 5.13a-b).

In underground headings the most striking feature of 2-2 Lens is the massive nature of the sulphides, with sharp contacts with the host rock. The hanging wall is the Nodular Marker and the footwall is an oolitic calcarenite. Minor fracture-fill mineralization occurs outside the sulphide horizon. The ore is composed of coarse galena in a matrix of finer sphalerite and barite (Zn:Pb around 2-3:1). The sulphides exhibit complex contortions, especially the galena, although a layered fabric is observed in places (Plates 5.13a-b).

#### 5.4.2 Description

A general paragenetic sequence representing open space infill and replacement can be established. Barite rosettes and laths, associated with fine-grained sphalerite crystals and subordinate galena cubes comprise the earliest mineralization and represent replacement of calcarenite. Within many of these rosettes, "ghost" oolitic structures are evident (Plate 5.14). These ghost ooliths are often in an open-packed form (in contrast to the closely-packed sphaleritised allochems (Section 5.2.1; Plate 5.5c) and carry the implication that some of the diagenetic cements had formed prior to replacement.

The rosettes show undulose extinction and occur as clusters. Between the rosettes mud/silt-size quartz grains are concentrated in dark seams, with pressure solution contacts between adjacent quartz grains. The detrital material has been squeezed aside as the barite has grown by carbonate replacement. Very fine barite laths or needles in layers dominated by mud-size, detrital quartz, resulted from primary barite growth within porous detrital horizons.

A complex sequence of mineralization followed and produced a texture of coarse galena growths (bands and contortions) in a "matrix" of sphalerite (Plate 5.13a). The galena occurs as layers/bands and aggregates of varying thickness (mm-3cm) and is highly contorted with a complex looped appearance, but is locally well-layered, resembling a symmetrical cockscomb vein growth (Plate 5.15). The galena grew in open space in all cases. Individual galena bands are asymmetrical and have grown as bladed crystals in one direction away from a substratum (Plate 5.15). Individual bands often coarsen in the direction of growth with a fine base and a coarse bladed top (Plate 5.15). In hand specimen, much of the galena occurs in a series of small, inter-connected, elongate cavities or pods which often exhibit an irregular outline (Fig. 5.14).

The sphalerite replaces carbonate as well as previously deposited barite, around the small cavities or pods, and is also present as crustiform overgrowths on the galena.

In thin section the sphalerite replacement exhibits a granular/amorphous texture through to well-developed crystals with one or two zones and up to more than ten zones in places (Plates 5.16a-c). The zoning is best developed adjacent to the galena and is picked out by darker orange-red bands in a paler crystal. A thin reddened "halo" is evident in the sphalerite at the contact with the base of a galena band and is due to a concentration of orange/red zones within the zoned sphalerite or else a dark orange generation of granular sphalerite (Plates 5.16c-e). This presumably reflects a change in the trace element content in the sphalerite associated with deposition of the galena. These well-zoned crystals are thought to be the result of recrystallization of finer grained more granular sphalerite as ore solutions continually pass through the system, a process used to explain the coarse zoned sphalerite observed in the Kuroko ores (Eldridge et al., 1983). Further evidence for recrystallization during sulphide deposition is observed where a transition occurs from sphalerite crystals, in places zoned, into a form of rhythmic crust directly below the base of the galena (Plate 5.17). The rhythmic crust appears to be a form of isochemical recrystallization as the sphalerite crystals have an orange-zoned core and a clear rim, whereas the rhythmic crust is clear at the base and has a fine orange band adjacent to the galena of the same generation as that at the centre of the sphalerite crystals (Plate 5.17). This is probably due to trace element(s) causing

the red colouration in the sphalerite being incorporated at the end of recrystallization.

Crustiform sphalerite overgrowths were precipitated on the galena (Plates 5.18a-c) and these overgrowths can be correlated from one sample to another within a given area. The deposition of these generations however was not a continuous event as is evidenced by local hiatuses and dissolutional contacts within the overgrowths (Plate 5.18c).

The small cavity structures were lastly infilled by a barite/detrital quartz mud with barite present as an intergrowth of fine needles. This material exhibits a geopetal relationship with coarse barite laths and lesser calcite and dolomite. Within the coarse barite, rare bournonite crystals are present. Pyrite occurs late in the paragenetic sequence as minor fractures in the galena, replacement of the sphalerite, and as localized small geopetal internal sediments at the top of one ore horizon (Plates 5.19 and 5.23b).

#### 5.4.3 Interpretation

The origin of the coarse, contorted galena is complicated, however two main possibilities exist. The first is that the galena was deposited within a series of small inter-connected cavities and locally as bedding-parallel veins, with sphalerite precipitated as replacement around the galena. The irregular nature of

the margins of the small cavities would control the geometry of the galena bands, and the bands would have been subsequently disrupted by slumping of the dense sulphide into the semi-lithified host material below (Fig. 5.15). There are two lines of evidence to suggest that the carbonate was semi-lithified:

a) The presence of sedimentary dykes of carbonate allochems and quartz-silt cutting across coarse galena/sphalerite bands shows that the limestone was not consolidated after the sulphide had formed, and host material was injected into the sulphide (Plate 5.20).

b) At the HW contact in 2-2 Lens, an upper coarse galena band deforms a pressure-solution seam developed in the Nodular Marker (Plate 5.21a-b). This suggests that the galena was deposited prior to lithification of the overlying host material, and either the galena was buckled up into the lithifying sediments above or the sediments were compacted around the sulphide.

The second possibility is that the contorted appearance is the result of the galena being deposited as encrustations or linings on the margins of relic fragments of host rock within some form of cavity or breccia system (Fig. 5.16). This would be similar to the mechanism suggested by Sass-Gustkiewicz et al. (1983) to explain the galena textures in the Silesian ores, where the galena is envisaged as encrusting fragments of rock (dolomite) in a cavity system, with the relic rock

fragments becoming progressively disaggregated with time.

The nature of the galena, often occurring in small, pod-shaped features and the lack of evidence for relic clasts of host rock favours the former interpretation. Also, the locally well-layered galena with symmetrical cockscomb growths is difficult to interpret in terms of anything except some form of bedding-parallel veining or infill of narrow, elongate cavities.

Although slumping of the galena may have produced the contorted appearance, brecciation of the sulphides is also evident and in places a splintering effect has totally disrupted the sulphides (Plate 5.22).

The slumping of the dense galena/sphalerite may have been enhanced by the initiation of vertical to sub-vertical fractures in the underlying lithifying carbonates, and in some cases, peculiar funnel-shaped structures have been produced by extension fractures into which the sulphide has slumped and been disrupted (this may be related to the observation that the hanging wall is essentially flat or planar whereas the footwall is undulating and irregular) (Fig. 5.17; Plates 5.23a-b). The interpretation of some of these structures is equivocal and some examples suggest that the basal section of the funnel had formed by fracturing and dissolution prior to the mineralization (Plate 5.23b). Onlapping relationships between layered sulphide and the host rock support this last interpretation (Plate 5.23b). The

orientation of the fracturing which controlled the formation and geometry of these funnels suggests that the direction of extension was approximately north to south, ie, roughly similar to the extensional direction on faults in the mine, but the funnels are seldom sufficiently well formed to establish unequivocal extension direction.

#### 5.4.4 2-5 Lens west

A variation on the bedding-parallel, massive galena/sphalerite mineralization is observed in the footwall of 2-5 Lens west (1190 Haulage Drift), is characterised by finely layered and occasionally coarsely cubic galena crystals in place of bladed growths. The galena occurs as cubes on the upper surface and as fine laminations on the lower surface of former small interconnected cavities. The sphalerite is often well-laminated and deposited as internal sediment prior to galena. The reddened sphalerite haloes adjacent to galena are best developed in this mineralization. Pyrite again occurs late in the paragenetic sequence as a replacement of the galena.

The contacts with the host rock are highly irregular but sharp, and the ore thickens and thins dramatically within an individual horizon (Plate 5.73).

## 5.5 BEDDING-PARALLEL INTERNAL SULPHIDE DEPOSITION IN HIGH-GRADE ORE HORIZONS

### 5.5.1 Introduction and morphology

A substantial amount of mineralization in the Pale Beds formed by an open space precipitation and growth below dolomitic lithologies with continual enlargement and deposition of sulphides within these spaces. The reason for mineralization at these contacts between dolomite and underlying calcarenite is the key to understanding the Navan deposit. Open space precipitation on a small scale has already been described in Sections 5.2 and 5.4, but in the following style of mineralization, it occurs on a larger scale with entire sulphide horizons deposited as open space growths, and with evidence for dissolution of adjacent limestone.

This style of mineralization was studied in 2-1 Lens (222W, 1315 level and 226-229N, 1435 level), 2-3/2-4 Lenses (252/253S, 1315 level and 224N, 1435 level) and numerous localities in 1-5 Lens (see Section 5.5)

In 1-5 Lens the mineralization occurs in the micrites and is considered in detail towards the end of this section since a more cross-cutting style of mineralization is evident.

The bedding-parallel sulphide horizons occur at the contact between a calcarenite or micrite and an overlying

dolomite (Plates 5.24a-b) and the characteristic features of the high-grade horizons are:-

- Distinct differences in the hangingwall and footwall lithologies.
- Sharp upper and lower contacts, often with a strongly undulating footwall containing depressions filled with argillite sediment.
- Pronounced thickening and thinning of the sulphide horizons.
- Layered sphalerite at the base, often inter-laminated with a fine detrital quartz mud, deposited as a sulphide sediment.
- Complex, chaotic assemblages of sulphide clasts with locally layered sulphides, frequently found in the bottom two-thirds of the horizon.
- An in-situ, open space solution growth assemblage of dendritic galena, rhythmically banded sphalerite and geopetal sphalerite sediments, with subsequent honeyblende sphalerite, barite and calcite with dolomite representing infill of remnant space within the massive sulphide.

#### 5.5.2 Evidence for dissolution of the host rock

Textures and features observed underground and in thin section indicate that there was some dissolution of the

host lithologies to form the space associated with precipitation of sulphides. This often occurred at the contact between two strongly differing lithologies, a micrite or calcarenite and an overlying dolomite.

An important feature found in these areas is a very irregular lower contact and the presence of small, rounded depressions filled with a dark, laminated mud (Fig. 5.18; Plate 5.25). This argillaceous material is a non-calcareous, quartz/feldspar sediment and is only found within these depressions where it may be up to 0.5 metres thick. In most cases layers of sphalerite, often disrupted and slumped, are also found interbedded with this material (Plate 5.25). The argillite can be seen onlapping the margins of the depressions indicating that the depression was present prior to argillite deposition (Fig. 5.18).

Graded bedding is observed within the argillite, with local silt to fine sand-size layers passing upwards into mud-size horizons. Similar depressions and infill are observed on thin section scale with a knife-edge contact between argillite and oolitic calcarenites below (Plate 5.26). The oolites are dissolved at the contact with the argillite.

It is probable that this argillite is the insoluble, residual material left after dissolution of the limestone below the dolomites. The argillite formation is clearly synchronous with the onset of mineralization, as is

evidenced by its interbedding with sphalerite layers. Graded bedding within the argillite implies that there was some degree of current action in the spaces or cavities created. The sphalerite was deposited as a sulphide sediment.

### 5.5.3 Internal sulphide (sphalerite) sediment

Sphalerite layers and laminations on a variety of scales and clearly visible underground can be traced for distances up to a few metres, where not disrupted (Plates 5.27a-c and 5.28a-c). This sphalerite sediment is found throughout an ore horizon but is preferentially developed at the base. The majority of the layers are dominated by sphalerite, but some contain up to 50% mud to fine silt-size detrital quartz/feldspar. Graded bedding can be seen within both the quartz-rich material and to a lesser extent the sphalerite-dominated layers, implying that there was some current action during deposition (Plates 5.27c and 5.28a). Current action is also suggested by the presence of asymmetrical growth folds in the sediment (Plate 5.27a). Sedimentary structures within this material include injections, draping features and density loading, and the layers are often disrupted (Plates 5.28b-c). The quartz/feldspar-rich sediment appears to have been less consolidated and is often squeezed and deformed by the sphalerite layers (Plate 5.29). Individual layers thin before they die out and this material is interpreted as being deposited and preserved

within a form of cavity structure.

Thin sections prepared from this sphalerite show that much of the mineralization is a microcrystalline sulphide mud. A proportion is made up of a coarser, granular sphalerite occasionally intergrown with barite. Galena mineralization is restricted to sporadic, porphyroblastic growths within and post-dating the sphalerite (Plate 5.30).

The sphalerite layers formed by rapid nucleation of sphalerite particles in the ore solution (Fig. 5.19). This resulted in a fine-grained suspension out of which the particulate sulphide then settled as a sediment on the base of the open spaces, with evidence for current action in the form of graded bedding and growth folds (Fig. 5.19).

#### 5.5.4 Complex, chaotic sulphide clasts

This term is applied to a complex assemblage of poorly sorted clasts of sulphide of sizes ranging from a few mm up to tens of cm set in a matrix of fine quartz silt and mud (Fig. 5.20; Plates 5.31a-b). Clasts are clearly matrix supported and represent active conditions during and after sulphide deposition, rather than the quieter conditions operating during the deposition of the layered sulphide sediment. A variety of clast types can be recognised:

- (1) Layered and laminated sphalerite sediment
- (2) Clasts of host rock containing galena/sphalerite veining.
- (3) Clasts made up of barite rosettes
- (4) Fragments of a coarse, bladed galena (see later).
- (5) Clasts of sphalerite replacing host rock.

We have already discussed a mechanism whereby clasts of sphalerite formed by replacement of carbonate sediment followed by disruption (Section 5.1). However, many of the clasts within this massive sulphide are of well-layered internal sediments and all the clasts are poorly sorted. The clasts are generally subangular and often have a very rugged outline suggesting that they have not been transported far.

This style of mineralization is interpreted as initial sulphide deposited within a cavity structure which has been disrupted and brecciated. The disruption could have been tectonically induced. During periods of quiescence, sphalerite sediment accumulated and was subsequently disrupted as a result of tectonic instability probably induced by faulting. Clasts of limestone with sulphide veinlets show that parts of the previously mineralized in situ host rock were also incorporated. This is envisaged as the result of collapse during the enlargement of existing spaces.

The sulphides described so far only make up part of a mineralized section. The upper parts of a horizon of massive sulphides are characteristically dominated by textures related to in-situ sulphide deposition which are distinctly different from the complex and layered sulphides described previously, and termed in-situ solution growths.

#### 5.5.5 In-situ solution growths

These appear as a complex intergrowth of galena, sphalerite +/- barite. In hand specimen and underground headings, the mineralization is characterised by coarse, pale yellow honeyblende sphalerite and large barite rosettes (Plate 5.32).

##### 5.5.5a Thin section petrography - Introduction

The main minerals are sphalerite, galena, barite and pyrite in order of abundance. The sequence of sulphide precipitation consists of early dendritic and skeletal galena and locally stalactitic pyrite overgrown by later rhythmically banded sphalerite and subsequently remnant porosity being infilled by honeyblende sphalerite crystals and coarse calcite, dolomite and barite.

##### 5.5.5b Galena

Galena is found as dendrites, skeletal crystals,

stalactitic coatings, platelets and cubic crystals. The most common form is a skeletal and dendritic crystal habit (Plates 5.33a-c). They are regarded as a precursor of the platelets and cubes which form as the skeletal crystals grow and "fill-in" (Plates 5.33b-c). The dendritic forms are typical of dendritic growths in other minerals (eg, silver) formed under experimental conditions (George and Vaidkin, 1981; Honjo and Sawada, 1982; Mason et al., 1982). Rapid growth from a supersaturated solution and the resulting instability during crystal growth is the main factor attributed to dendrite formation, although incorporation of certain trace elements may have a poisoning effect and also result in non-cubic growth. Rapid growth is thought to be due to rapid cooling (Honjo and Sawada, 1982; Jones and Kahle, 1985). In some sections there are clear indications where the skeletal crystals have started to "fill-in" and the result is a cubic crystal. The dendrites can vary in size from those only visible in thin section to examples which are greater than 3 cm in length and clearly visible in hand-specimen.

Dendrites and skeletal crystals are the result of primary, open space growth and are not a replacement texture. The delicate nature of these structures would imply that they formed in a protected environment.

Galena also occurs as crystals coating pyrite "stalactites" or "rods" (see next section). In one example the galena was observed as a primary stalactite,

and in this sample it is transitional to a dendritic structure.

It appears that when a free surface is available on the pyrite rods, the galena will nucleate and grow as crystals. Otherwise the galena crystallizes as fine dendrites. This implies that there is an excess of sulphur on the outside of the pyrite "stalactite" with which the lead combines.

#### 5.5.5c "Stalactitic" structures

These peculiar structures are locally observed throughout the deposit, both within massive sulphides and in bedding-parallel veins in unmineralized host rock (Plates 5.34a-b). The term "stalactitic" is used due to their overall morphological resemblance to present day stalactites but they are genetically dissimilar as they grew in a fluid as opposed to air. They consist of a pyrite core with later galena and sphalerite overgrowths (Plate 5.35). The pyrite takes two forms: a central rod structure which consists of successive generations of a concentric ring-type growth, and later overgrowths (often marcasite) of a botryoidal, radiating form (Plate 5.35). The stalactitic structures are overgrown by galena crystals and generations of rhythmically banded sphalerite. Geopetal sediments are synchronous with the rhythmic overgrowths. The stalactites are regarded as resulting from gravity-induced crystal growth. A central

column or rod is initially precipitated as successive concentric generations, prior to later overgrowths of radiating, botryoidal crystals. Unlike modern-day stalactites observed in cave systems, they occasionally thicken towards the base rather than tapering out. This is due to the fact that these structures pull away from the upper surface to which they are attached in a fluid-filled environment due to density contrast under the influence of gravity, as opposed to a simple drip process. Similar structures have been produced experimentally by chemical garden growth by Russell (1987), who demonstrated a process whereby mixing of an acidic and an alkaline solution could produce rod-type structures. This mixing of two solutions is essential in forming these growths and is significant in terms of ore depositional processes. At Navan, the mixing of a metal-rich, acidic fluid with a bacteriogenic sulphide-rich, more alkaline solution at the site of ore deposition is proposed and may have produced these features (Chapters 6 and 7). Fontebote and Amstutz (1986) proposed that the stalactitic structures at Navan formed by diagenetic replacement of barite, however in all the samples examined in the present study the stalactitic pyrite growths are primary and no evidence was found for a replacement origin.

5.5.5d Microscopic, rhythmically banded, crustiform sphalerite and geopetal sphalerite sediments

Rhythmically banded or collomorphic sphalerite (Plates 5.36a-c) occurs as coatings on the dendritic and skeletal galena, on the stalactitic growths, and on clasts within the sulphide. The sphalerite consists of microscopic bands of varying colour from shades of pale orange through to darker brown-red (Plate 5.36a). The banding is botryoidal to colloform and is coated around the galena nucleus. There are two main fabrics developed: the concentric banding and an acicular growth perpendicular to the banding. Under high magnification the acicular texture protrudes through the boundaries of these bands, resulting in an imbricated, rugged contact between adjacent bands. Contacts between adjacent bands are generally diffuse under high magnification. The outline of the banded sphalerite is controlled by the shape of the galena nucleus. All these features are similar to those described by Roedder (1968) in samples from the Pine Point deposit and Zn/Pb deposits in Europe, such as Bleiberg in Austria and the Silesian deposits in Poland. Adjacent nuclei may coalesce during the precipitation of the sphalerite bands and later generations encompass both nuclei. In this way, a "grape-like" texture forms in which these structures become mutually supporting and inter-connected (Plate 5.36c). These delicate structures are always well preserved. There are distinct hiatuses in the deposition of the sphalerite as illustrated by

dissolution of early bands prior to precipitation of later bands. Between the sphalerite bands, microscopic galena crystals may occur with the overlying band, being deflected around the outward crystal face.

Finely laminated geopetal sphalerite sediment was deposited synchronously with, and can be traced into the rhythmic growths (Plates 5.37a-b). These laminations cannot be traced over distances greater than a few centimetres. Numerous small geopetal structures can be seen in individual hand specimens, deposited in small spaces that existed within the crystallizing dendritic galena. Some of the best developed geopetal textures are associated with stalactitic growths (Plate 5.34a).

In thin section the sphalerite geopetal sediment is present as a microcrystalline mud, zoned crystals with different layers having different zones, and a form of concretion, like small spherules which appear to be a transitional growth into crystals (Plates 5.37a-b and 5.38a-c). The cause for the last style of sphalerite is unclear but may be due to supersaturation and consequent high rate of precipitation being too rapid for well-formed crystal growth (Roedder, 1968). The laminations are a dark orange/brown colour both in hand specimen and thin section and display pronounced vertical variations in colour over a few mm with a general sequence of upward darkening (Plate 5.38a). Sedimentary structures, including injections and slumps are particularly well-preserved.

Late-stage geopetal sediments are often found on disrupted clasts of previously deposited dendritic galena/rhythmic banded and geopetal sulphides. Detrital quartz grains within the sphalerite sediment are only observed in one or two examples and authigenic quartz overgrowths are always developed.

The origin of the rhythmically banded texture is controversial and terms including colloform, colloidal and botryoidal have all been used to describe it. It has been recognised in many Zn-Pb deposits and for this reason has been a subject of much discussion (eg, Pine Point; Roedder, 1968). The main dispute is to whether the sphalerite is precipitated as a gel or as minute crystals, and whether the banding is primary or diffusional in origin. Roedder (1968) advocates a mechanism of continual precipitation of euhedral crystals as minute druses directly from a fluid. This occurs as the result of relatively high supersaturation which gives rise to high rates of nucleation and crystallization/growth rate (cf, galena dendrites and skeletal crystals). Roedder argues for a non-colloidal origin of deposition.

#### 5.5.5e Honeyblende sphalerite

This is a term given to coarse, well-developed, pale yellow sphalerite crystals readily visible in hand-specimen. It is nearly always the last sulphide mineral

precipitated and is accompanied by barite, dolomite and calcite (Plates 5.32 and 5.39a-b). The sphalerite is usually precipitated on top of the rhythmic sphalerite and there is often a transitional boundary between the two (Plate 5.39a). In transmitted light little internal structure is visible, but under cathodoluminescence yellow growth zones are apparent. Occasionally where the honeyblende is found in narrow, bedding-parallel veinlets, it exhibits a geopetal-type deposition (Plate 5.11b). In all sections studied it brecciates the previously precipitated sulphides which suggests that the fluids that deposited the honeyblende were forcefully injected into the previously deposited sulphides as well as filling pre-existing spaces (Plate 5.40). In one section the honeyblende appears to force open rhythmic layers of sphalerite. Precipitation must be slower in contrast to the dendritic/skeletal galena and the rhythmic banded sphalerite to allow the well-formed crystals to grow.

#### 5.5.5f Late barite and calcite

This assemblage represents the last stage infill in the bedding-parallel sulphide and blocks up all the remaining porosity in the massive sulphides, forming up to 20% of the rock in places and indicating that considerable space was retained after the main phases of mineralization (Plates 5.32 and 5.41). It is associated with the honeyblende, and comprises coarse crystals. In thin

section, large patches of barite/carbonate in optical continuity over-print and replace the sphalerite and the galena and can also occur as a "halo" around small fractures within internal sphalerite sediment (Plate 5.38a). Two or three skeletal galena growths and later rhythmic sphalerite are overgrown and replaced by calcite which is in optical continuity. The sphalerite appears to be preferentially replaced and the original banded fabric is preserved as numerous small inclusions within the calcite (Plates 5.42a-b). Within the sphalerite banding, individual bands are selectively replaced and the surrounding material untouched. In places this replacement is best developed where reentrant angles are present in the rhythmically banded sphalerite (Fig. 5.21). The barite is found as large laths, brecciating galena and rhythmic sphalerite in a similar fashion to the honeyblende. Relationships between this material and the honeyblende suggest that the barite and calcite both pre-date and post-date the honeyblende.

#### 5.5.6 Bedding-parallel and cross-cutting mineralization in the micrites

The features ascribed to open space sulphide growth are particularly well-developed in the micrites which are now studied in detail as they host much of the ore in the Navan mine. The main areas studied underground are in 1-5 Lens in Blocks 2 (181-183N, 1330 level), Block 6 (FW contour drifts, 1315 level), Block 7 (panel 7) and Block

14 (131-133W, 1230 level). 1-5 and 2-5 Lenses were also extensively examined in core.

The main features of the sulphides in the micrites are illustrated in Figs. 5.22-5.31 and Plates 5.43-5.51. There are two gross forms of mineralization: 1) bedding-parallel, 0.5-2.5m thick, high-grade horizons, and 2) more anastomosing, cross-cutting ore extending vertically over larger sections of the micrites. Both styles exhibit sharp contacts with the micritic host rock which may be either bedding-parallel, low-angle cross-cutting, and in the case of 2), frequently high-angle cross-cutting.

The mineralization within these two gross forms is essentially similar and dominated by 3 styles: laminated argillite and sphalerite, complex chaotic clasts of sulphides within an argillaceous matrix, and in-situ solution growth textures. These have been described earlier, however they exhibit features in micrites which warrant further discussion.

#### 5.5.6a Laminated sphalerite/argillite

Towards the footwall in 1-5 Lens in Blocks 14, 15, 17 and 18, bedding-parallel sulphide horizons are commonly 0.5-1.0m thick and have a dark, laminated quartz mud at the base, grading up into laminated and layered sphalerite and sphalerite clasts. These horizons occur at the contact between micrite and an overlying dolomite (Figs.

5.22-5.23; Plate 5.43) and the layered material has been deposited in open space. The base of the dolomite is commonly fractured with sphalerite locally replacing the margins of the fractures (Fig. 5.22). In places the sulphide and the dolomite break off as clasts, and fall into and deform laminated sulphide below (Fig. 5.22). The sphalerite is subsequently replaced by new generations. The basal contact between argillite and micrite is sharp, sub-rounded, and truncates stylolites where present (Fig. 5.22). Clearly open space developed below the dolomite, with some subsequent collapse of the dolomite into the accumulating sulphide below. In a few cases, thin sulphide horizons have micrite below and above, and in these examples the layered sulphide/argillite have low-angle, cross-cutting contacts with the host rock. The hanging wall is commonly brecciated (Plate 5.44).

In the more anastomosing, cross-cutting mineralization, eg Block 14, laminated sphalerite occurs in a complex network of former cavities. Some of this sulphide appears to have been deposited in sub-horizontal "tubes" in the micrite whereas other examples appear to be high-angle fractures which have subsequently been modified by dissolution. The initial space clearly existed prior to the mineralization. The layered sphalerite is often graded and fills the entire space available with no evidence for deposition on the top or sides of the cavity. This must be related to either the rate of sulphide precipitation being too rapid to allow growth on

the tops and sides of the existing space and/or the sphalerite nucleation occurred rapidly in the solution flowing through the space, with subsequent deposition out of suspension.

#### 5.5.6b Complex, chaotic clasts

This chaotic material comprises more massive, higher grade sulphides and in places this style of mineralization is gradational into the laminated argillite. This style well-developed in both the bedding-parallel and anastomosing sulphides (Figs. 5.24-5.26; Plates 5.45-5.47). Sulphide clasts are unsorted, mm-15cm in size, with no overall layering observed. The clasts are varied, consisting of disrupted layered and laminated sphalerite, galena/pyrite crystal growths, rhythmic sphalerite bands and in-situ solution growths. Clasts of unmineralized or unaltered host micrite frequently occur within the complex sulphides (Fig. 5.26; Plate 5.47). They vary in size from millimetres up to 2.0m in diameter and are always subrounded with dissolved margins. The matrix to all these clasts is a detrital quartz and feldspar mud-fine silt. In thin section, the sulphide clasts show that the mineralization was continuous, with sphalerite replacing galena and pyrite fracturing and replacing both galena and sphalerite (Plate 5.48). Small spherical growths are present with a galena core and a rim of pyrite (Fig. 5.24). The galena has replaced the host rock with preservation of the allochems and some

diagenetic cements (Plate 5.49) and has subsequently been disrupted into a series of fragments which acted as a nucleus for later pyrite overgrowths. Rhythmically banded sphalerite occurs as overgrowths on previously deposited sulphides and clasts of host rock, however it is also found as disrupted veins cutting through the accumulating clasts and mud-silt matrix (Fig. 5.27). Disrupted barite veins were formed in a similar manner.

The complex assemblage must have formed by a process of continual sulphide deposition and disruption in a dynamic environment in contrast to the quieter conditions that produced the well-layered sphalerite. The presence of a detrital mud/silt to these clasts is again interpreted as residual, insoluble material accumulated during dissolution of the micrites. However, the features in the anastomosing, cross-cutting mineralization indicate that initial spaces in this case may have been created by extension and "tearing-apart" of partially lithified micrite (Fig. 5.28a). Distortion of the laminated sphalerite by the micrite host rock shows that the micrite was still compacting during the mineralization and was not fully consolidated. Extension, resulting in a fracture network in the micrites, would allow fluids into these rocks and deposition of the sulphides could occur on the fracture surfaces (Fig. 5.28b; Plate 5.50). If there was a continual series of pulses of such extension and fracturing, collapse and disruption of the sulphides

would occur, existing fractures would be enlarged and new fractures initiated. The fracture network would also become enlarged by dissolution by the warm mineralizing fluids. In this way a complex assemblage of clasts would be generated (Fig. 5.28c).

The complex clasts are particularly well-developed in the bedding-parallel horizons where they may form up to 75% of the sulphide, however it is also within these horizons that the in-situ growth textures are best-developed.

#### 5.5.6c In-situ solution growths

These textures form a greater proportion of the massive sulphides in the micrites than elsewhere in the deposit, occurring as intersections over 1.0m thick in places, and also as disrupted clasts within the chaotic sulphides previously described. Where present as clasts, these deform argillite and sphalerite sediment, implying that they have collapsed into the sediment (Fig. 5.25). Pyrite is absent from this textural assemblage, although late fractures brecciating this mineralization commonly contain pyrite and pyrite/sphalerite geopetal sediments and associated coatings (Plate 5.51). Within an individual area, the paragenesis within the rhythmic sphalerite overgrowths can be correlated from one sample to another, indicating that within that area, the in-situ textures were deposited in one main event, ie there were existing spaces prior to that particular mineralizing

event.

Clearly the delicate nature of the textural assemblage (dendritic growths are abundant) as well as the thick accumulation suggests that there were distinct periods of "quiescence" with significant open space present during the formation of the massive sulphides.

The in-situ sulphides may have been subsequently disrupted into clasts (Fig. 5.25; Plate 5.51), although they are usually essentially undisturbed. The passive style of mineralization contrasts with the more dynamic style of the chaotic clasts.

#### 5.5.7 Interpretation

Widespread sulphide deposition in open spaces beneath the dolomites clearly indicates very major lateral flow of the ore fluids along the bases of the dolomites, presumably away from sources where vertical ascent of the ore fluids occurred. The dolomite must therefore either have acted as a physical barrier to the ascending ore fluids and/or there was some form of permeability at the contact between limestone and overlying dolomite which was exploited by the fluids, or a combination of both. The dolomite may also have acted as a chemical barrier as dolomite is more stable than calcite in weakly acidic solutions of the type involved in the transport of metals, and would therefore be less likely to dissolve. The dolomitic horizons definitely acted as a physical

barrier in places as vertical veins cutting through micrites die out on encountering a dolomitized horizon as a few small fractures in the basal 0.5m of the dolomitic lithology (Fig. 5.29). Was there an initial zone of permeability at the contact?. Clearly the sulphide textures indicate that deposition occurred in open spaces below dolomitic horizons and that precipitation and crystal growth was rapid. How did the open space develop. There are several lines of evidence showing that dissolution occurred below the dolomite:

- 1) Rounded depressions in the footwall of an ore horizon filled with insoluble, residual mud,
- 2) Accumulations of black, insoluble residual material at the contacts between micrite and sulphide (Fig. 5.25),
- 3) Layered birdseye fabrics in the FW truncated by the sulphides (Fig. 5.30).
- 4) Stylolites in the micrites truncated by the sulphides (Plate 5.45).

The question arises as to whether widespread dissolution resulted in the formation of cavities within which the sulphides were later deposited (ie, a form of karst process completely separate from the mineralizing process) or was permeability at the dolomite/calcarenite contact (initiated), exploited and enlarged during the mineralization. The presence of sphalerite layers within

the argillite in dissolutional depressions in the base of some sulphide horizons indicates that the mineralization and dissolution in these instances were synchronous. The depressions may have been initiated closer to the base of the overlying dolomite and subsequently slumped down and away from the base of the dolomite during mineralization and compaction of the stratigraphic section, creating space for further sulphide deposition. The difference in rheology between a competent dolomitic horizon and an underlying, semi-lithified calcarenite may have been sufficient to initiate this process, however it would have been propagated and enhanced by the accumulating dense sulphides (Chapter 7).

With the development of open spaces below the dolomite, some fracturing and collapse of the base of the dolomite would be expected, however the lack of major collapse structures and breccias suggests that large cavity systems were not present prior to the mineralization, and that the generation of much of the open space was approximately synchronous with the mineralization. The development of these open spaces is addressed in detail in Chapter 7.

The ore fluids obviously penetrated into and through the dolomites and accessed higher levels, as indicated by the multiple tabular ore layers. The penetration of the dolomite would have occurred during periods of extension with rupturing of the dolomite allowing the ore fluids to ascend and perpetuate sulphide deposition at higher

levels (Chapter 7).

The cross-cutting, anastomosing open space mineralization restricted to the micrites, represents a process of extension and tearing-apart of the host lithology associated with deposition and disruption of sulphides.

Apart from dolomites, two other examples of a lithological barrier-effect include an intensely stylolitized micrite near the footwall in 1-5 Lens in Block 6, and 10cm thick shales in 2-1 and 2-5 Lens. The stylolitic micrite forms the hanging wall to a continuous 1.5-2.0m massive sulphide horizon. In one sidewall small veins extend above the main sulphide horizon into the stylolitic micrite, however these die out 0.5 metres above the massive sulphides (Fig. 5.31). There is a dark 2-3 cm thick argillite at the top of the sulphide horizon and the contact between the argillite and micrite is sharp. This contact is regarded as dissolutional and the shale is the residue from dissolving the basal section of stylolite-rich micrites (Fig. 5.31). A constraint can therefore be placed on the timing of the mineralization in that it post-dated the stylolite formation. This is also indicated by stylolites that are truncated by the sulphides (Plate 5.45).

In the 2-5 Lens footwall and 2-1 Lens hanging wall mineralization, thin shale bands clearly acted as local impermeable layers through which sulphide veins were unable to pass, directly below which narrow sulphide

horizons were deposited (Plate 5.52).

## 5.6 MASSIVE, CENTRAL 2-5 LENS-STYLE MINERALIZATION

### 5.6.1 Introduction

The main areas studied were the 242S headings on 1330 and 1315 levels. The mineralization displays many features in common with the massive galena/sphalerite sulphides discussed in Section 5.4, but differs distinctly in that it exhibits little bedding-parallel layering or fabric, and is more massive and often cross-cutting and brecciated (Plate 5.53). This mineralization forms the most massive horizon in the mine, and may have grades of around 40% Zn+Pb over thicknesses of 15m. One of the most significant features is the abundance of galena, and the sulphide in 2-5 Lens shows a low Zn:Pb ratio relative to the deposit as a whole, around 3:1 (Andrew and Ashton, 1982, 1985). The mineralization occurs in calcarenites and medium to fine-grained pale buff dolomites which display several stages of dolomitization. The ore itself consists almost entirely of sphalerite and galena with marcasite developed locally close to the FW of the T Fault. Barite is found in various paragenetic stages but is usually late and is associated with calcite. The massive sulphides consist of a coarse galena which is similar to that in 2-2 Lens, but is more disrupted in this area. Individual bands of galena cannot generally be traced more than 10 cm. Although the sphalerite is fine-grained

and massive, there are also small, minor internal sediments.

Brecciation of the dolomite occurs at the contacts between sulphide and host rock, and within the massive sulphides blocks of dolomite are common.

Lower grade areas consist of cross-cutting veins of sphalerite/galena/barite of the same generations as those in massive sulphides and these interconnect the more massive mineralized areas.

#### 5.6.2 Description

The general paragenesis is as follows:

The first sulphides, predominantly sphalerite, were deposited by replacement of calcarenites at the margins of a series of interconnected fractures or veins and within the fractures themselves. Where fracturing was extensive, the host rock was essentially brecciated. Replacement occurred as a coarse, granular, amorphous textured sulphide which grades into coarse poorly-zoned bands of sphalerite in the vein itself (Plate 5.54). The bands are up to 4 mm thick and in thin section contain two widely spaced orange/yellow diffuse zones. Under cathodoluminescence, this sphalerite shows a blocky texture and the only zoning observed is a distinct purple-blue horizon which separates a dark, non-luminescent base from blue-yellow luminescent upper

horizons (Fig. 5.32). Barite laths were also deposited at this stage but unlike 2-2 Lens, did not preserve the allochems. Galena and minor pyrite deposited at this stage formed small crystals or disseminations. In section these replace the carbonate allochems, with inclusions of calcite preserved within the pyrite (Plate 5.55). The allochems, like those replaced by barite in 2-2 Lens, show some degree of open packing and cementation. A significant feature is that all the allochems in the host rock both within and surrounding the sulphides are now dolomitized, whereas the inclusions in the galena are calcite. Therefore the galena replacement occurred prior to the dolomitizing event. Sphalerite was also precipitated around pellets in the dolomitized host rock replacing the original cements (Plate 5.56).

Most of the galena was subsequently deposited on top of coarse sphalerite in the fractures (Plate 5.57). The galena is texturally similar to that seen in the bedding-parallel sulphides in that it is coarse and bladed, however the galena bands are usually sub-vertical as opposed to bedding-parallel and the complex contorted texture is absent. The galena within the massive sulphides can also be traced down into vertical veins leading up into the massive sulphide.

Sphalerite, often in the form of zoned crystals, was deposited by a complex sequence of replacement of host material, recrystallization similar to the bedding-parallel mineralization (Section 5.4), and rhythmically

banded overgrowths on the galena in the fractures. Continual brecciation and in places, fragmentation of previously deposited generations including galena resulted in a complex textural assemblage. Under cathodoluminescence, various complex generations of zoned sphalerite crystals are evident (Plates 5.58a-b and 5.59a-b). Early generations of zoned sphalerite crystals replacing host rock are cut by fractures containing later generations, and zoning within sphalerite crystals under CL is often brecciated.

In one thin section taken across a vein, small fragments of the host rock are coated by a rhythmically banded sphalerite and replacement by zoned sphalerite crystals is evident at the margins of the clast. The surrounding matrix also contains zoned sphalerite and the margins of the vein or fracture have symmetrical galena/rhythmic sphalerite growths (Plate 5.60). In most cases the galena is coated with a rhythmically banded sphalerite and the sphalerite generations are the same as those in zoned crystals. The two styles are therefore synchronous.

Well-laminated dark brown geopetal sphalerite sediments are common as a later stage of mineralization, synchronous with rhythmically banded growths (Plate 5.61). They are more evident in thin section than in underground exposures and are also disrupted and brecciated (Plate 5.62). The sphalerite is not always developed as one simple geopetal. The geopetal sphalerite sediment is often absent and rhythmic banded sphalerite

lines both sides of the fracture, especially where the fractures are sub-vertical. Where the rhythmically banded sphalerite was deposited directly on the early, coarse, poorly-zoned sphalerite there was frequently dissolution of the coarse sphalerite prior to deposition of the rhythmic banding (Plate 5.63).

Compiling observations from sections prepared from 242S pillar in 1330 and 1315 levels, and in particular one section which exhibited an apparently complete sequence of sulphide deposition from coarse sphalerite bands and galena through to rhythmic and geopetal styles, a paragenesis can be established using transmitted light and cathodoluminescence (Fig. 5.32). Zoned crystals show the same generations as the rhythmic sphalerite and were precipitated synchronously. From this, it can be seen that there is a change in the style of sphalerite deposition shortly after precipitation of the galena, and the later ZnS generations are finely banded or zoned compared to the earlier more blocky form. A general trend within the sphalerite with regards to changing chemistries is from a blue to a yellow luminescence, and this occurs in 3 or 4 cycles. The last stage sphalerite observed in any section is always yellow-zoned, and where cross-cutting relationships are found, it is always yellow cutting blue. Individual crystals show blue centres and yellow outer zones. The reason for different luminescence colours is related to the trace element chemistry of the sphalerite, however the actual elements

causing the luminescence are unknown and would require detailed probing of the sections under cathodoluminescence.

Coarse, late-stage, white dolomite and barite infilled the final porosity within the massive sulphide. Numerous small inclusions of lead/antimony sulphosalts result in a purple colouration to parts of the dolomite in hand specimen (Plates 5.64a-b). This late, coarse dolomite/barite assemblage is identical to that observed as the last stage of deposition in the other styles of mineralization.

Veins and aggregates of marcasite occur adjacent to the T Fault and generally appear to post-date the bulk of the Zn/Pb mineralization. The proximity to the fault and the late-stage nature of the marcasite is regarded as evidence for the T Fault being involved in the channelling of late Fe-rich hydrothermal fluids, possibly those fluids responsible for the Fe-rich mineralization in 2-1 Lens and the CGO at stratigraphically higher levels (Andrew and Ashton, 1982, 1985).

### 5.6.3 Interpretation

The mineralization formed by fracture-infill/brecciation and replacement of the host rock. After initial sphalerite and a main phase of galena deposition there was a complex sequence of sphalerite precipitation in the form of zoned crystals, rhythmically banded growths and

geopetal sediments, with continual brecciation and precipitation of new generations. The principal differences between this mineralization and the bedding-parallel sphalerite/galena previously described (Section 4.4) are:

- 1) Mineralization extending over vertical distances of up to 15m.
- 2) Significant vertical to sub-vertical fracturing and brecciation of the host rock.
- 3) Absence of contorted textures within the sulphides.

These differences can be explained in terms of the mineralization occurring as a more forceful process in the central 2-5 Lens area suggesting that it was more proximal to the site of ore fluid influx, whereas in the bedding-parallel mineralization the ore fluids moved laterally. Also, the lack of contorted sulphides in the massive 2-5 Lens as opposed to say 2-2 Lens style is due to the difference in rheology of the host material encountered by the ore fluids. The host rock was more lithified than say in the 2-2 Lens as indicated by the extensive fracturing, and therefore slumping of the sulphides would not be an operative process.

#### 5.6.4 Dolomitization

Dolomite is present both within the massive sulphides and

the surrounding host rock, and most of the dolomite post-dates the mineralization.

Ghost relicts of oolites and pellets are observed throughout the dolomite host rock (Plates 5.65a), with the dolomite being of varying coarseness both in hand specimen and thin section, with well-developed rhombs (up to 750  $\mu\text{m}$  in diameter). Under cathodoluminescence, there is a complicated sequence of precipitating events and growth zones. There are 5 main sequential stages of growth (Plates 5.65b and d and Plate 5.66b) and several stages can be correlated with those observed in the unmineralized host rocks in Chapter 4 and the dolomite associated with the stringer mineralization in 2-4/2-3 Lenses. The stages are:

- (a) Dark, almost non-luminescent granular growth precipitated only as replacement of both pellets or intraclasts,
- (b) A dull brown-red luminescent dolomite (possibly correlated with Stage 1) and often best developed as replacement of the outermost sections of original oolites (Plate 5.65b),
- (c) A zone of dark non-luminescent dolomite (correlated with Stage 2) precipitated as a replacement of the original cements and often after dissolution of Stage b) dolomite (Plate 5.65b),
- (d) A bright red/dark luminescent dolomite (correlated

with Stage 3) precipitated as a cement within the "casts" of original oolites and as a cement within the matrix (Plates 5.65b and d),

- (e) A medium to bright yellow-orange luminescent calcite (correlated with Stage 4) precipitated as a cement on top of Stage d) dolomite.

Stages d) and e) form cements both in the host rock and the massive sulphides, post-dating the mineralization (Plates 5.65d and 5.66b), however the relationships between Stages a), b) and c), formed by replacement, and the mineralization are ambiguous. There is evidence in places to suggest that they pre-date the mineralization in that the host rock is dominated by Stages b) and c) as a replacement with Stages d) and e) precipitated in localized areas as a late cement (Plates 5.65d and 5.66b), but within the massive sulphide there is a dominance of generations d) and e). This suggests that Stages a), b) and c) dolomitization of the host limestone had occurred prior to the mineralization and Stages d) and e) associated with and post-dating the mineralization were precipitated in secondary pore space generated by earlier Stage b) dolomitization.

The presence of calcite inclusions in pyrite and galena however, shows that some of the rock was undolomitized at the time of that mineralization. Also, Stages a), b) and c) are present within the sulphides in places. The fact

that dolomites are essentially unmineralized in the rest of the deposit implies that they were not suitable host rocks and may indicate that the host rock in the 2-5 Lens footwall was a limestone at the time of mineralization.

## 5.7 BRECCIA STYLES OF MINERALIZATION

Angular, breccia mineralization is essentially confined to the silty dolomitic lithologies and consists of angular clasts and fragments of host rock, cemented by various sulphide generations and textures. It occurs on a local scale, and is commonly developed above massive sulphide horizons (Plates 5.67-5.70). The brecciation generally occurred in-situ.

Breccia and fracture-fill sulphides occur at the base of the LDM and BDM where the mineralization occurs in narrow bedding-parallel sulphide horizons linked by vertical to sub-vertical mineralized breccia structures (Plate 5.69). Where bedding-parallel permeability existed the ore solutions moved laterally and precipitated sulphides, with upward movement of the fluids through the vertical breccias. This is a feature observed in many MVT deposits (Heyl, 1983). The mineralization in the massive sulphides, below the LDM and BDM is bedding-parallel replacement and contrasts with the breccias. A degree of bedding-parallel permeability in the LDM and BDM existed after the mineralization and numerous calcite-filled vugs with a bedding-parallel fabric are present. The calcite

is the same generation as that occurring as a last stage infill within the breccia sulphides. Sulphides occur as coatings on the clasts of host rock and also as stalactitic growths between clasts and in adjacent bedding-parallel horizons.

The origin of the fracture-fill, breccia-infill textures is thought to be in situ brecciation of the dolomite as a result of fluids forcing their way upwards through permeability at points of weakness which were exploited during extension and when the fluid pressures were high. Collapse breccias are also evident, eg 1-5 Lens Block 2, with clasts of overlying, dark BDM present in a wedge structure within the underlying pale limestones (Plate 5.70). The clasts are cemented by sulphide. It is therefore envisaged that some of the bedding-parallel space in which stalactitic growths are well-developed, formed during subsidence of underlying host rock as opposed to being forced open hydraulically. If a process of hydraulic "jacking" is the only process invoked, with high fluid pressures forcing open bedding-parallel zones of weakness and resultant deposition of sulphides, these features would be expected to close as a result of a decrease in fluid pressure and we would not expect to find such delicate stalactitic structures preserved.

#### 5.8 CROSS-CUTTING VEINS

High-angle veins occur throughout the deposit although they are probably most frequent and best-developed in the

5 Lens (Plate 5.71). The veins are NE to ENE-trending and vary in width from cm-scale up to 0.5m. The veins are dominated by two textural styles: banded, symmetrical, crustiform growths with coarse galena and occasionally marcasite overgrown by rhythmically banded sphalerite, and collomorphic sphalerite associated with skeletal and cubic galena with late stage honeyblende (in-situ solution growth textures). A large vein swarm present in 2-5 Lens with numerous high-angle veins around 0.5m wide, is dominated by the latter style of mineralization. These veins extend up into 2-4 Lens and cut the LDM (C.J. Andrew, pers comm).

In 2-5 and 3-5 Lenses, crustiform veins can be traced up into high-grade bedding-parallel sulphide horizons that formed by veining and replacement.

The high-angle veining indicates that the ore fluids ascended vertically through the Pale Beds as well as laterally below dolomites.

#### 5.9 LOW-GRADE DISSEMINATED SULPHIDES

This is only a minor constituent of the mineralization at Navan and does not form ore by itself. The only two examples examined occur in drill core and are dominated by sphalerite. In the Upper Sandstone Marker, fine disseminations of sphalerite were examined in two surface holes in the west. These consist of pale sphalerite grains enclosed within detrital quartz. Thin sections

show that the sphalerite is made up of angular crystals which appear to be detrital. In one section, disseminated ZnS occurs as a replacement of a crinoid ossicle in a sand-rich limestone, and sphalerite in this section is confined to replacement of the biodebris.

Samples of core from the microconglomerates in the 3 Lens interval in the west show sparsely disseminated sphalerite, which on thin sectioning consists of fragments of well-zoned crystals confined to intraclasts within the rock and is totally absent from the matrix (Plate 5.72). At the edges of the intraclasts the zoned crystals are broken and these features are interpreted as replacement of limestone by zoned sphalerite, followed by subsequent erosion and re-deposition of this material as mineralized intraclasts. This places constraints on the timing of mineralisation, in that some mineralization had occurred prior to the ripping up and re-deposition of the intraclasts during erosion.

## 5.10 EXAMPLES OF THE RELATIONSHIPS BETWEEN DIFFERENT STYLES OF MINERALIZATION

### 5.10.1 2-5 Lens FW mineralization

The sulphides in the 2-5 Lens footwall in the central mine area (eg, 242S) are dominated by massive, coarse galena/sphalerite (Section 5.6), with brecciation and fracturing of the host rocks (Plate 5.53). High-grade

mineralization extends continuously over a vertical distance of up to 15m. Further west (eg 2-5 Lens west, 1190 haulage) the ore is made up of a discrete horizon (1-3m thick) of massive, bedding-parallel galena and sphalerite with sharp, dissolutional contacts present between sulphide and host calcarenite with lesser micrite (Plate 5.73 and Section 5.4.4). This variation in the nature of the mineralization is thought to be a result of hydrothermal fluids forcefully ascending in the central 2 Zone area, with fracturing and brecciation of the host rock. Further to the west the mineralization formed less forcefully and bedding-parallel indicating that the ore fluids migrated towards this area (Fig. 5.33). It is worth noting that the host rock in the central 2-5 Lens footwall is often a pale dolomite and the relative timing of the earliest dolomitizing event and the mineralization are ambiguous. If the earliest dolomitization pre-dated the mineralization, then this may explain why the host rock is so fractured, as the dolomitization would probably have altered the rheology of the rock, perhaps making it more susceptible to fracturing. The vertically continuous mineralization is still consistent with hydrothermal fluids ascending in the central 2 Zone area.

#### 5.10.2 2-4/2-3 Lenses

Relationships between the bedding-parallel, massive sulphides deposited as internal sediments and the

"stringer" veinlet replacement described in Section 5.3 are clearly illustrated in headings in 1315 level, 253S access (Plate 5.10). There are 3 major sulphide horizons occurring below the SLS, LSM and a silty dolomite in 3 Lens. In the latter example, the massive sulphides are overlain by lower grade stringer sulphides present in the basal 0.5 to 1m of the dolomite above. This relationship is the result of metal-bearing fluids encountering a horizon which suffered an earlier dolomitizing event (Chapter 4). The dolomite acted as a barrier. Some solutions were able to penetrate into the base and sulphides were deposited here as sub-horizontal veinlets (Fig. 5.34). The bulk of the ore was precipitated below the dolomite as open space growth. There is also evidence for collapse of the mineralization in the overlying, silty dolomite into the space and sulphides generated below (Plate 5.74), which illustrates that the mineralizing event was an ongoing process.

### 5.10.3 2-2 Lens

In the central mine area, this lens consists of stratiform, high-grade massive sulphides (Section 5.4) which formed as bedding-parallel mineralization of oolitic limestones below the Nodular Marker. Towards the west, this style dies out and is replaced by low-grade, sphalerite replacement of allochems (Section 5.2), which is very discontinuous. This is interpreted as a peripheral replacement by Zn-rich solutions away from the

high-grade Pb+Zn mineralization (Fig. 5.35). The zinc would have been more soluble than lead in the ore fluid (Barret and Anderson, 1982) and therefore some zinc would tend remain in solution and migrate to more distal areas. This migration could occur both laterally and upwards (Fig. 5.35), and it is interesting to note that the Zn-rich allochemical replacement is best developed in 2-3, 2-2 and 2-1 Lenses, ie the stratigraphically higher mineralization.

The 2 Lens mineralization is very poorly developed in 1 Zone and consists of the allochemical replacement.

#### 5.10.4 2-1 Lens

The sulphides in 2-1 Lens West are dominated by 2 main styles: high-grade, stratiform horizons with the sulphides deposited in open spaces (Section 5.5), abundant in the footwall and middle sections of 2-1 Lens, and lower grade replacement and small bedding-parallel cavity infill (Section 5.2), dominant in the hanging-wall mineralization. The lateral relationships between the two are shown in Fig. 5.36, with the most obvious feature being the fingering out of the hanging-wall mineralization down-dip towards the west. This is due to the fact that the dolomitic lithologies dominant in the middle-basal sections of 2-1 Lens controlling the higher grade mineralization allowed the fluids to move laterally towards the west, whereas the fluids which deposited the

small, bedding-parallel cavity infill and replacement sulphides dominant in the hanging-wall had no such trap and therefore sulphides were deposited more locally (Fig. 5.36).

## 5.11 DISTRIBUTION OF ORE IN THE PALE BEDS

There are two major controls on the distribution of high-grade ore horizons in the Pale Beds: lithological and structural.

### 5.11.1 Lithological control

The presence of a silty or muddy dolomitic lithology, even if only partially dolomitized (eg, the Nodular Marker), overlying a clean limestone, whether it be an oolitic, micritic or biopellisparitic lithology, acted as a site for ore deposition producing bedding-parallel sulphide horizons with a variety of textures. This situation is found throughout the Pale Beds from 5 to 1 Lens. In parts of 5 Lens and the centre of 2 Zone, mineralization is more vertically extensive, however even in these areas however, the dolomitic lithologies are commonly less well mineralized and the limestones between the dolomites are more extensively mineralized.

The best example of the control exerted by the dolomites is found in 5 Lens where the micrite thickens substantially towards the west, and a thick dolomitic

siltstone-sandstone (6-10m) is developed about 20m above the base of the micrites (Chapter 3).

#### 5.11.2 Structural control

Accumulation of sulphides is evident adjacent to some of the main NE-SW trending faults in the mine, however, the faults themselves are unmineralized. In other areas there are linear trends of higher grade mineralization in a similar orientation or at slightly oblique angles which are non-coincident with the main faults. A general genetic connection is inferred with the trend of the faulting but not to the individual fault planes as currently exposed (Andrew and Ashton, 1985). This suggests a structural control on ore deposition along precursors of the presently observed fault systems, prior to major displacement. Three examples are presented:-

##### 5.11.2a F3 Fault between Blocks 14 and 15

This consists of a horst structure between Blocks 14 and 15 with a substantial thickening of the ore on both sides of the structure (Fig. 5.37a). In Block 14 the ore is better developed overall than in Block 15 to the north. As the F3 Fault is approached from the south, the ore thickness increases in 5 Lens and ore grade mineralization extends from the footwall right up to the LDQ (Fig. 5.37a). In Block 15 there is a dramatic accumulation adjacent to the horst, which dies out

rapidly to the north. The build-up of ore in this region coincides with the maximum throw (20m) on the F3 Fault. The F3 structure presently seen is unmineralized and displacement post-dates the mineralization.

#### 5.11.2b F2 Fault between Blocks 6 and 7

This is illustrated in Fig. 5.37b and consists of a southerly dipping fault which separates the two blocks in 1-5 Lens. Block 7 contains relatively little ore, with a good 1.52.5m thick footwall horizon developed and relatively little above. Adjacent to the fault however, there is a thickening of ore. Mineralization and ore grades are higher and better developed in Block 6, with good intersections occurring up to 15m above the main footwall horizon.

#### 5.11.2c F1 Fault in Block 2

As the F1 Fault is approached from the south there is a build-up of sulphide where the throw on the fault is at a maximum of 20 metres. The throw decreases to the SW and the mineralization is less well developed. Across the fault into the north of Block 2 the mineralization is more continuous vertically and may extend right up to the base of the LDM.

In underground drillholes logged in Blocks 18 and 19 there is a large variation in the development of the

sulphide over lateral distances in the order of 30 metres. Holes drilled this distance apart show essentially the same stratigraphy, however high-grade sulphides present in one hole are totally absent from another, which illustrates the laterally discontinuous nature of the ore in the Micrite Unit in this area. The high-grade intersections define a trend running in an ENE-WSW direction. There is no known faulting coincident with sulphide enrichment and as there is no variation in the stratigraphy, this is regarded as an early, very subtle structural control.

Countouring of the metal distribution within the deposit by Andrew and Ashton (1982,1985) has shown that localized areas of higher grade mineralization are NE to ENE-trending, particularly in 4 and 5 Lenses, with local swings in the strike to a more easterly trend (Fig. 5.38). These trends are often slightly oblique to the faults presently observed in the mine area. The sulphide veins in the deposit generally strike NE although a more easterly trend occurs in the up-dip part of the deposit. Andrew and Ashton conclude that NE fracturing and faulting was a primary control on the mineralization. The patterns of Fe-enrichment only partially follow the Zn+Pb trends and it is suggested that the factors controlling the iron distribution were possibly different to those controlling the lead and zinc. Texturally and paragenetically the pyrite is generally late stage within an individual area and a later control on its

distribution may be inferred. The presence of marcasite very close to the T Fault suggests that the Fe influx occurred when the larger movements or growth of this fault was initiated.

## 5.12 THE CONGLOMERATE GROUP ORE (CGO)

### 5.12.1 Introduction

The CGO occurs in the Boulder Conglomerate on top of the submarine erosion/slump surface and has been studied at 2 Zone Upper on 1420 level and the 3 Zone accesses on 1390 and 1405 levels (Fig. 5.1). It occurs inter-digitated with the Boulder Conglomerate and is distinctly different to the Pale Beds ore in style and metal composition. The ore has a very high iron content (up to 27%) dominated by pyrite/marcasite and high-grade Zn+Pb. It comprises < 3% of the total ore reserves (Ashton et al., 1986).

### 5.12.2 Description

There are two main styles of mineralization encountered: 1) well-laminated pyrite horizons and 2) high-grade, massive sulphides consisting of intergrowths and breccias of pyrite, sphalerite and galena.

1) Laminated pyrite is found throughout the CGO and to a lesser extent in thin laminae in the UDL, with individual

laminae traceable for distances greater than 5 or 6m (Fig. 5.39, Plates 5.75-5.76) and locally replaced by sphalerite. The pyrite laminae often exhibit soft-sediment deformation structures possibly indicating that active faulting was synchronous with the deposition of the laminae. In places the pyrite laminations are clearly deformed by clasts in the Boulder Conglomerate (Plate 5.75). The layered pyrite horizons persist into the basal 20-30m of the overlying Upper Dark Limestones where they are present as thin isolated laminae within dark calc-argillites. In polished thin section, the pyrite is dominated by framboidal growths which are locally concentrated into concretions (Plate 5.77). Euhedral, cubic pyrite forms are rarely observed and the paragenetic relationships between the framboids and cubes are unclear. It has been noted at Mt. Isa that pyrite layers consist of cubic crystals that may contain framboids at their centres and it has been proposed that the framboidal pyrite pre-dated the later cubic overgrowths (Eldridge et al., 1986). Samples from the Mt. Isa deposit bare a striking similarity to those from the Navan CGO. The pyrite in the CGO is inter-layered with dark mudstone which is packed with calcified sponge spicules. Cherty horizons present in the UDL may have derived their  $\text{SiO}_2$  from the de-silicification of the sponge spicules.

The laminated pyrite can be traced laterally and in places vertically into more massive chaotic areas of

massive pyrite-sphalerite-galena mineralization.

2) The principal feature of the high-grade mineralization is massive pyrite, sphalerite and galena occurring as complex intergrowths. Breccias occur within the massive sulphides in a variety of forms consisting of: rare, angular clasts of Pale Beds ore and Pale Beds clasts replaced at their margins by disseminated sphalerite and pyrite, transported clasts of pyrite from the CGO, presumably reworked, and in-situ breccias (Plates 5.78a-b). Within a lateral distance of 2 or 3m, all of these styles of breccia can be found and trying to interpret the relationships between each style is extremely difficult. It is evident however that the mineralization was clearly a continuous event during disruption, as clasts of pyrite/sphalerite occur in a later pyrite matrix and this has subsequently brecciated into clasts in an argillaceous matrix. Clasts of limestone and dark mud in a pyrite matrix are graded and it may be that the pyrite was precipitated in the porosity between the clasts which themselves were deposited as part of the Boulder Conglomerate debris flow (Plate 5.78b). The galena and sphalerite appear to post-date the pyrite in almost all cases, by replacement of the pyrite, deposition in fractures and infill of porosity left after the pyrite precipitation, and in one case open-space deposition in a solutional tube within pyrite in 3 Zone (J.H. Ashton, pers comm).

### 5.12.3 Interpretation

The CGO formed as the result of syn-sedimentary to diagenetic mineralization, with a general superimposition of galena/sphalerite on earlier pyrite. Sedimentary and early diagenetic pyrite layers were deposited during periods of quiescence, only to be ripped-up and incorporated into complex breccias during the periods of instability associated with the formation of the Boulder Conglomerate. The mineralization is interpreted as a result of the exhumation of the hydrothermal system that was still depositing the Fe-rich mineralization in the 2-1 Lens in the Pale Beds, due to removal of large sections in the stratigraphy by the submarine erosion/slumping (Andrew and Ashton, 1985), and indicates that the hydrothermal system was active at the time of deposition of the Boulder Conglomerate (Chapter 7). The high Fe-content of sulphide in the CGO may be related to the concentration of marcasite adjacent to the T Fault (particularly well-developed in the 2-5 Lens) indicating that the fault acted as a feeder for the Fe-rich hydrothermal fluids during deposition of the CGO.

### 5.13 CONCLUSIONS AND OBSERVATIONS

(1) There are a variety of textural styles within the massive sulphides in the Pale Beds, reflecting different processes involved in the sulphide deposition, and the

state of lithification of the host rock during mineralization. The main sulphides observed are sphalerite, galena and pyrite, with pyrite deposition generally post-dating the main sphalerite and galena event(s). The depositional processes are:-

(a) Bedding-parallel, sphalerite-rich replacement of calcarenites occurred along semi-consolidated lithologies with allochems in the host rock pseudomorphed and preserved. This replacement often occurred around narrow, bedding-parallel, permeable horizons, or open, bedding-parallel veins. Subsequent in situ disruption of the sulphides resulted from compaction and local collapse. Soft-sediment, pull-apart structures, compaction of sulphides around unreplaced clasts of host rock, and buckled, cross-cutting veins indicate that sulphide deposition occurred during the compaction of the stratigraphic section. This style of mineralization is best-developed in 3 to 1 Lenses and may indicate that the upper sections of the Pale Beds were least lithified at the time of mineralization. The dominance of sphalerite may be explained by the precipitation of the lead in the hydrothermal fluid at an earlier stage in galena/sphalerite massive sulphides, and the vertical and lateral migration of zinc-rich fluids.

(b) More massive bedding-parallel replacement and infill of small, inter-connected cavities by galena/sphalerite/barite produced high-grade sulphide horizons (eg, 2-2 Lens). Again the host rocks were semi-lithified

as evidenced by carbonate allochem dykes cutting the massive sulphides and contorted slumping of the dense sulphide into carbonate below. This slumping may have been initiated or enhanced by extensional fractures opening up in the footwall limestone.

(c) Dolomitization of silt-rich calcarenite horizons occurred prior to the ore deposition (also see Chapter 4) and the later ascending ore fluids migrated laterally along the base of these dolomites. The sulphides were deposited as a variety of open space growth forms. Evidence suggests that some degree of dissolution below the dolomitic lithologies, synchronous with the mineralization, provided at least some of the open space within which the sulphides were deposited. Sulphide precipitation and growth was rapid, and initial precipitation frequently occurred within laterally flowing ore fluids and sulphides were deposited out of suspension as sediments.

(d) Massive galena and sphalerite in central 2-5 Lens formed by brecciation and replacement of the host rock indicating that the host rocks were in a more lithified state than a) and b) above. Galena was precipitated early in this system.

Post-ore dolomite cements are evident around the massive sulphides in parts of 2-5 Lens and the same generations occur as a late-stage gangue within the sulphides; they are the same as those observed in the host rocks

elsewhere. Relationships and timing of earlier replacement dolomite in the host rocks and the mineralization however are ambiguous. The complexities of the dolomitization can only be unravelled by further detailed thin section petrography, fluid inclusion and carbon/oxygen isotopes.

(2) Ore distribution was also controlled by early structural features which were precursors to the faults now seen in the mine area (NE-SW trending). The major sulphide veins exhibit a similar trend. Virtually all the faults are unmineralized and have developed roughly coincident with the earlier, less distinct features which controlled the mineralization. In places the trend in the metal zoning plots suggests that the earlier structures were slightly oblique to the presently observed faults (Andrew and Ashton, 1985). Accumulation of sulphides occurs close to several faults in the 1-5 area. The presence of marcasite adjacent to the T Fault in 2 Zone is regarded as evidence for the initiation of this structure channelling Fe-rich fluids, probably related to the pyrite-rich mineralization in 2-1 Lens and the CGO.

3) The Conglomerate Group Ore was deposited during the formation of the Boulder Conglomerate essentially as sedimentary to early diagenetic pyrite followed and accompanied by soft-sediment disruption and brecciation. Later pyrite, sphalerite and galena mineralization

occurred as replacement of the earlier pyrite laminations and infilling interstices of complex breccias. The increased Fe at this stage may be related to the presence of marcasite adjacent to the T Fault, suggesting that the Fe content in the hydrothermal fluid increased during major extension on the T Fault.

## CHAPTER 6   SULPHUR ISOTOPES

### 6.1 INTRODUCTION

A sulphur isotope study was carried out on two hundred and fifty one samples of sulphides and sulphates selected throughout the deposit and representing the differing styles of mineralization and processes of ore deposition. The study was undertaken after detailed petrographic and paragenetic relationships had been established, to help understand the origin(s) of the sulphur and construct a model for the mineralization.

Sulphur has four stable isotopes,  $^{32}\text{S}$ ,  $^{33}\text{S}$ ,  $^{34}\text{S}$  and  $^{36}\text{S}$ , with percentage abundances 95.02, 0.75, 4.21 and 0.02 respectively. Sulphur isotope measurements are made on  $^{34}\text{S}/^{32}\text{S}$  and are expressed as per mil (‰) deviations relative to a standard; troilite from the Canyon Diablo meteorite (CDT). The sulphur isotope ratio for a given sample is defined as:

$$\delta^{34}\text{S} = \left[ \frac{R_{\text{sample}} - R_{\text{standard}}}{R_{\text{standard}}} \right] \times 1000,$$

where  $R = ^{34}\text{S}/^{32}\text{S}$ .

### 6.2 POTENTIAL SULPHUR SOURCES

Sphalerite, galena, pyrite and barite represent the

precipitation of both metals and sulphur as sulphide and sulphate. The sulphur that combines with these metals can be either transported in a hydrothermal fluid with the metals to the site of deposition, supplied to the metals at the site of deposition, or a combination of both. Sulphur transported with the metals is termed "deep-seated" or "hydrothermal" sulphur and for some Irish deposits, eg Silvermines, has been regarded as magmatic in origin (Greig et al., 1971). However, hydrothermal sulphur may also be derived by leaching and alteration of basement lithologies and/or thermal reduction of sulphate in deeply circulating ground or sea water. Sulphur supplied to the metals at the site of deposition, unless a separate sulphur-rich hydrothermal fluid is invoked, has an ultimate origin from seawater sulphate which can provide a source of reduced sulphur by:

- 1) Bacterial reduction of sulphate
- 2) Abiological reduction of sulphate by the oxidation of iron
- 3) Thermochemical reduction of sulphate using organic matter.

#### 6.2.1 Sulphur transported with the metals - Hydrothermal Sulphur

A detailed review of hydrothermal sulphur and controls on

sulphide signatures precipitated from this source is given in Ohmoto (1972) and Rye and Ohmoto (1974).

If the sulphur is transported in the hydrothermal fluid, then the isotopic signature of that sulphur and the mineral phases precipitated is controlled by both the isotopic composition of the source and the factors affecting equilibrium isotopic exchange in the fluid.

#### 6.2.1a Potential sources of hydrothermal sulphur

##### a) Lower Carboniferous Seawater

Convection of Lower Carboniferous seawater to depths as great as 15km at temperatures of  $\approx 250^{\circ}\text{C}$  has been proposed by Russell (1978). This provides the initial fluid which interacts with the Lower Palaeozoic or older lithologies below a potential deposit to produce a metal-bearing brine. This fluid would contain large quantities of seawater sulphate, which if reduced either thermochemically or abiologically to sulphide would potentially be available for combination with the metals. Bischoff, Radtke and Rosenbaur (1981) demonstrated experimentally that sulphate in seawater, on encountering Lower Palaeozoic-type greywackes and reacting with them at around  $200^{\circ}\text{C}$ , will be precipitated as anhydrite. The sulphate would therefore be lost from the hydrothermal fluid. It is possible however, that the anhydrite could be subsequently reduced abiologically or

thermochemically and incorporated into the hydrothermal fluid.

b) Magmatic Sulphur

Magmatic sulphur is unlikely to have contributed to the hydrothermal sulphur because any intrusives in the area have been dated around 400Ma and pre-date the mineralization by at least 40Ma. There is no evidence for igneous activity contemporaneous with the mineralization. Lead isotope data (Mills et al., 1987) suggest that there is no igneous component in the Pb source, implying that it is unlikely that the fluid involved any igneous or magmatic sulphur, assuming that the lead and sulphur were transported in the same fluid. It will be shown that the sulphur isotope results themselves are inconsistent with an igneous source.

c) Lower Palaeozoic rocks

Leaching of diagenetic sulphides within Lower Palaeozoic greywackes, shales and volcanics which underlie the Navan deposit could have provided a source of sulphur for the mineralization. This possibility is discussed in Sections 6.8 and 6.9.

### 6.2.1b Factors affecting isotopic equilibrium exchange in the ore fluid and minerals precipitated

The main process affecting the sulphur isotope composition of the hydrothermal solution and the mineral phases precipitated is equilibrium fractionation.

The isotopic composition of the sulphur in the solution,  $\delta^{34}\text{S}_{\text{TS}}$ , is a combination of the isotopic composition of all the aqueous sulphur species, including:  $\text{H}_2\text{S}$ ,  $\text{HS}^-$ ,  $\text{S}^{2-}$ ,  $\text{SO}_4^{2-}$ ,  $\text{HSO}_4^{2-}$ ,  $\text{KSO}_4^{2-}$ , and  $\text{NaSO}_4^{2-}$ . One of the primary controls of equilibrium fractionation between these phases is temperature and there is a constant fractionation between the different species at a given temperature (Ohmoto, 1972). For example at  $250^\circ\text{C}$ , the fractionation between  $\text{H}_2\text{S}$  and  $\text{SO}_4^{2-}$  will be  $+26.5^\circ/\text{‰}$ , whereas at  $150^\circ\text{C}$  it will be  $+39^\circ/\text{‰}$ . If the sulphides are precipitated from  $\text{H}_2\text{S}$  in the ore fluid, then the relative proportion of reduced to oxidized sulphur species will also control the isotopic composition of the  $\text{H}_2\text{S}$ , as will the pH of the ore fluid (Fig. 6.1). Thus assuming  $\delta^{34}\text{S}_{\text{TS}} = 0^\circ/\text{‰}$  at a temperature of say  $200^\circ\text{C}$ , then if  $\text{H}_2\text{S}/\text{SO}_4^{2-}$  in the hydrothermal fluid is 9/1,  $\delta^{34}\text{S}_{\text{H}_2\text{S}} = -3.2^\circ/\text{‰}$  (Fig. 6.2a). If the fluid becomes more oxidized and the ratio becomes 1/9, then  $\delta^{34}\text{S}_{\text{H}_2\text{S}} = -28.8^\circ/\text{‰}$  (Fig. 6.2a). The isotopic signature inherited by the sulphides which precipitate from the fluid under equilibrium conditions is similarly controlled by temperature, pH and  $f_{\text{O}_2}$ , as the sulphur isotopes are partitioned among the

precipitating minerals (Ohmoto, 1972). Changes or fluctuations in these parameters will result in a shift in the  $\delta^{34}\text{S}$  of the minerals precipitated. For example, at a temperature of  $250^\circ\text{C}$ ,  $\delta^{34}\text{S}_{\text{H}_2\text{S}}=0^\circ/\text{‰}$  and given that  $\text{H}_2\text{S}$  is the only sulphur species in the fluid, ie  $\delta^{34}\text{S}=0^\circ/\text{‰}$ , then sphalerite and galena precipitated would have isotopic signatures of  $-1.2$  and  $-4.1^\circ/\text{‰}$  respectively. However, if 50% of the  $\text{H}_2\text{S}$  in the fluid was oxidized to  $\text{SO}_4^{2-}$  prior to the mineral phases being precipitated, then the sphalerite and galena would inherit isotopic signatures of approximately  $-17.2$ , and  $-20.5^\circ/\text{‰}$  respectively, and any barite precipitated would have  $\delta^{34}\text{S}=+16.0^\circ/\text{‰}$  (Fig. 6.2b).

With regard to the transport of sulphur in the solution, the presence of considerable amounts of barite at Navan and in most Irish deposits, suggests that sulphate was not a major component in the hydrothermal fluid due to the difficulty of transporting barium and sulphate in the same fluid (Lydon, 1983). Therefore any hydrothermal sulphur would be in the form of sulphide in a more reducing solution. One consequence of there being little or no sulphate in the fluid is that precipitation of mineral phases from the hydrothermal fluid could not produce a spread in the data (see above). This means that all the sulphide minerals precipitated would possess a fairly constant isotopic signature which would be close to that of the initial sulphide in the hydrothermal solution.

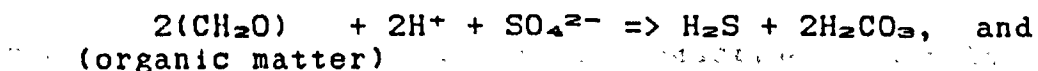
Experiments on the solubility of zinc and lead, and studies on oilfield brines, indicate that the two metals are most soluble and easily transported as chloride complexes in NaCl brines (Lydon, 1983); these were probable ore transporting fluids. However, it is not considered possible to transport enough metal and reduced sulphur in the same solution to form an economic Zn-Pb deposit under realistic conditions (Anderson, 1975, 1983), thus it is almost certain that a substantial proportion of H<sub>2</sub>S must have been supplied to the metals at the site of deposition.

#### 6.2.2 Sulphur supplied at the site of ore deposition

Unless a separate hydrothermal sulphur-rich fluid is invoked, then the ultimate source of sulphur supplied at the site of ore deposition is seawater sulphate, which can be reduced by:

##### 6.2.2a Bacteriogenic sulphate reduction

This involves the reduction of sulphate in the presence of a supply of suitable organic material, by anaerobic, dissimilatory, sulphate-reducing bacteria (Kemp and Thode, 1968; Postgate, 1984). It is a non-equilibrium reaction and can be expressed as:-



is combined with oxidation of the organic material.

Bacteriogenic reduction in the natural environment can result in extensive fractionation, with a preferential enrichment of the light isotope ( $^{32}\text{S}$ ) in the sulphide produced, due to its relatively weaker bond strength. Harrison and Thode (1957) demonstrated experimentally that  $^{32}\text{S}-\text{O}$  bonds are more easily broken than  $^{34}\text{S}-\text{O}$  bonds. Bachinski (1969) also demonstrated that bonds in sulphur-bearing minerals are more easily broken for the lighter isotope. Enrichment up to 50‰ has been observed in the Black Sea (Vinogradov et al., 1962) and the Bay of Kiel (Hartmann and Nielson, 1969), although the maximum fractionation produced in the laboratory is only 27‰ due to ideal, single-stage reduction conditions.

The fractionation resulting from bacteriogenic reduction is controlled both by the type of bacteria and by other "external" factors in the surrounding environment which affect the rate of reduction. There is an inverse correlation between the rate of reduction and the resulting fractionation (Goldhaber and Kaplan 1975). This means that slower rates of reduction result in a greater fractionation. The fractionation is therefore controlled by the:

#### Rate of sedimentation

There is a positive correlation between the rate of sedimentation and the rate of reduction (Goldhaber and

Kaplan, 1975) and therefore the fractionation. Faster rates of sedimentation can preserve any organic material before it gets oxidized and therefore influence the rate of reduction, as the bacteria will reduce at a faster rate if there is an abundance of organic material.

#### Type of bacteria

Kemp and Thode (1968) have demonstrated that different strains of bacteria can produce different fractionations. It is impossible to determine what strain of bacteria was operating and so this is of little use in our interpretation.

#### Temperature

There is a positive correlation between increased temperature and increased rates of reduction (Kaplan and Rittenberg, 1964), although this correlation is not systematic. This means that small changes in temperature, eg 10°C, can indirectly influence the  $\delta^{34}\text{S}$  of the sulphides precipitated.

#### "Open vs closed" system bacteriogenic sulphate reduction

Bacteriogenic sulphate reduction occurs both in the water column and in the sediment, as is well illustrated in the Black Sea (Janasch et al., 1972). The environment however must be anoxic. If there is a continuous supply and replenishment of the sulphate source, termed an

"open" system, then the isotopic signature of the sulphide produced by bacteriogenic reduction will remain roughly constant and will be isotopically light or negative. However, if these environments are, or become restricted with regard to the supply of sulphate, then this can result in a spread in the  $\delta^{34}\text{S}$  of the sulphide produced towards isotopically heavier or more positive values. This is because bacteriogenic reduction is removing the light isotope in the source and therefore making the source sulphate heavier (Schwartz and Burnie, 1973). This restriction is termed "closed" system reduction. Closed systems are most obvious in seafloor sediments where the sulphate supply is often limited to interstitial pore waters; for example the Bay of Kiel in the Baltic Sea (Hartmann and Nielsen, 1969). The relationship between closed system fractionation and the  $\delta^{34}\text{S}$  value of the sulphide produced is shown in Figure 6.3. Closed system fractionation is used to explain secular variations in the  $\delta^{34}\text{S}$  value of diagenetic pyrite from Ordovician to Lower Carboniferous sediments in the Selwyn Basin (Goodfellow and Jonasson, 1984), and the vertical variations in the isotopic composition of the sulphides in the stratiform, McArthur River deposit in the Northwest Territory, Australia (Williams and Rye, 1974).

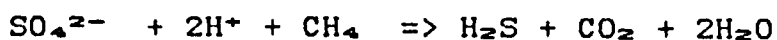
#### 6.2.2b Chemical or abiological reduction

Chemical or abiological reduction may occur when the

seawater sulphate is reduced by the ore fluid at temperatures greater than 300-350°C (Ohmoto and Lasaga, 1982; Trudinger and Chambers, 1985), with the oxidation of Fe<sup>2+</sup> to Fe<sup>3+</sup>. These temperatures are unrealistically high for those invoked in the formation of the the Irish Zn+Pb deposits (≈150-250°C: Probert, 1981; Samson and Russell, 1983, 1987). It must be pointed out that the length of time involved in such experiments does not rule out the possibility that given a longer period of time, tens or hundreds of years or more, that the reactions producing the sulphide could operate at significantly lower temperatures.

#### 6.2.2c Thermochemical reduction of sulphate by organic matter

This non-biogenic reaction has been thought to be impossible below 250-300°C (Kiyosu, 1980; Trudinger and Chambers, 1985), although Krouse et al. (1988) have demonstrated that it may occur in the natural environment at temperatures as low as 100°C, with light hydrocarbon gases as the reducing agent. Thermochemical reduction involves the reduction of sulphate in two stages, with the formation of native sulphur as a necessary intermediate step in this process. The fractionation between the initial sulphate and the sulphide produced is generally less than 7‰ (Krouse et al., 1988). The net reaction can be expressed as:



### 6.3 SEAWATER SULPHATE

The secular variation in seawater sulphate  $\delta^{34}\text{S}$  can be deduced from evaporites in the geological record (Claypool et al., 1980). This is because precipitation of sulphate minerals from seawater results in little isotopic fractionation between the sulphate mineral produced and the original seawater sulphate (Thode and Monster, 1965). A curve of the changing isotopic composition of global seawater sulphate through time has been constructed by Claypool et al. (1980) (Figure 6.4). The isotopic composition of Lower Carboniferous seawater sulphate is estimated to be around  $+19\text{‰}$ . Sulphates forming at this time will inherit such a signature, although it may be modified by features such as the removal of light sulphide in a closed system (Section 6.2.2) or oxidation of sulphides.

### 6.4 PREVIOUS WORK ON THE DEPOSIT

Boast (1978) carried out twelve sulphur isotope analyses on sphalerite, galena and barite samples from the deposit (Table 6.1). The sulphides were interpreted as incorporating bacteriogenically reduced Lower Carboniferous seawater sulphate, with the barite being precipitated directly from this sulphate. He suggested that the slightly heavier barite analyses may have been

the product of a localized closed system reduction. A detailed description of the style of mineralization sampled is not given, except for "...banded sulphide ores...", which may indicate the internal sulphide sediments (Chapter 5).

## 6.5 SUMMARY OF SULPHUR ISOTOPE RESULTS FROM NAVAN

A summary of the sulphur isotope results is presented Figure 6.5 and Tables 6.2a-f.

## 6.6 INTERPRETATION

### 6.6.1 Replacement of carbonate allochems (Figs. 6.6-6.7)

The isotopically light results (ie, enriched in  $^{32}\text{S}$ ) in the allochemical replacement mineralization are interpreted as the result of bacteriogenic reduction of sulphate with a Lower Carboniferous seawater sulphate isotopic composition ( $\approx +19\text{‰}$ ). The results fall into two tight groups,  $-23.0$  to  $-19.2\text{‰}$  and  $-16.6$  to  $-14.5\text{‰}$ . The former group of relatively lighter results is dominated by samples from 1-2 to 1-4 Lenses, whereas the latter group is made up of samples from 2-2 to 2-4 Lenses. The variation between the two areas, ie. 1 and 2 Zone, may therefore reflect local differences in the environment of bacteriogenic sulphide generation such as discussed in Section 6.2.2a. For example the values ranging from  $-23.0$  to  $-19.2\text{‰}$  could be the result of

relatively slower rates of reduction producing a greater fractionation and relatively lighter results in 1 Zone compared to 2 Zone.

The results represent a fractionation of around 35 to 45‰ which is consistent with fractionations observed at the present day (Hallberg and Bagander, 1985). The range from -23.0 to -14.5‰ implies that the reduction took place under open system conditions, as there is no major spread in the data towards isotopically heavy values close to contemporaneous seawater sulphate. The textural evidence suggests that the sediments were semi-consolidated when replaced and therefore initial bacteriogenic H<sub>2</sub>S may have been present in the pore spaces in the sediment and continually replenished, perhaps from reduction in the seawater and top few metres of the sediment column, above.

Colloform marcasite and pyrite precipitated as narrow bedding-parallel, cavity-infills associated with the sphalerite replacement in 2-1 Lens exhibit more negative values from -37.3 to -28.2‰ (Figs. 6.6-6.7). These values are also interpreted as incorporating bacteriogenic sulphide, but are substantially lighter than the bacteriogenic sulphide in the sphalerite replacement. The pyrite and marcasite appear to be paragenetically later than the sphalerite, both in hand specimen and in thin section. An explanation for similar extremely negative values has been put forward by Boyce et al. (1984) to explain similar results at Silvermines,

by a process of "fractionation loops". Essentially this involves two stages of bacteriogenic reduction of sulphate. Seawater sulphate is reduced to sulphide and then re-oxidized prior to combining with the metals. The new sulphate produced therefore inherits the isotopically light signature from the bacteriogenic sulphide as there is little if any fractionation during the oxidation. A second reduction of this sulphate gives rise to extremely negative values. The above process has been demonstrated in recent sediments (Hallberg, 1984).

However, if these extremely negative values were produced by a fractionation loop then we would expect to see a range of values from -38 down to -20‰, similar to Silvermines (A.J. Boyce, pers comm), but the results are generally concentrated around -33 to -28‰. This implies that either the entire starting sulphate was lighter or the fractionation was greater. There is no evidence for isotopically light sulphate in the deposit (ie starting sulphate would require  $\delta^{34}\text{S}$  values around +5 to +10‰), so unless none of this light sulphate was fixed then this possibility seems unlikely. The most likely interpretation is a change in the environment in which the bacteria were operating, which therefore controlled the fractionation and is discussed in Section 6.7.

### 6.6.2 Coarse galena/sphalerite (Figs. 6.8-6.10)

The following section includes the bedding-parallel mineralization (eg, 2-2 Lens) and the more massive 2-5 Lens mineralization. These sulphides have a different range of  $\delta^{34}\text{S}$  values with an abundance of significantly heavier results (Fig. 6.8 and 6.10). This is exemplified by the coarse bladed galena. With the exception of two analyses of  $-0.7$  and  $-1.1\text{‰}$ , the coarse bladed galena throughout the deposit has  $\delta^{34}\text{S}$  values greater than  $0\text{‰}$  (Fig.6.10)

A possibility for this heavy sulphide is that of thermochemical reduction of seawater sulphate by organic matter or hydrocarbons occurring in the host lithologies at the site of deposition (Section 6.8), which results in a limited fractionation between the initial sulphate and the sulphide produced (Krouse et al., 1988). Trudinger and Chambers (1985) have demonstrated experimentally that thermochemical reduction does not take place at temperatures below  $250^\circ\text{C}$  in the laboratory. However, recently Krouse et al. (1988) have demonstrated thermochemical reduction of sulphate by light hydrocarbon gases at temperatures as low as  $100^\circ\text{C}$  in the natural environment, with fractionations of up to  $7\text{‰}$ . Thermochemical reduction has been used to explain the genesis of the Pine Point deposit in the NW Territories, Canada. Here, fluid inclusion data suggests ore deposition temperatures of  $80\text{-}150^\circ\text{C}$ . (Roedder, 1968), and

importantly; the field and geochemical evidence point overwhelmingly to the thermochemical reduction of sulphate producing the sulphide. Therefore the experimental data in the laboratory may differ from the geological environment. If the process is accepted as operating at lower temperatures, then using Pine Point as an example, the isotopic composition of the sulphides (118 samples,  $\bar{x} = +20.1\text{‰}$ ,  $sd = +2.6\text{‰}$ ; Sasaki and Krouse, 1969) is essentially the same the postulated initial sulphate source (+19 to +20‰; Sasaki and Krouse, 1969). There is also an abundance of altered and unaltered organic matter at Pine Point with the sulphur isotopic composition and geochemistry of the organic material consistent with thermochemical reduction. Native sulphur is also observed which is an essential intermediate stage in the reaction (Maqueen, 1986). There is a greater spread in isotopic values in the relevant textures at Navan, only minor amounts of organic material are present and no native sulphur is observed, and therefore in-situ thermochemical reduction seems an unlikely possibility for the heavy sulphide.

An attractive alternative origin to explain the data is that the sulphides incorporated a component of hydrothermal sulphur transported with the metals which had an isotopically heavy  $\delta^{34}\text{S}$  signature. Textural studies on the ore paragenesis are essential in this interpretation, particularly since we are often looking at isotopic variations on a small scale.

A significant feature to emerge from the isotope results is the overall trend towards isotopically lighter  $\delta^{34}\text{S}$  values in subsequent paragenetic stages of sulphide deposition (Figs. 6.11(1-4) and 6.12). This is best illustrated in samples from 2-5 Lens, where a sequence of sulphide deposition is clearly established and  $\delta^{34}\text{S}$  values in many samples change from around +8 to +11‰ in the early coarse zoned sphalerite and galena, to about -3‰ and then to around -15‰ in the later rhythmic sphalerite (Fig. 6.12). This variation occurs over a distance of less than one centimetre. The later generations of rhythmic sphalerite are cogenetic with geopetal sediments which also have light values from around -16 to -11‰. One sample from 1-5 Lens shows colloform pyrite overgrowths on a coarse galena band, with the top of the galena band having  $\delta^{34}\text{S} = +11.8\text{‰}$ , and  $\delta^{34}\text{S} = -26.3\text{‰}$  in the pyrite above (Fig. 6.11(4)). In 2-2 Lens, rhythmic sphalerite is in the range +2.1 to +11.3‰ but is always isotopically lighter than the earlier galena (Fig. 6.11(2-3)). The last stage of sulphide deposition in this lens involved minor amounts of bournonite associated with late-stage calcite and barite. The one sample of bournonite analysed yielded a value of -4.2‰ and again confirms the trend towards isotopically lighter results with time.

To explain all the isotopic values by sulphide precipitation involving only  $\text{H}_2\text{S}$  in the hydrothermal fluid would require fairly major fluctuations in either

temperature, pH,  $f_{O_2}$  or a combination of these parameters (Ohmoto, 1972; Rye and Ohmoto, 1974). Alternatively, mixing of a hydrothermal component carried with the metals with  $\delta^{34}S > +14\text{‰}$ , with an isotopically light endmember,  $\delta^{34}S < -16\text{‰}$ , would explain the spread and general trends in the data, with the latter being dominant in the later stages of sulphide deposition. The most likely candidate for the isotopically light component would be bacteriogenic sulphide which has already been identified in the allochemical sphalerite replacements ( $\delta^{34}S = -23.0$  to  $-14.5\text{‰}$ ). To assess these two interpretations and to ascertain whether variations or trends existed within individual sulphide phases it was decided to look in detail at the coarse galena. Galena was chosen as it displayed a distinct range of isotopically heavy  $\delta^{34}S$  values and was coarse enough in places to obtain several samples across the bladed growths in an individual band.

An isotope traverse was conducted on a sample from 2-1 Lens across a coarse galena band in the direction of crystal growth. The band is 25mm thick and there is a distinct textural break 6mm above the base which marks a change from finer (lower band) to coarser (upper band) galena. The sample is therefore regarded as representing two phases of galena deposition. The upper, coarser galena band has rhythmically banded sphalerite overgrowths. The results obtained from the traverse is illustrated in Figure 6.13.

The hand-drilled traverse (12 samples) indicated that:

- a) The range of  $\delta^{34}\text{S}$  values across a single galena band from 2-1 Lens is almost the same as that obtained from the coarse galena throughout the entire deposit. Thus interpretation of this sample would apply to and explain the range of values observed throughout the deposit.
- b) The observed textural break in the sample corresponds to a major shift in the isotopic composition of the galena.
- c) There is an apparent trend towards isotopically lighter values towards the top of the both the lower and upper bands, relative to values towards the base of each band.
- d) There is an apparent trend in the lower 2/3 of the upper band for the  $\delta^{34}\text{S}$  values to become slightly heavier passing upwards.
- e) The trend towards isotopically lighter values in the top 5-6mm of the upper band is continued within subsequent overgrowths of rhythmically banded sphalerite with  $\delta^{34}\text{S}$  values approaching a bacteriogenic signature.

Two possibilities are considered to explain the range of values:

### 6.6.2a Precipitation from hydrothermal sulphur only

To explain the variations and trends within this individual sample by deposition involving hydrothermal sulphur only would require major fluctuations or changes in the physio-chemical conditions during ore deposition, namely pH and  $f_{O_2}$ . For example, the decrease in values from +5.5 to +0.7‰ in the lower band would involve an increase in the oxidation state of the hydrothermal fluid, i.e. a decrease in  $H_2S/SO_4^{2-}$  or an increase in the pH of the ore fluid during galena deposition (Ohmoto, 1972; Rye and Ohmoto, 1974). An increase in pH could be achieved by the hydrothermal fluids reacting with the carbonate host rocks and calcium being released into the ore solution. A decrease in the  $\delta^{34}S$  values for individual minerals with respect to time and space has been reported in the carbonate/calcsilicate-hosted Darwin Zn+Pb deposit in southern California (Rye et al., 1974). This decrease is attributed to an increase in pH due to the hydrothermal fluid reacting and equilibrating with the host rocks. However, the decrease in  $\delta^{34}S$  values observed within individual sulphide samples is around 0.5‰ (from centre to outer edge of zoned sphalerite crystals) and substantially less than observed within an individual galena sample at Navan.

The trend towards more positive  $\delta^{34}S$  values moving up through the galena in the bottom two thirds of the upper band led to the possibility of closed system equilibrium

fractionation between sulphur in the ore fluid and the galena precipitating being considered to explain all the values. If for example sulphide in the hydrothermal solution had a signature of say  $+12\text{‰}$  then galena precipitated from this fluid would preferentially be enriched in the lighter isotope relative to the sulphide in the hydrothermal fluid (Ohmoto, 1972). Assuming ore depositional temperature between 150 and 250°C, then the galena would have inherited a  $\delta^{34}\text{S}$  value approximately 4 to 5‰ less than the original  $\text{H}_2\text{S}$  in the solution, ie  $\approx +7$  to  $+8\text{‰}$  (Ohmoto, 1972). If this pulse of fluid was not replenished, then the remaining  $\text{H}_2\text{S}$  would have been slightly enriched in  $^{34}\text{S}$ , ie, operate as a closed system. The above process could continue during the deposition of the galena and so produce a trend towards heavier values with time, until the hydrothermal  $\text{H}_2\text{S}$  was exhausted or "swamped" by a new input. However, this does not explain the zig-zag effect as we move up the coarser galena band, because we would expect the values to get consistently heavier. Therefore although there is an overall simple trend towards heavier  $\delta^{34}\text{S}$  values moving up through the lower two thirds of the upper band, closed system equilibrium fractionation does not seem to explain this. The model is also likely to be more dynamic than this static closed system envisaged. The Raleigh distribution calculated for the trend is not as would be expected for this process either.

To try and explain the range of values observed within

the galena sample (and by extrapolation throughout the deposit) by precipitation involving hydrothermal  $H_2S$  only seems unacceptable. Firstly, major fluctuations in pH and/or  $f_{O_2}$  would be required, eg, to explain the trend towards decreasing  $\delta^{34}S$  values in the lower galena band and then increasing values with the onset of the upper band. Secondly, the process must take into account the decrease in values down to  $-9.3\text{‰}$  in sphalerite coating the upper band, and values around  $-16.0\text{‰}$  in other samples, which approach and are better approximated by a bacteriogenic component.

#### 6.6.2b Mixing of hydrothermal and bacteriogenically-derived sulphur

Mixing of bacteriogenic and hydrothermal  $H_2S$  is supported by the presence of late-stage barite in samples containing the isotopically heavy sulphides, with the barite isotopic composition indistinguishable from Lower Carboniferous seawater sulphate. This implies that seawater accessed into the mineralizing zones and could have provided a fluid for transporting a component of bacteriogenically-derived  $H_2S$ .

Mixing of hydrothermal and bacteriogenically-derived sulphur has been invoked to explain the isotopic composition of clasts of sulphide in the Rammelsberg deposit (Eldridge et al., 1988), the isotopic composition of sulphides in the Silvermines deposit (Coomer and

Robinson, 1976; Boyce et al., 1984) and sulphides in the Kanmantoo mine in South Australia (Seccombe et al., 1985). In these examples the isotopic composition estimated for the hydrothermal  $H_2S$  is different, for example  $\approx +3\text{‰}$  at Silvermines (Boyce et al., 1984), and  $\approx +15\text{‰}$  in the Kanmantoo mine (Seccombe et al., 1985) and essentially reflects the source of the hydrothermal sulphur.

The isotopic composition of the hydrothermal  $H_2S$  endmember would be greater than the isotopically heaviest value obtained from the sulphides (Figs. 6.8-6.9). Therefore, if we take the isotopically heaviest value in the galena throughout the deposit to represent the most "pristine" hydrothermal signature in the sulphides, then this gives a  $\delta^{34}S$  value of around  $+14\text{‰}$ . This is close to the isotopically heaviest value observed in the traverse sample. At estimated temperatures of ore deposition from the hydrothermal fluids of  $150\text{--}250^\circ\text{C}$  (Probert, 1981; Samson and Russell, 1983, 1987), this would indicate  $\delta^{34}S \approx +18$  to  $+19\text{‰}$  for  $H_2S$  in the hydrothermal fluid (Ohmoto, 1972). The bacteriogenic sulphide would have  $\delta^{34}S$  values in the range  $-23.0$  to  $-14.5\text{‰}$  (Section 6.6.1). Mixing of these two components and increasing or decreasing the relative proportions of each, ie varying the ratio of hydrothermal/bacteriogenic  $H_2S$ , would produce the variations observed both in the individual sample and throughout the deposit as a whole. If this increase or decrease was systematic, then trends

towards relatively lighter or heavier  $\delta^{34}\text{S}$  values could arise. Trends would most likely be produced if the supply of one endmember remained constant whilst the supply of the other varied. Applying this to the traversed sample would suggest that the hydrothermal sulphur was incorporated into the earliest galena deposited along with a bacteriogenic component, however the hydrothermal/bacteriogenic  $\text{H}_2\text{S}$  ratio decreased during precipitation of the lower galena band. This decrease could be the result of either the hydrothermal sulphur supply not being replenished, ie a single pulse of fluid, whilst the bacteriogenic component was continually supplied, or else the supply of bacteriogenic sulphide increased during growth of the lower band. The latter could have been caused by the onset of a period of extension affecting the carbonate lithologies, allowing increased quantities of bacteriogenic sulphide-rich fluid down into the system.

The trend towards less positive values in the lower band was arrested at a point corresponding to the textural break in the sample by an increase in the hydrothermal/bacteriogenic  $\text{H}_2\text{S}$  ratio. It is possible that the lead in a pulse of ore fluid was consumed along with a substantial amount of the hydrothermal sulphur and the textural break corresponds to a new input of hydrothermal fluid at the onset of the upper band. This is corroborated by the presence of microscopic quantities of sphalerite locally coating the top of the lower band and

possibly indicating that the lead in the initial pulse of fluid was exhausted at the end of galena deposition in the lower band, thereby allowing the zinc to be precipitated. The new pulse of hydrothermal fluid replenished the supply of hydrothermal  $H_2S$ , thus increasing the hydrothermal/bacteriogenic sulphide ratio and producing a shift in the isotopic composition of galena deposited to more positive values. If the hydrothermal fluid was continually supplied, then the isotopic composition of the galena would be dominated by relatively more positive values during crystal growth. A final input of hydrothermal  $H_2S$  can be inferred around 6mm from the top of the upper band. Subsequent galena precipitated during mixing of this pulse of hydrothermal sulphur with a continual supply of bacteriogenic sulphide and gave rise to a gradual decrease in the hydrothermal/bacteriogenic sulphur ratio, similar to the lower band. Sphalerite was deposited after precipitation of all the lead from the ore fluid and most of the hydrothermal sulphur, resulting in  $\delta^{34}S$  values ( $-9.3\text{‰}$ ) which began to approach a bacteriogenic signature.

As a result of the trends in the isotopic composition of the galena band and its clear importance in understanding the sources of sulphur and processes operative during galena deposition, a more detailed traverse over approximately the same area was conducted using a laser probe (Fig. 6.14; the traverse was conducted by Dr. Simon Kelly at SURRC). The system used

was Laser Spectrophysics 164, run in multimode producing 8 watts of power (all lines). The precision is  $\approx 0.25\text{‰}$ , however a calibration factor of  $+2.5\text{‰}$  is added to the values due to a fractionation occurring at the point of impact on the sample ( $\approx 1500^\circ\text{C}$ ). This calibration is based on multiple analysis of standards.

The three most important observations arising from the laser traverse are:

- 1) The traverse extended the sampling almost down to the base of the lower band which gives values  $\approx +12\text{‰}$ , ie similar to the most "pristine" hydrothermal sulphide. This supports the idea of hydrothermal sulphur in the fluid being incorporated and dominant in the earliest galena deposited from a pulse of hydrothermal fluid.
- 2) Clear trends towards isotopically lighter values throughout the lower band and the top of the upper band are enhanced, and other trends and variations are apparent.
- 3) There are major shifts in the isotopic composition of the galena over minute vertical distances in the band (eg,  $+3.9\text{‰}$  to  $+14.4\text{‰}$  and then back down to  $+6.5\text{‰}$  over a vertical distance of  $< 1\text{mm}$ ).

The interpretation of the isotopic variations during galena and later sphalerite precipitation remains the same, however clearly there are more complex interplays

regarding the mixing of the two sulphur sources and must reflect the source and supply of sulphur during precipitation of the metals.

In summary, the range of values observed throughout the textural assemblage characterized by coarse galena and later rhythmic and geopetal sphalerite can best be explained by mixing of an isotopically heavy hydrothermal sulphur ( $\delta^{34}\text{S}_{\text{H}_2\text{S}} \approx +18$  to  $+19\text{‰}$ ) and an isotopically light bacteriogenically-derived component ( $\delta^{34}\text{S}_{\text{H}_2\text{S}} = -23.0$  to  $-14.5\text{‰}$ ). The relative proportion of these two components governed the isotopic composition of sulphur incorporated into the galena. As a general rule, the earliest mineralization within a band of galena was dominated by hydrothermal sulphide, however the hydrothermal/bacteriogenic ratio decreased during subsequent deposition, as exemplified by the rhythmically banded sphalerite overgrowths, with bacteriogenic sulphide-rich fluids finally becoming dominant. It is interesting to note that the  $\delta^{34}\text{S}$  values in the galena are never less than  $-1.1\text{‰}$ . Simple mass balance calculations assuming  $+19\text{‰}$  and say  $-18\text{‰}$  to represent the endmembers, indicate that the minimum amount of hydrothermal  $\text{H}_2\text{S}$  present during galena growth was 40-45% of the total sulphide incorporated, and implies that hydrothermal  $\text{H}_2\text{S}$  was always available during deposition of the coarse galena.

The reasons for the relative increase/decrease of the isotopic composition in the galena and therefore the

interpreted variations in bacteriogenic/hydrothermal  $H_2S$  must be complex (as apparent from laser traverse). Incorporation of hydrothermal sulphur into the earliest stage of mineralization and the dominance of bacteriogenically-derived sulphide in the later stages would suggest that the hydrothermal component was consumed whilst the bacteriogenic sulphide was continually supplied. It is more likely that the introduction of the hydrothermal solution would occur as pulses, ascending from depths of up to 15km (Russell, 1978), whereas the bacteriogenic sulphide derived from contemporaneous Lower Carboniferous seawater sulphate would be continually available. However, it is postulated above that a component of hydrothermal  $H_2S$  was always available during deposition of the galena and may imply that the supply of bacteriogenic  $H_2S$  varied.

Finally, looking at the trace element geochemistry within the galena may shed some light on the complex trends observed within the laser traverse, in trying to recognise inputs of hydrothermal  $H_2S$ -bearing fluid. For example, it could be predicted that the Ag/Pb ratio would be relatively greater at the base of a galena band where hydrothermal sulphide is dominant, as Ag is commonly enriched in the paragenetically earliest mineralization in many deposits (Gustafson and Williams, 1981; Large, 1980, 1983). If the arresting of the trends towards isotopically lighter values in the isotopic composition of the galena were due to an input and replenishment of

the hydrothermal fluid, then an increase in the Ag/Pb ratio could be expected at the onset of the reverse back to increasing  $\delta^{34}\text{S}$  values.

The inter-lens variations of the range in the sulphur isotopic composition of the coarse galena throughout the deposit (Fig. 6.10) probably reflect the sampling, with more detailed analyses of both the lenses and individual specimens, eg the individual sample from 2-1 Lens, giving a greater spread in the data. It could be argued however, that the only two samples analysed from 2-4 Lens gave almost the same range of values as 26 samples from 2-2 Lens and therefore the tighter grouping of the values in 1-5 and 2-5 Lenses (Fig. 6.10) from 5 and 8 samples respectively does reflect the actual isotopic composition of both lenses. If this is the case, then it would appear that the ratio of hydrothermal/bacteriogenic sulphur remained higher during galena deposition in 1-5 and 2-5 Lenses than elsewhere.

### 6.6.3 Bedding-parallel massive sulphides indicative of open space deposition (Figs. 6.15-6.16).

The bedding-parallel, massive sulphide horizons deposited as a variety of open space growths exhibit a range of values from  $-32.6$  to  $+0.2\text{‰}$ . With the exception of the value  $-32.6\text{‰}$ , the more negative end of this population is similar to the  $\delta^{34}\text{S}$  values obtained from the sphalerite replacement of allochems (Figs. 6.7 and

6.16), interpreted as bacteriogenically reduced sulphide in an open system, however open system bacteriogenic reduction alone does not explain the spread in the data. The value of  $-32.6\text{‰}$  was obtained from a late-stage "stalactitic" pyrite growth, post-dating the sphalerite and galena, and is regarded as representing a different source of bacteriogenic sulphide, addressed in Section 6.6.6.

One significant feature is the general trend towards isotopically lighter values within later sulphides in the paragenetic sequence in a given sample (Fig. 6.11(5)), a feature which bears similarities to the coarse galena/sphalerite previously discussed (Section 6.6.2). There are 3 possible explanations considered to explain the range  $-24.8$  to  $+0.2\text{‰}$ :

#### 6.6.3a Closed system bacteriogenic reduction

The spread of values could be explained by a closed system reduction of sulphate, perhaps where the sulphate is trapped in the sediment, with the reduction taking place in pore spaces. However, late stage barite associated with the sulphides has a range of values from  $+17.9$  to  $+23.6\text{‰}$ , which is not consistent with closed system reduction. Also, the isotopically lighter  $\delta^{34}\text{S}$  values in the paragenetically later sulphides is the opposite of what would be expected from closed system reduction.

### 6.6.3b Precipitation from hydrothermal sulphur only

Precipitation from hydrothermally-derived sulphur is rejected because the late stage barite exhibits values that are consistent with seawater sulphate and not hydrothermal sulphur. It has already been argued that hydrothermal sulphur was involved in the precipitation of coarse galena, however  $\delta^{34}\text{S}_{\text{H}_2\text{S}} \approx +18$  to  $+19\text{‰}$  and no values remotely near this signature are observed in these open space growths.

### 6.6.3c Mixing of isotopically light bacteriogenic and heavy hydrothermal sulphur

A substantial quantity of isotopically light  $\text{H}_2\text{S}$  generated by bacteriogenic reduction ( $\delta^{34}\text{S} = -23.0$  to  $-14.5\text{‰}$ ), mixing with a far lesser amount of isotopically heavier hydrothermal component carried along with the metals ( $\delta^{34}\text{S} \approx +18$  to  $+19\text{‰}$ ), could explain the range of values and also the overall trend in lightening of the isotopic signature with time. If a substantial amount of bacteriogenically-derived sulphide was present and encountered by the hydrothermal fluid, then the limited amount of hydrothermal sulphur would literally be "swamped" by the abundant bacteriogenic component. It is also likely that any hydrothermal sulphur would be incorporated in the earlier sulphides precipitated, become exhausted during ore deposition and so the bacteriogenic component would become dominant with time.

Thus later sulphides precipitated would possess lighter  $\delta^{34}\text{S}$  signatures. The original hydrothermal sulphide signature would not be preserved as in the coarse galena-style mineralization (Section 6.6.2) because it would be by far the lesser component in the system described and ultimately swamped by bacteriogenic  $\text{H}_2\text{S}$ .

Textural evidence of dendritic galena, finely banded rhythmic sphalerite and internal sphalerite sediment within the open spaces is evidence for the rapid precipitation of the lead and zinc from supersaturated solutions (Roedder, 1968). This arose from the mixing or "quenching effect" of metals encountering a plentiful supply of bacteriogenic  $\text{H}_2\text{S}$ . Stalactitic growths in the sulphides formed by a process of "chemical garden" growth (Chapter 5, Section 5.5.5c), are also indicative of the mixing of two solutions (Russell 1988, in press), in this case metal-rich and bacteriogenic  $\text{H}_2\text{S}$ -bearing fluids. The mixing model offers the most satisfactory explanation of the trends within the sulphides and the textural features observed.

#### 6.6.4 2-5 Lens west (footwall) (Figs. 6.8-6.9)

In parts of 2-5 Lens west, the massive sulphides contain a finer layered galena, with local coarser cubic growths. These sulphides all give light results from  $-20.3$  to  $-14.9\text{‰}$  (including late-stage bournonite) and the source of sulphur is bacteriogenic. The relationships

between this and the coarser, bladed galena are looked at in Section 6.10.

#### 6.6.5 Vein sulphides (Figs. 6.8, 6.10, 6.15 and 6.17)

Cross-cutting sulphide veins in the deposit are not characterized by a distinct sulphur isotopic composition. Instead, the isotopic signature of sulphides within the veins is related to the textures displayed by the sulphides, which exhibit a similar range in values to the same textures within the massive sulphides previously discussed. For example, cockscomb vein growths of galena, and locally marcasite adjacent to the T Fault, with subsequent overgrowths of crustiform sphalerite, exhibit a range of isotopically heavy values indistinguishable from the range of results obtained from similar textures in massive sulphide horizons throughout the deposit (Fig. 6.8). The results from these veins are likewise interpreted as the dominance of a component of hydrothermal  $H_2S$  travelling with the metals and preferentially incorporated into sulphides deposited within the veins.

The large vein swarm in 2-5/2-4 Lenses characterized by dendritic and cubic galena, rhythmically banded sphalerite and late-stage honeyblende (Chapter 5, Section 5.8), and again exhibiting a similar range of values to the same textures within the massive sulphides (Fig. 6.15), is interpreted as being dominated by a component

of bacteriogenically-derived  $H_2S$ . The nature and size of this vein swarm implies a major phase of extension and fracturing associated with the formation of the veins, possibly related to the initiation of the B and T Faults (Section 5.8), ie, in the latter stages in the evolution of the deposit. Vast quantities of Lower Carboniferous seawater and entrained bacteriogenic  $H_2S$  could have permeated down these fractures, encountered ascending ore fluids, and thus precipitated sulphides as veins dominated by bacteriogenically-derived  $H_2S$ . Alternatively, such large vein systems may have initiated small convection cells which continually drew bacteriogenic sulphide into the veins.

Clearly, as with the massive sulphides previously discussed, the nature of the  $H_2S$  which combined with the metals controlled the texture of the sulphides precipitated.

#### 6.6.6 Pyrite in the Conglomerate Group Ore (Figs. 6.6 and 6.18)

Pyrite in the CGO has a range of very light  $\delta^{34}S$  values interpreted as bacteriogenically-derived  $H_2S$  and is similar to those values from parts of 2-1 Lens described in Section 6.6.1.

The pyrite in the CGO was deposited as syn-sedimentary to early diagenetic growths, often as framboids, and would therefore readily have access to bacteriogenic sulphur

produced in the seawater column. Deposition of the CGO resulted from the exhumation of the mineralizing system in the Pale Beds (Andrew and Ashton, 1985). The Fe-rich nature of the 2-1 Lens makes it likely that exhumation occurred during deposition of at least the pyrite in the Lens and thus it is acceptable to assume that the CGO and pyrite in 2-1 Lens were deposited roughly synchronously. Therefore interpretation of the  $\delta^{34}\text{S}$  values in the CGO would apply directly to 2-1 Lens.

The strongest candidate to explain the change in the isotopic composition of bacteriogenic sulphide in the CGO and 2-1 Lens is a change in the environment of bacteriogenic reduction as opposed to a lighter sulphate source than that observed throughout the Pale Beds. The age of the mineralization in the CGO is constrained by the fact that it was deposited above a pre-Arundian erosion/slump surface and was therefore considerably later than the Zn/Pb mineralization in the Pale beds (Ashton et al., 1986). The carbonate lithologies at the time of the deposition of the CGO are indicative of a shelf margin-carbonate slope depositional environment and thus by analoge with present day systems are suggestive of water depths  $>\approx 500\text{m}$  (McIlreath and Jones, 1984). This carbonate depositional environment and water depth contrasts dramatically with the shallow water (probably less than 10m in many cases), inter to sub-tidal environment during the deposition of the Pale Beds (during which time much of the Zn/Pb mineralization is

thought to have been deposited). Clearly the major difference in the carbonate environment would directly affect the rate of sedimentation, the nature of the bacteria operating and the temperatures at which the bacteriogenic reduction took place. For example, it is conceivable that the seawater temperature in the shallow marine environment could have been as much as 10-15°C warmer than say that in water depths of 500m. Kaplan and Rittenberg (1964) have demonstrated that increasing the temperature at which sulphate-reducing bacteria are operating by as little as 10°C, increases the rate of reduction. Increased rates of reduction result in relatively smaller fractionations (Goldhaber and Kaplan, 1975). Thus it may be expected that the fractionations in warmer waters would be less than in relatively colder waters and may partly explain the more negative isotopic signatures in the CGO.

The value of  $-32.6\text{‰}$  obtained from a late-stage "stalactitic" pyrite growth in 2-4 Lens (see Section 6.6.3 and Fig. 6.11) implies that some of this extremely isotopically light bacteriogenic sulphide accessed down through the Pale Beds after the Zn-Pb mineralization that formed the 5 to 2 Lenses in the Pale Beds.

#### 6.6.7 Barite (plus minor gypsum and celestite) (Figs. 6.19-6.21)

Barite samples from Navan exhibit a range of  $\delta^{34}\text{S}$  values

from +17.7 to +39.1‰ with the bulk of the data in the range +18 to +24‰. The Navan data shows a greater spread than reported from elsewhere in Ireland, eg Silvermines with a range +14.2 to +20.0‰ (Coomer and Robinson, 1976; Boyce et al., 1984) and Tynagh with a range +17.4 to +21.1‰ (Boast et al., 1981), both of which are interpreted as incorporating Lower Carboniferous seawater sulphate. The bulk of the barite at Navan is also interpreted as incorporating Lower Carboniferous seawater sulphate. The greater spread in the data at Navan is related to the carbonate depositional environment. The Pale Beds are dominated by inter to sub-tidal carbonate deposition which would present the possibility of a more restricted sulphate supply, compared to the deeper water facies and a more open-system at say Silvermines (around 250m water depth, Samson and Russell, 1988). This restricted supply of sulphate is reflected in a sample of gypsum obtained from the Quartz Marker in the Laminated Beds below the Pale Beds, which gives a value of +24.9‰. It is also interesting to note that the average isotopic composition of barite at Navan, +22.8‰, is the same as the average value of any gypsum present in the deposit (Fig. 6.19), also supporting a Lower Carboniferous seawater origin for the sulphate in the barite (however it is probably coincidence that the average values are exactly the same).

It is interesting that the isotopically heavier barite

within the massive sulphides (ie, excluding the that in late-stage veins) occurs in the stratigraphically lowest lenses, ie 1-5 and 2-5 Lenses, whereas barite in stratigraphically higher lenses, particularly 2-2 and 2-1 Lenses are characterized by isotopic signatures closer to normal Lower Carboniferous sea water, ie  $\approx +19\text{‰}$  (Fig. 6.21). Accepting that there are only two results from both 2-3 and 2-4 Lenses, the tendency of  $\delta^{34}\text{S}$  values in barite in the upper lenses towards values approaching normal Lower Carboniferous sea water may reflect a change in the carbonate depositional environment and associated sea water sulphate supply, to more open system conditions at the time of mineralization in the upper ore lenses. A more open system with regards to the sea water sulphate supply could arise from an increase in the water depth at this time. It is therefore significant that the Navan and ABC Group lithologies reflect an overall increase in water depth (Chapter 3, Fig. 3.10) from shallow water Pale Beds through to deeper water Shaley Pales, ABC and Waulsortian mudbank. The implication from this is that at least part of the mineralization in the upper ore lenses (barite is generally the last stage of mineralization (Chapter 5) could have been synchronous with an increase in the depth of sea water, possibly during the transition from deposition of the Pale Beds to the Shaley Pales and ABC and thus put a broad time constraint on this aspect of the mineralization.

The isotopically heaviest barite sample,  $\delta^{34}\text{S} = +35.0\text{‰}$ ,

and one celestite sample,  $\delta^{34}\text{S}=+39.1\text{‰}$ , occur as a coarse laths and crystals in late-stage veins in 2-3 Lens near the B Fault which cut the massive sulphides and which are quantitatively insignificant. However, these extraordinarily isotopically heavy results require some explanation.

Any explanation of these results must invoke a process of closed system bacteriogenic reduction or redox equilibrium reactions in a hydrothermal fluid. In one example from a late-stage vein in 2-3 Lens (224N on 1435 level), sphalerite coexisting with barite ( $\delta^{34}\text{S}_{\text{barite}}=+35.0\text{‰}$ ) has a value of  $-16.4\text{‰}$ . If equilibrium had been attained, then this gives a realistic depositional temperature of around  $120^\circ\text{C}$ . However, sulphate-sulphide pairs have been shown to be of limited value in determining temperatures (Ohmoto and Lasaga, 1982), but as it is the only pair available (due to sphalerite being the only sulphide present) it must be considered further. At this temperature the isotopic composition of the  $\text{H}_2\text{S}$  in the hydrothermal fluid would be approximately the same as the isotopic composition of the sphalerite (Ohmoto, 1972). Thus, assuming that little or no sulphate was present in the initial hydrothermal fluid, and from previous sections, assuming  $\delta^{34}\text{S}_{\text{H}_2\text{S}}=\delta^{34}\text{S}_{\text{Zn}}\approx+18\text{‰}$ , then to produce sulphate with an isotopic composition of  $+35.0\text{‰}$  and co-existing sphalerite of  $-16.4\text{‰}$  would require a  $\text{SO}_4^{2-}/\text{H}_2\text{S}$  ratio of  $\approx 7/3$ , i.e. the hydrothermal fluid would be relatively

oxidized. This oxidized fluid would be consistent with the abundance of barite in these late-stage veins, in places comprising 90-100% of the vein. The isotopic composition of the sphalerite co-existing with the barite is not consistent with a closed system bacteriogenic reduction assuming a fractionation of 35 to 45‰. However, it is worth considering that the veins are late-stage, and it has been proposed that the environment of bacteriogenic reduction involved in the final stages of mineralization represented by the CGO and pyrite in 2-1 Lens resulted in a greater fractionation, up to 60‰. Thus it is possible that an isotopic signature of -16.4‰ could be the result of closed system reduction and explain both the barite and the sphalerite.

A small fracture from 1-5 Lens (Block 14) containing internal sulphides and barite gives a  $\delta^{34}\text{S}$  value of +27.9‰ for the barite, precipitated after the sulphides, and values of -17.2 and -12.5‰ for the galena and sphalerite respectively. The galena pre-dates the sphalerite. This example of isotopically heavy barite may be better explained by a closed system bacteriogenic reduction. Initial fractionation from sulphate with an isotopic signature of between +18 and +25‰ produced a value of -17.2‰ in the galena and the remaining sulphate in the small fracture became heavier. Subsequent bacteriogenic reduction produced sulphide which was slightly heavier, -12.5‰, which was incorporated into the sphalerite and the sulphate again became slightly

heavier. The final batch of sulphate had an isotopic signature of  $+27.9\text{‰}$  in contrast to  $+18$  to  $+25\text{‰}$  at the start, and was incorporated into the late-stage barite.

It therefore remains uncertain as to the exact origin of the extraordinarily heavy barite. Other tests would be required to determine whether it is seawater sulphate or hydrothermal, for example oxygen isotopes on the sulphate. If the isotopically heavy sulphate was due to a closed system in a shallow water, locally inter-tidal carbonate depositional environment, then we may expect to find enrichment in the  $\delta^{18}\text{O}$  values in this sulphate relative to Lower Carboniferous sea water sulphate values because of the removal of the lighter oxygen isotope by local evaporation.

#### 6.7 THE ORIGIN OF THE BACTERIOGENIC SULPHIDE

The lack of evidence for the presence or former presence of evaporites in the stratigraphy makes it highly unlikely that bacteriogenic reduction of gypsum or anhydrite provided the quantities of sulphide involved in the formation of the orebody. Gypsum is present in the Pale Beds around 45-50 miles east of Navan at Keel and further east at Strokestown, presenting the possibility of a sulphate-rich brine derived from dissolution of these evaporites and migrating during diagenesis. This origin is regarded as unlikely due to the difficulty

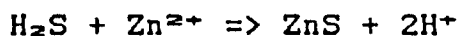
envisaged in migration of a brine across the the strike of the structural grain at that time, and the discontinuity in the stratigraphy between Navan and for example Keel. There is no obvious aquifer present. The only realistic possibility would be permeable conglomerates and sandstones in the basal Reds Beds, which are however discontinuously developed across the Central Midlands (Philcox, 1984). A Lower Carboniferous seawater source for the sulphate is therefore favoured. Accepting this origin, there are factors which must be considered when invoking bacteriogenic sulphide.

Anderson (1983) has pointed out that the amount of bacteriogenic sulphur in an economic Pb-Zn deposit is too great to have been present in a static fluid prior to the introduction of metals, and it is essential to have a continuous supply of sulphur to the metals to produce the quantities of ore observed. This means that there must be a continuous in-situ reduction of sulphate or a supply of sulphur brought to the metals. In exhalative mineralization continuous in-situ reduction can occur in a seawater brine, easily accessed by the metals. This could possibly apply to the CGO and pyrite in 2-1 Lens, however for the bulk of the Navan deposit in a sub-seafloor environment it is less likely. The textural evidence suggests that the rocks had undergone some diagenesis prior to the mineralization, including dolomitization, and it is unlikely that quantities of bacteria could operate and continually produce sulphide

in the remaining pore space. Also, in areas where the fluids were passing through at temperatures of 180 to 250°C (Probert, 1983), sulphate-reducing bacteria would be unable to survive (Postgate, 1984).

It is concluded that the bulk of the bacteriogenic sulphide must have been transported to the site of deposition at Navan and mechanisms for the derivation of the sulphide are addressed in Chapter 7.

Finally, dissolution of limestone occurred below dolomitic lithologies at Navan as a result of ore fluids passing laterally below the dolomites (Chapter 5). Anderson (1983) showed that if bacteriogenic reduction does not take place at the depositional site, then acid formed during the precipitation of sulphide by the reaction:



is not consumed by in situ reduction (Section 6.2.2a) and therefore becomes available for host rock dissolution. Precipitation of sulphides, with introduced bacteriogenic H<sub>2</sub>S, is acid-generating and explains the dissolution of the limestones at Navan.

## 6.8 THE ORIGIN OF THE HYDROTHERMAL SULPHUR (Fig. 6.22)

Clearly interpreting the isotopically heavy sulphur component ( $\delta^{34}\text{S} = +18$  to  $+19\text{‰}$ ) in the deposit as

hydrothermal in origin poses the question as to the ultimate origin of the sulphur and why it is heavier than the hydrothermal sulphur interpreted Silvermines and Keel deposits (Boyce et al., 1984; Caulfield et al., 1986; Coomer and Robinson, 1976).

The potential sources for hydrothermal sulphur were addressed in Section 6.2.1a. The lack of contemporaneous igneous activity associated with the mineralization and the variations seen in the data are not consistent with an igneous origin for the hydrothermal sulphur (Section 6.2.1a).

The similarity between the isotopic composition of the hydrothermal component and that of Lower Carboniferous sea water sulphate presents the possibility of chemical or thermochemical reduction of such sulphate to produce the sulphide. The possibility of seawater sulphate being convected and chemically reduced at temperatures of around 250°C has been ruled out on the basis of experimental evidence, although if organic molecules were transported down with the seawater sulphate, they could theoretically thermochemically reduce the sulphate at  $\approx 250^\circ\text{C}$  (M.J. Russell, pers comm). There is no way of testing this latter model.

Thermochemical reduction of Lower Carboniferous seawater sulphate below the deposit may have taken place if the organic material was present in the underlying Lower Palaeozoic rocks (Fig. 6.22).

Bischoff, Radtke and Rosenbaeur (1981) have demonstrated that sulphate carried down in the convecting seawater would be precipitated on reacting with Lower Palaeozoic shales and greywackes and therefore be lost to the hydrothermal solution. If this was the case, then with the vast quantities of seawater and sulphate involved, we might expect to see sulphate minerals in the Lower Palaeozoic stratigraphy below the deposit. There are no such occurrences recorded in the Navan region. If the sulphate was thermochemically reduced either prior to or after precipitation, this could generate substantial quantities of  $H_2S$  and explain the lack of sulphate minerals in the Lower Palaeozoic column. Organic matter in the Lower Palaeozoics would be altered by convecting fluids to produce hydrocarbons, in a similar way to the presently active convecting system of the Guaymas Basin, where metamorphism of organic material in the sediments by the action of hydrothermal fluids (around  $300^{\circ}C$ ) is generating petroleum (Simoneit, 1986). Temperatures invoked during hydrothermal convection are up to  $250^{\circ}C$  (Russell, 1983). The resultant petroleum would then react with the sulphate, generating sulphide. In oil fields, sulphate in brines pumped down into wells reacts with oil in the strata to produce thousands of ppm of  $H_2S$  at temperatures often less than  $150^{\circ}C$ , with little isotopic fractionation between the sulphate and sulphide (M.J. Russell, pers comm).

A variation on the above model is the thermochemical

reduction of Lower Carboniferous seawater sulphate contained in the Red Beds by organic gases within the hydrothermal solution (cf, Guaymas Basin), to produce isotopically heavy sulphide which was entrained in the rising hydrothermal fluid (Fig. 6.22). The fact that the Red Beds have generally not been reduced by the mineralizing fluids (except locally in close proximity to the B Fault) could be explained by the presence of a dense  $SO_4^{2-}$ -bearing brine derived from a Lower Carboniferous sabkha which drained down into and along the Red Beds and kept out the mineralizing solutions (M.J. Russell, pers comm). However, there is a general absence of evaporites or evidence for the former presence of evaporites in the Pale Beds stratigraphy around the Navan area, which is inconsistent with a sabkha environment where the precipitation of evaporites from such concentrated brines would be common. There is also an absence gypsum, anhydrite or barite in the Red Beds, sulphate minerals that would be expected to have been precipitated within the Red Beds from such a brine. Therefore thermochemical reduction of sulphate contained within a dense brine within the Red Beds and derived from a Lower Carboniferous sabkha environment seems unlikely. However, thermochemical reduction occurring in the Lower Palaeozoic pile could provide a mechanism for generating hydrothermal sulphur.

An alternative model is one whereby hydrothermal sulphur was leached from diagenetic pyrite in the underlying

Lower Palaeozoic rocks by the circulating fluids (Fig. 6.22). This model can be tested by looking at the isotopic composition of such diagenetic sulphides. If there were systematic geographical variations in the  $\delta^{34}\text{S}$  of Lower Palaeozoic diagenetic pyrite, then leaching of that pyrite would produce different hydrothermal signatures in different deposits.

### 6.9 DIAGENETIC PYRITE IN THE LOWER PALAEOZOICS

It is contended that sulphur transported in the ore fluids had  $\delta^{34}\text{S} \approx +18$  to  $+19\text{‰}$ . This implies that if the metals were leached from the Lower Palaeozoics below the deposit, then original diagenetic sulphides within these rocks would also have a correspondingly isotopically heavy signature. We would not expect to see a preponderance of isotopically light values.

Diagenetic mineralization in the Lower Palaeozoics below Navan encountered in drilling is in the form of pyrite "clots", concretions and disseminations. Textural evidence shows that the pyrite is diagenetic, as concretions which deform mud laminae around them (Fig. 6.23). The samples collected are restricted to 3 holes (N168, N837 and U80) and from depths of up to 200m below the base of the Lower Carboniferous sequence. Ten results have been obtained and range from  $+6.0$  to  $+61.1\text{‰}$ , with the majority occurring between  $+6$  and  $+31\text{‰}$  (Figs. 6.24-6.25). The data shows that diagenetic

sulphide in the Lower Palaeozoic pile is isotopically heavy.

The pyrite is unaltered and the lack of leaching or alteration in these samples may be due to the fact that the ascending solutions were saturated with respect to sulphur on encountering this pyrite or that the fluids did not have access to this pyrite.

The range of values and especially the values of +52.7 and +61.1‰ are explained by closed system bacteriogenic reduction, producing an enrichment of  $\delta^{34}\text{S}$  in the sulphate source. Ordovician seawater sulphate had a  $\delta^{34}\text{S}$  value of around +30‰ (Claypool et al., 1980). Bacteriogenic reduction with a fractionation of 30 to 40‰ would result in initial sulphides with values -10 to 0‰. Closed system reduction would result in an increased enrichment of  $\delta^{34}\text{S}$  in the sulphate and also the sulphide produced, with the result that the sulphate could become as isotopically heavy as +60 to +70‰. If this final batch of sulphate was totally reduced and pyrite precipitated essentially instantaneously, then the resultant sulphide would inherit the same signature. An essential feature in this interpretation is that sulphide must have been precipitated during this closed system reduction. If it was not, then the  $\delta^{34}\text{S}$  in the  $\text{H}_2\text{S}$  could only reach the initial sulphate value of around +30‰ (Ohmoto and Rye, 1974). This is the only effective way of explaining the observed values in the diagenetic sulphides, and we would expect to find only minor amounts

of the very heavy sulphide as it represents the final stages of reduction.

Finally it is accepted that there are vast areas of the Lower Palaeozoic rocks in the Navan area which we know little about regarding the isotopic composition of diagenetic sulphides, for example the volcanoclastic lithologies, and this is an area for future research.

#### 6.10 MINOR ZnS, PbS AND CuFeS<sub>2</sub>-BEARING VEINLETS IN LOWER PALAEOZOIC ROCKS BELOW THE DEPOSIT

Very minor quartz/carbonate veinlets containing sulphides were encountered in Lower Palaeozoic lithologies directly below 2 Zone. They are presumably the same age as the ore stage mineralization in the overlying limestones. Results from sphalerite, galena and chalcopyrite samples are shown in Figs. 6.24-6.25, and range from +1.8 to +4.5‰. Temperatures calculated from sphalerite-galena and chalcopyrite-galena pairs, assuming isotopic equilibrium, are 359 and 210°C respectively. If we assume 210°C as a more plausible temperature (Probert, 1983), then either  $\delta^{34}\text{S}_{\text{H}_2\text{S}}$  in the hydrothermal fluid had a value around +5 to +6‰ for that sample or else bacteriogenic sulphide derived from Lower Carboniferous seawater sulphate was able to penetrate down into the Lower Palaeozoics where it mixed with the hydrothermal fluid with  $\delta^{34}\text{S}_{\text{H}_2\text{S}} \approx +18$  to +19‰.

## 6.11 LATERAL VARIATIONS IN THE SULPHUR ISOTOPIC DATA

Individual textures exhibit no systematic lateral or vertical variation in  $\delta^{34}\text{S}$  values throughout the deposit, i.e. the coarse bladed galena has similar values in all the lenses studied and the same applies to the internal sphalerite sediments for example. However, different textural styles clearly have different ranges of values and therefore the lateral variations in textural style across the deposit are also reflected in the sulphur isotopes. This is best illustrated by two examples which have been described in Sections 5.10.1 and 3 and 6.6.1, 2 and 4.

The 2-5 Lens footwall mineralization exhibits different textural styles towards the west, away from the central mine area (Fig. 6.26), with the galena deposited as fine layers and cubic growths instead of coarse, bladed crystals in the central mine area. The  $\delta^{34}\text{S}$  values in galenas are significantly different in the two areas, with isotopically heavy values +7.7 to +11.0‰ in the central 2-5 Lens footwall and lighter values, -20.3 to -19.5‰ towards the west (Fig. 6.26). These results back up the textural interpretation of solutions ascending through the central region with abundant veining and brecciation of the host rock and massive mineralization, precipitating any hydrothermal sulphur. The fluids then migrated towards the west, depleted in hydrothermal  $\text{H}_2\text{S}$  from this earlier precipitation, and

here bacteriogenic sulphur would consequently dominate.

In 2-2 Lens, the mineralization in the central mine area is dominated by bedding-parallel, coarse galena/sphalerite with an isotopically heavy, hydrothermal component (Fig. 6.27). Towards the west and in 1-2 Lens, the sulphide occurs as low-grade sphalerite replacement, with a tight grouping of light, bacteriogenic values (Fig. 6.27). This again is interpreted as the result of the solutions ascending in the central 2-2 Lens area, precipitating hydrothermal sulphur and all the lead, and the resultant Zn-rich fluids migrating laterally to encounter bacteriogenic sulphur in more distal areas.

## 6.12 COMPARISONS WITH OTHER IRISH DEPOSITS

### 6.12.1 Tynagh

Boast et al. (1981) carried out a sulphur isotope study on the four paragenetic stages of mineralization identified within Waulsortian "Reef" limestones at Tynagh. They interpreted much of the ore as having been deposited in a dilatant cavity system in the limestones (Stage 2), which has features in common with open space deposition at Navan, for example internal sphalerite sediments. The results for this mineralization show a very similar range in values to the internal sulphides at Navan,  $-26.0$  to  $-4.1\text{‰}$ , with a mean of  $-17.2\text{‰}$ , which

the authors interpreted as bacteriogenic in origin. Later mineralization (Stage 3) is dominated by tenantite and galena, and exhibits a spread of data from  $-23.0$  to  $+11.1\text{‰}$ , with a mean of  $-8.7\text{‰}$ . The relatively heavier values and the spatial relationship with the Tynagh fault led Boast et al. (1981) to conclude that there was an input of hydrothermal sulphur at this time.

There are clear similarities in the data from Navan and Tynagh, and some similarities in the style of ore emplacement. The authors noted that the Stage 2 sulphides showed evidence for a mixing of two solutions, one rich in metals and the other in  $\text{H}_2\text{S}$ . However Boast et al. (1981) interpreted all the  $\delta^{34}\text{S}$  values as bacteriogenic. The internal sulphides at Navan have a similar range in values, also with evidence for mixing and rapid precipitation, although it is considered that the spread towards values closer to  $0\text{‰}$  at Navan represents an input of hydrothermal sulphur mixing with the bacteriogenic component prior to and during sulphide deposition. The heavier signatures in the later stage of deposition at Tynagh, which attain values of up to  $+11.1\text{‰}$ , show some values consistent with interpreted hydrothermal sulphur at Navan, although at Navan the hydrothermal sulphur is incorporated into the earliest sulphides.

#### 6.12.2 Silvermines

Several studies have been carried out on the Silvermines

deposit, notably Greig et al. (1971), Coomer and Robinson (1976) and Boyce et al. (1984). Greig et al. (1971) proposed that all the  $\delta^{34}\text{S}$  values obtained from sulphides in the deposit could be explained by precipitation from hydrothermal sulphur. However, a more detailed study by Coomer and Robinson (1976) suggested that both hydrothermal and bacteriogenic sulphur were involved in the deposition of the ore body. This is supported by the work of Boyce et al. (1984). The stratiform mineralization is characterized by a large spread of light results from  $-42.5$  to  $-4.0\text{‰}$ , with most of the values in the range  $-10$  to  $-30\text{‰}$ , interpreted as bacteriogenic sulphide. This range is broadly similar to that of the sulphides at Navan interpreted as having a component of bacteriogenic sulphur. The discordant Lower G Zone and the veining in the Shallee pit hosted by ORS, exhibit a tighter group of results from  $-10.0$  to  $+12.0\text{‰}$ , however the bulk of the analyses are spread between  $-10.0$  and  $+5.0\text{‰}$ . This is interpreted as incorporating hydrothermal sulphur, in agreement with Greig et al (1971). Boyce et al. (1984) estimate the  $\delta^{34}\text{S}_{\text{HS}}$  value of sulphur in the hydrothermal solution to be  $\approx +3\text{‰}$ . This value is isotopically lighter than that proposed at Navan (cf.  $\approx +18$  to  $+19\text{‰}$ ) and is interpreted as reflecting heterogeneity in the isotopic composition of diagenetic pyrite in the Lower Palaeozoic rocks from which the hydrothermal sulphur was probably derived.

### 6.12.3 Tatestown

Caulfield et al. (1986) published data from the Tatestown prospect, 3km NW of Navan (Andrew and Poustie, 1986). The ore-stage sulphides range from -23.6 to +14.4‰, however the majority of the samples, excepting pyrite, are in the range -3.0 to +12.0‰. The pyrite analyses are generally clustered between -24.0 and -19.0‰ and are interpreted as bacteriogenic sulphur incorporated in clearly diagenetic sulphide. The range of values of galena and sphalerite is similar to Navan, i.e. hydrothermal, although the authors favour an origin of in-situ abiogenic reduction of evaporites for this heavy sulphur, while not completely discarding the possibility of a hydrothermal source. The main argument against abiogenic reduction is the lack of evidence for evaporites in the succession, and the example of replaced evaporite cited in their paper occurs in the Laminated Beds succession, is only around 10cm thick and well below the mineralization (Chapter 3). This is unlikely to have produced the quantities of sulphide involved. The similarity in values with hydrothermal sulphur at Navan suggests that the origin of this heavy sulphur is the same in both deposits.

### 6.12.4 Ballinalack

The Ballinalack deposit, hosted in Waulsortian limestones (Jones and Brand, 1986) has a range of values from -36.4

to  $0.0\text{‰}$  which Caulfield et al. (1986) interpreted as essentially bacteriogenic reduction of Lower Carboniferous seawater sulphate with the possibility of mixing with a component of hydrothermal sulphur with a value between  $-5.0$  and  $0.0\text{‰}$ . The textures in the ores are dominated by internal sphalerite sediment in stromatactis cavities, and mixing of a bacteriogenic and a hydrothermal sulphur component is consistent with the internal sulphide sediments at Navan. Caulfield et al. (1986) interpreted the origin of the bacteriogenic sulphide as being derived from pre-existing pyrite, possibly of diagenetic origin, with evidence for galena and sphalerite replacing pyrite (Jones and Brand, 1986). This seems unlikely to have been the case at Navan due to the vast quantities of sulphide with a bacteriogenic sulphur isotope signature now observed in the deposit and the primary nature of the sphalerite and galena which certainly have not replaced pyrite.

### 6.13 SUMMARY

The sulphur isotopes suggest that there were two sources of sulphur involved in the deposition of the bulk of the deposit: a bacteriogenic component ( $\delta^{34}\text{S} = -23.0$  to  $-14.5\text{‰}$ ) and a hydrothermal component ( $\delta^{34}\text{S} \approx +18$  to  $+19\text{‰}$ ). The former was the dominant sulphur source and was derived from the bacteriogenic reduction of Lower Carboniferous seawater sulphate in a shallow marine environment, which subsequently permeated through

carbonate lithologies and migrated to the site of ore deposition. The hydrothermal sulphur was probably leached from diagenetic pyrite in the Lower Palaeozoic lithologies below the deposit, however thermochemical reduction of convected Lower Carboniferous seawater sulphate to produce sulphur in the hydrothermal fluid is not ruled out.

Sulphur isotopes from coarse galena-rich sulphides show that during a pulse of hydrothermal fluid and mineralization a component of isotopically heavy hydrothermal  $H_2S$  was incorporated into the earliest galena precipitated. However, the ratio of hydrothermal/bacteriogenic sulphide generally decreased during deposition of the coarse galena band due the hydrothermal sulphur being used up and the bacteriogenic component continually supplied. In places, subsequent pulses of the hydrothermal fluid replenished the hydrothermal component. The overall result is that the later stages of mineralization are dominated by sulphide with a bacteriogenic signature.

High-grade ore horizons deposited as open space internal sulphides incorporated both hydrothermal and bacteriogenic sulphur, the latter being dominant, with sulphide textures indicative of a mixing of two fluids. The plentiful supply of bacteriogenic sulphide available during ore deposition meant that the hydrothermal  $H_2S$  component was essentially "swamped", but it was still

incorporated into the earliest phases of mineralization as evidenced by trend of isotopically lighter  $\delta^{34}\text{S}$  values with time.

Bedding-parallel replacement of carbonate allochems incorporated bacteriogenic sulphide only giving rise to a grouping of isotopically light  $\delta^{34}\text{S}$  values. This mineralization is dominated by sphalerite, and combined with the textural evidence, implies that virtually all the lead had already been precipitated elsewhere, probably having removed any component of hydrothermal sulphur.

In the latter stages in the genesis of the deposit, pyrite in the Conglomerate Group Ore was deposited approximately synchronously with Fe-rich mineralization in 2-1 Lens, both incorporating mostly bacteriogenically-derived sulphide. The change in the environment in which the bacteria were operating at this time to water depths of >500m, resulted in a greater fractionation between initial sulphate and the sulphide produced.

The sulphur isotopic composition of barite within the massive sulphides in the Pale Beds suggests that the sea water sulphate supply was partially restricted at the time of the mineralization in the basal lenses, however operated as a more open system during the mineralization in the upper lenses.

The internal sulphides at Navan exhibit a similar range of values to those described by Boast et al. (1981) as

being internal at Tynagh, and also internal sulphides in stromatactis cavities at Ballinalack. In these examples, mixing of two solutions is evident and I would suggest that the range in data within the sulphides represents a hydrothermal component carried with the metals, mixing with a more dominant bacteriogenic component at the site of deposition. The relative proportion of these two sulphur sources governed the isotopic composition of the sulphides precipitated and to a certain extent the ore textures produced.

## CHAPTER 7 CONCLUSIONS, DISCUSSION AND THE MODEL

### 7.1 CONCLUSIONS

#### 7.1.1 Host Rock Depositional Environment

The Navan deposit is largely hosted in the shallow-water Pale Beds carbonate sequence near the base of the Lower Carboniferous succession, which unconformably overlies Lower Palaeozoic, low-grade metamorphic sediments, volcanics and intrusives. The Lower Carboniferous succession begins with fluviatile Red Beds deposits, overlain by tidal-flat muds and sands representing the onset of a marine transgression. Detailed stratigraphic logging and correlation suggests that the overall depositional environment evolved from shallow, marine conditions depositing sub to inter-tidal oolites and micrites in the Pale Beds, deepening with time to deeper water, muddy, bioclastic limestones and Waulsortian mudbanks, and finally into calc-turbidites of the UDL. This sequence may be explained by the evolution of a carbonate ramp to slope depositional environment, similar to that envisaged by Gawthorpe (1986) for the Dinantian carbonates in the Bowland Basin, England.

Lateral variation in the stratigraphy shows that the primary control on the carbonate facies development had a NNW-SSE trend and can be attributed to tidal channel deposition. A thinning of the micrites, erosion of parts

of the shallow marine sequence during deposition of the Laminated Beds and Pale Beds succession, with deposition of coarse microconglomerates were consequences of these channels.

Proximity to land during carbonate deposition is implied by the presence of terrigenous silt and sand in horizons that were subsequently preferentially dolomitized. The most pronounced terrigenous incursion resulted in deposition of the LDM in the central mine area.

The NNW-SSE trend can also be traced on a more regional scale within the Laminated Beds, with the well-defined CG to CB units only being developed in trend from Carlanstown in the Kells Outlier to Clogherboy, through the Navan deposit, a distance of around 12 to 15 kilometres and again illustrating the facies control exerted by this trend. It is significant that the Tatestown/Scallanstown and Clogherboy deposits lie along the north-western and south-eastern extensions of the NNW-SSE trend defined by the facies variations in the central mine area and indicates a NNW-SSE host rock control on the localization of mineralization in the Navan area.

#### 7.1.2 Carbonate Diagenesis

Studies on the diagenesis of the host rocks in the deposit reveal that there are three main stages of

calcite cement, often ferroan, with the sequence best interpreted as marine cements precipitated within the oxidation zone through to the sulphate reduction zone in the sedimentary column. Dolomitic lithologies in the stratigraphy are of two main styles; bedding-parallel, silt-rich dolomites, usually 3-4m thick but up to 12m thick in the micrites, and more pervasive, pitted dolomites which may extend over a vertical interval of 50m or more, often confined by muddy marker horizons in the stratigraphy and occurring in the middle to upper Pale Beds. There is a complex sequence of ferroan dolomitization, with both types exhibiting early replacement and later cements. There is evidence for pre and post-ore dolomitization. The pre-ore dolomitization of bedding-parallel, silt-rich horizons was shallow burial, diagenetic in origin, whereas the pervasive dolomitization in the western mine area is thought to have been related to the mineralizing event. Later stages of dolomite in both types exhibit the same generations and are often saddle dolomites. These late saddle dolomites are found associated with many MVT deposits in carbonate rocks and are thought to form under elevated temperatures (60-150°C, Radtke and Mathis, 1980). The last stage cement is a non-ferroan calcite.

### 7.1.3 Sulphide Deposition

The sulphides in the Pale Beds formed by a variety of depositional processes involving replacement and open

space fill. This occurred during the diagenesis of the host rocks (ie, syn-diagenetically) and should not be regarded as epigenetic mineralization merely superimposed on lithified host rocks. There is no evidence for seafloor sedimentary mineralization in the Pale Beds; however the host calcarenites and micrites within which the sulphides were deposited were semi-lithified at the time of mineralization and the rheology of the host rock controlled the gross geometry and style of the mineralization to a significant extent.

Bedding-parallel replacement and infill of small, interconnected cavities ranged from low-grade replacement of allochems to high-grade coarse galena/sphalerite mineralization. The ore textures and mineral relationships indicate that frequent disruption of the sulphides occurred during compaction of the semi-consolidated host succession.

The bulk of 2-5 Lens east formed as a result of fracturing and replacement of the host rock with the formation of high-grade mineralization over considerable vertical distances. This probably represents an area where the hydrothermal fluids entered into the Pale Beds succession.

Pre-sulphide dolomitization of silt-rich horizons reduced the permeability of these lithologies and increased their competency. Massive sulphides accumulated below these dolomitized horizons with the majority of the sulphide

textures indicative of open space growth. There is strong evidence that dissolution provided at least some of this space, and that the insoluble, residual material accumulated within the sulphide horizons. Some of the sulphide was deposited as a fine-grained sphalerite sediment which was initially precipitated rapidly within the hydrothermal fluid due to fluid mixing and then settled out of suspension as the fluid moved through the space available. Other textures such as dendritic galena growths were the result of rapid in-situ crystal growth out of a super-saturated solution. The mixing of two fluids is also suggested by stalactitic growths. The mineralization was a continuous event with disruption of previously deposited sulphides as the existing spaces were continually enlarged.

High-angle, cross-cutting, anastomosing mineralization in the micrites, with the sulphides deposited as internal sediments and open space growths and continually disrupted, resulted from the rheology of the partially lithified micrite which was "torn apart" during periods of extension.

Breccia mineralization is largely confined to silty dolomitic lithologies and is the result of dolomitization which increased the competence of the rock, and allowed only minor fracturing and brecciation. Sulphides deposited along bedding-planes in the form of stalactitic growths are frequently associated with the breccia mineralization and have been interpreted as

precipitation in "jacked-joints". However, it is clear in some underground headings that a collapse origin for the space along the bedding is more likely.

The Conglomerate Group Ore contrasts with the Pale Beds ore in that sedimentary to early diagenetic pyrite formed as framboids within thin, continuous laminae and in more complex sedimentary breccias. Zinc and lead mineralization essentially post-dated the pyrite and was deposited as replacement of the laminae and massive pyrite lenses.

#### 7.1.4 Relationship between Faulting and Mineralization

An early structural control on localization of the ore had a NE to ENE trend. Several minor faults in 1 Zone with this trend, have accumulations of sulphide on the HW side, often at the area of greatest throw on the fault. The faults themselves are unmineralized and are not thought to have controlled sulphide deposition but to have developed along a precursor, possibly a zone of structural weakness with relatively minor fracturing, which influenced the location of sulphide deposition and subsequently the presently observed faults. Areas of high-grade mineralization flanked by lower grades have been logged in core, with no faulting apparent, and these too strike ENE. They represent areas where fracturing and mineralization were not superceded by larger scale faulting.

### 7.1.5 Source(s) of the Sulphur

Sulphur isotope studies reveal that there were two sources of sulphur involved in the bulk of the Pale Beds ore deposition; isotopically heavy sulphur ( $\delta^{34}\text{S} \approx +18$  to  $+19\text{‰}$ ) transported with the metals in the hydrothermal solution and derived from leaching of diagenetic pyrite in the Lower Palaeozoic basement lithologies below the deposit, and secondly a more abundant isotopically light sulphur ( $\delta^{34}\text{S} = -23.0$  to  $-14.5\text{‰}$ ) derived from the bacteriogenic reduction of contemporaneous Lower Carboniferous seawater sulphate and supplied at the site of ore deposition. Various degrees of mixing of these two components occurred during precipitation of the metals resulting in a varying ratio of bacteriogenic/hydrothermal sulphur. Different styles of mineralization partly reflect the dominance of one component relative to the other. The most "pristine" hydrothermal signatures occur in the earliest sulphides deposited (galena-dominated). However the hydrothermal component was often "swamped" when the ore fluids encountered a plentiful supply of bacteriogenically-derived sulphide.

As a result of a major change in the environment in which the bacteria were operating at the time of deposition of the CGO and contemporaneous pyrite in 2-1 Lens, the bacteriogenic fractionation was greater and sulphur incorporated into this pyrite had extremely negative values ( $\delta^{34}\text{S} = -37.3$  to  $-28.2\text{‰}$ ).

Barite has a range of isotopic values reflecting a Lower Carboniferous, shallow marine, inter to sub-tidal seawater source for the sulphate.

## 7.2 EVIDENCE FOR THE TIMING OF SULPHIDE EMLACEMENT

The mineralizing event in the Pale Beds was clearly occurring during deposition of the pre-Arundian Boulder Conglomerate as evidenced by the syn-sedimentary/diagenetic pyrite layers and breccias in the Boulder Conglomerate, and probably continued in its waning stage into the basal Upper Dark Limestones (Arundian) as evidenced by the presence of sedimentary pyrite laminae (Ashton et al., 1986) and a Mn/Zn/As enrichment (Finlay et al., 1984). However, Ashton et al. (1986) put forward several lines of evidence to suggest that the bulk of the Pale Beds ore formed prior to the deposition of the Boulder Conglomerate. These include:

- a) The Fe-rich nature of the CGO and the 2-1 Lens suggests that the exhumation of the Pale Beds mineralizing event occurred during the deposition of the stratigraphically highest ore and post-dated the formation of the basal lenses. Related to the late Fe-rich mineralization is marcasite cross-cutting Zn+Pb sulphides adjacent to the T Fault.
- b) The presence of clasts of mineralized Pale Beds in the BC.

- c) The presence of soft-sediment deformation fabrics in layered sphalerite in the Pale Beds.
- d) Displacement of the Pale Beds ore by the essentially pre-erosion B and T Faults.

Other lines of evidence relating to the timing of sulphide emplacement are:

- 1) The preferential development of sulphides formed by replacement of semi-lithified sediment in the upper lenses is consistent with the ore fluids entering a host succession that was still undergoing lithification and compaction (ie, during diagenesis).
- 2) Buckled or squashed, cross-cutting sulphide veins indicate that the sediment was still compacting after the mineralization.
- 3) Carbonate dykes containing allochems and cross-cutting the mineralization indicate that the host limestones were not fully lithified.
- 4) The isotopic composition of barite in the Pale Beds ore suggests a shallow marine, possibly partially restricted source for the seawater sulphate during the mineralization. This is more consistent with the environment of deposition of the Pale Beds than the deeper water open system conditions inferred during deposition of the Chadian-Arundian carbonates, and the CGO.

- 5) The presence of low-grade mineralization in the Shaly Pales on the hanging wall side of the T Fault adjacent to the 2-5 Lens mineralization possibly indicates that some mineralization occurred after displacement along the fault.
- 6) The presence of high-grade sulphides in a large late-stage vein swarm in central 2-5 Lens regarded as forming during the main phase of extension, ie probably synchronous with initiation of the B and T Faults.
- 7) The presence of mineralized intraclasts in the 3 Lens microconglomerates indicates that some mineralization had occurred just prior to the deposition of that section of the Pale Beds. However, the general absence of sulphide clasts in the microconglomerates would suggest that the mineralization was very limited or else the intraclasts were derived from the periphery of the main mineralization.

Ashton et al. (1986) concluded that the mineralization "...could not have formed below sediment depths greater than around 700m, and a significant proportion of this is thought to have formed at substantially shallower depths...". The earliest constraint that can be put on the timing and depth of mineralization is the fact that the host rocks were semi-lithified in many places and that sulphate in the barite was derived from seawater during deposition of at least part of the Pale Beds

sequence. Andrew and Ashton (1982,1985) and Ashton et al. (1986) proposed that some of the mineralization in the Pale Beds occurred contemporaneously with sedimentation, however there is no evidence from the present study to support this. The most important implication arising from the timing of mineralization is that ore deposition in the Pale Beds was syn-diagenetic.

### 7.3 ORIGIN OF THE METALS

Two main genetic models have been advocated for the origin of the metal-bearing fluids in the Irish Zn+Pb deposits: hydrothermal convection (Russell, 1978,1983 and 1986; Russell et al., 1981; Boyce et al., 1983; Samson and Russell, 1983,1987; Hills et al., 1987) and variants of basinal brine expulsion (Badham 1981; Brown and Williams 1985; Williams and Brown, 1986; Lydon, 1986). A third mechanism (a variant of brine expulsion) involving seismic pumping of formation waters (Sibson et al., 1975) has been suggested by Boast et al. (1981) and Le Hurray et al. (1987). Of these mechanisms, hydrothermal convection of Lower Carboniferous sea water through Lower Palaeozoic lithologies below a deposit appears to be the most plausible for the following reasons:

Lead isotope compositions suggest that the lead in the Irish Lower Carboniferous deposits was derived from underlying Lower Palaeozoic and Pre-Cambrian basement lithologies (Boast et al., 1981; Le Hurray et al., 1986;

Mills et al., 1987), with localized derivation of the lead (Caulfield et al., 1986; Le Hurray et al., 1987). Within the Navan deposit, lead mineralization evolved with a relatively less radiogenic component becoming evident with time, consistent with the orebody having formed from a hydrothermal convection cell which enlarged and leached metals from progressively deeper parts of the continental crust (Mills et al., 1987).

Fluid inclusion and stable isotope compositions from the Silvermines deposit (Samson and Russell, 1983, 1987) are best interpreted in terms of Carboniferous sea water which travelled through and equilibrated with Lower Palaeozoic sediments and associated granites below the deposit.

The above features combined with the small size of the Lower Carboniferous shale and sandstone-filled basins (ie, source areas for the first model) and the thickness of the sediment infill needed to achieve the temperatures recorded in fluid inclusions (up to 250°C), rules out basin brine expulsion as a realistic model (Samson and Russell, 1983, 1987). The only basin that could have provided the required thickness of sediment would be the South Munster Basin, with up to 6km of sediment, however it is unlikely that expelled fluids emanating from this source could have travelled 100-200km across the structural grain of the basement (Lydon, 1986).

The seismic pumping model is difficult to assess, however

Samson and Russell (1987) suggest that more fluid would be required to form the Irish deposits than the amount of formation water that would be available in the Lower Palaeozoic succession.

#### 7.4 DISCUSSION

##### 7.4.1 The significance of early dolomitization at Navan, and comparisons with dolomitization in other Irish deposits

The early dolomitizing event prior to and controlling the ore distribution explains why the ore is approximately stratiform. The dolomitized lithologies have a higher detrital silt content than the surrounding limestones, and this may have been responsible for creating/increasing the permeability of these rocks and enabling flow of the dolomitizing fluids. The dolomitization eventually decreased the permeability of these horizons. The presence of post-mineralization dolomite shows that some permeability was retained, and these later generations are best-developed in localized pockets formed as a result of the volume reduction after dolomitization and a probable increase in porosity.

Dolomitization is evident in most of the carbonate-hosted Zn+Pb deposits in Ireland, however relationships between dolomite formation and ore deposition are varied. It is important to understand that dolomitization occurred in

stages in deposits such as Navan (this thesis), Silvermines (Andrew, 1986b) and Tynagh (Boast et al., 1981), and the formation of pre-ore dolomite may have been important in ore genesis. There is clear evidence for both pre and post-ore dolomitization at Navan, with early replacement and later cements. The later generations are more ferroan. At Silvermines, the stratigraphically lowest mineralization in the Lower Carboniferous limestones is epigenetic (Taylor and Andrew, 1978; Andrew, 1986b) and is hosted by a dolomitized oolitic grainstone (the Lower Dolomite). The dolomitization of the limestone is regarded as pre-mineralization (Andrew, 1986b). The dolomitizing event(s) is thought to have generated the permeability and space in which the sulphides were then deposited as epigenetic mineralization (Andrew, 1986b). A comparison may be made between the dolomite-hosted mineralization at Silvermines and the 2-5 Lens dolomite-hosted ore at Navan. In both cases, the original host rock was an oolitic grainstone, the mineralization is the stratigraphically lowest in the carbonate sequence and the host rock was extensively fractured. At Navan however, there are clearly post-ore dolomite cements within both the host rocks and the massive sulphides.

At Tynagh, pre-ore, ore-stage and post-ore dolomites are evident (Boast et al., 1981; Clifford et al., 1986). The last stage in the paragenesis of the deposit consists of coarse, vuggy dolomite, with calcite and chalcopyrite

associated, with saddle-type dolomite crystals evident.

At Tatestown the mineralization is essentially confined to a horizon in the micrites, directly below a dolomitized limestone (Andrew and Poustie, 1986). Mineralization is absent in the dolomite. Detailed studies using staining techniques have shown that there are both pre and post-ore dolomitizing events, again with the later dolomites often coarse, saddle-type, and being more ferroan than the pre-ore dolomite (Andrew and Ashton, 1985; Andrew and Poustie, 1986). The early dolomitization is regarded as resulting from alteration by pore waters of marine and freshwater origin, with the late dolomites derived from the hydrothermal fluids. Andrew and Poustie (1986) suggest that the reasons for ore localization between the dolomite and underlying micrite were the contrasting physical properties of the two lithologies and the proximity to the Tatestown Fault. It is likely that the compressive and tensile strengths of the dolomites and micrites were quite different, with the micrites fracturing more easily (Andrew and Poustie, 1986).

Pre-ore dolomitization therefore generated the conditions for ore deposition in different ways. At Silvermines and possibly parts of 2-5 Lens at Navan, it provided the permeability and space for deposition of the epigenetic mineralization. For the bulk of the Navan deposit, pre-mineralization dolomitization controlled the later deposition of bedding-parallel sulphides directly below

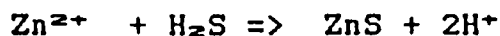
the dolomitic horizons and little or no sulphide was deposited in the dolomite itself.

#### 7.4.2 Dolomitization related to the creation of open spaces

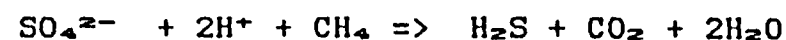
From the previous chapters it is clear that abundant bedding-parallel sulphide deposition occurred in open spaces directly below the dolomites. The evidence from sulphide-host rock relationships shows that dissolution produced at least some of that space. One obvious mechanism for the generation of this space would be karstification by meteoric waters moving below the dolomite. The karstification could occur prior to the mineralization, such as that proposed for the stratabound Zn+Pb mineralization in the Alpine Middle and Upper Triassic deposits (Klau and Mostler, 1983, 1986), Nanisivik (Olson, 1984) and Pine Point (Rhodes et al., 1984). In these examples, a palaeokarst origin involving subsurface mixing of meteoric and marine water has been proposed for the cavities, however at Nanisivik the initial karstic network may have been enlarged by the later hydrothermal fluids (Ford, 1986). The absence of internal carbonate sediments which would be expected if the karstic network was present prior to the mineralization (Klau and Mostler, 1983), of major collapse and other karst features, and the presence of sphalerite layers inter-bedded with the residual material accumulated during dissolution are inconsistent with

karstification at Navan. Also, if this process provided the open space then the space would be more likely to be generated at the contact between the top of the dolomite and overlying limestone as opposed to the base of the dolomite, as the meteoric waters passed down into the succession. The opposite is observed and implies that any dissolution involved ascending fluids.

A more plausible interpretation is that any dissolution was related to the mineralizing event, a process often misleadingly termed "hydrothermal karst", such as in the Zn+Pb deposits in the Upper Silesian District (Sass-Gustkiewicz et al., 1982; Sass-Gustkiewicz 1983). The acidic nature of probable ore transporting fluids (Anderson, 1973) would be sufficient to cause initial dissolution of the limestones. However Anderson (1983) points out that if the H<sub>2</sub>S that combines with the metals to form the ore is not produced at the site of deposition, then sulphide deposition is an acid generating process, ie



Conversely, if the H<sub>2</sub>S is generated at the site of deposition, then the acid produced by sulphide precipitation will be used up by sulphate reduction, eg



The sulphur isotope study (Chapter 6), proposed that the  $H_2S$  involved in the deposition of the internal sulphides had an essentially bacteriogenic origin and that with the quantities of sulphide now observed and the temperatures involved during the mineralization that this  $H_2S$  must have been supplied to the site of deposition. This also provides a mechanism of generating acid for the limestone dissolution.

It is envisaged that some form of initial permeability must have existed directly below the dolomitized lithologies (as well as the dolomites acting as barriers) and this was exploited and enhanced by the later ore fluids. We have seen evidence in the bedding-parallel, massive sphalerite/galena for small, inter-connected, bedding-parallel cavities which were subsequently infilled by galena. These may have been diagenetic in origin, formed directly below a partially dolomitized Nodular Marker and drastically increased the permeability of the calcarenites below the Nodular Marker. At other levels in the stratigraphy, these diagenetic spaces providing the permeability below the dolomite could have been exploited and enlarged by dissolution, creating the bedding-parallel internal sulphide horizons.

Why did the diagenetic space form directly below the dolomite? The answer lies in the competency contrast between dolomites and calcarenites/micrites in a sequence of semi-consolidated lime-rich sediments undergoing compaction. The dolomites are envisaged as forming rigid

layers within a less-lithified sequence, and would therefore act as large "crusts" below which the limestones would compact and tend to sink unevenly below the base of the dolomite (Fig. 7.1). This sinking-effect could create small cavities in the host limestones and provide the initial permeability along which the ore fluids could migrate. Subsequent deposition of dense sulphides could also enhance the sinking-effect and lead to the enlargement of existing spaces within which sulphides could continue to be deposited (Fig. 7.1).

The dolomite still provided a physical barrier to the ore fluids as evidenced by vertical veins in the micrite which die out as they pass upwards into a dolomitic horizon.

The geometry of the open space cross-cutting mineralization restricted to the thick micrites (eg, that seen in Block 14) could also be related to extension that occurred during compaction. The micrites have a low tensile/compressive strength (Tara Mines Company Reports) and these weak micrites would therefore fracture and be torn apart very easily during periods of extension. The sharp, often sub-rounded contacts between sulphide and micrite with accumulations of dark insoluble residue indicate that dissolution of the micrites did occur in the cross-cutting mineralization.

A similar style of mineralization to the cross-cutting, anastomosing ore seen in the micrite at Navan is

described from Waulsortian micrites in the Tynagh deposit by Boast (1978), where the main sulphide deposition occurred in a dilatant fracture/cavity system initiated by the forceful injection of metal-bearing brines into the Waulsortian mudbanks adjacent to the Tynagh fault.

In summary, it is envisaged that the formation of bedding-parallel open spaces was related to the presence of competent dolomitic horizons overlying calcarenites and/or micrites, and this space formed by a combination of dissolution of the limestones and the sinking of semi-lithified calcarenites away from the base of the dolomites. The latter process was enhanced by the deposition of dense sulphides in the spaces being created below the dolomites.

#### 7.4.3 The intersection of two trends at Navan

There was clearly a NE to ENE-trending structural control on the distribution of the mineralization as evidenced by the metal distribution in the deposit and the accumulation of sulphides adjacent to faults with a similar orientation. However the facies and thickness variations within the deposit indicate a NNW-trending control on the carbonate deposition (Chapter 3; Fig. 3.5). The NNW-SSE trend is not observed in the main structural features around the mine area, and indeed throughout the Central Midlands, where NE and ENE-striking structures are the norm. However, Russell (1975)

has postulated that N-S trending crustal lineaments or fractures exerted a major control on the localization of Lower Carboniferous Pb-Zn deposits and veins both in Ireland and Scotland, even though local structures within many of the deposits are NE and ENE-trending. One of Russell's proposed "geofractures" runs from south of the Navan deposit, northwards through the NNW-trending lead veins at Clontibret. This lineament also runs through the axis of the Upper Carboniferous-Triassic N-S trending Kingscourt Basin, which he regards as having developed as a consequence of the geofracture and indeed facies and thickness variations within the basin are N to NNW striking (M.J.Russell, pers comm).

#### 7.4.4 The reason for such vast quantities of ore at Navan

The amount of metal present at Navan is substantially greater than in any other known carbonate-hosted deposit Ireland. This is a consequence of:

- 1) The presence of suitable dolomitization-related barrier and traps which controlled the location of sulphide deposition: pre-mineralization, selective, bedding-parallel dolomitization created traps which subsequently prevented the ore fluids escaping and becoming dispersed. This resulted in continual lateral migration of the ore fluid enabling the sulphides to accumulate and form the

high-grade, tabular ore.

- 2) The presence of a plentiful source/supply of bacteriogenically-derived sulphur which was continually supplied to the site of ore deposition to combine with the ascending and laterally migrating metal-bearing solutions.

#### 7.4.5 Derivation of the bacteriogenic sulphur

It was concluded in Chapter 6 that the origin of the bacteriogenic sulphur was the reduction of sulphate in Lower Carboniferous seawater as opposed to sulphate in evaporites. Two plausible derivations of this bacteriogenic sulphur are:

- 1) Reduction of sulphate in the Lower Carboniferous sea and top few metres of the sediment column (eg, present day Bay of Kiel) stratigraphically above the mineralization, with subsequent downwards and lateral migration to the site of ore deposition (Fig. 7.2). It has been postulated that dolomitic horizons were essentially impermeable to the mineralizing solutions and therefore it is unlikely that seawater containing bacteriogenic sulphide could have permeated down through these dolomites, below which the sulphides were deposited. Consequently, if any seawater containing bacteriogenic sulphide did access the carbonate sequence it must have done so by passing either around the margins

of the dolomite horizons or through fault zones cutting the dolomites, and subsequently migrated laterally through more permeable limestones to the site of ore deposition.

Russell (1978, 1983 and 1986) proposed a mechanism of hydrothermal convection for the origin of the Irish Zn/Pb deposits, whereby Lower Carboniferous seawater permeated down through the Lower Palaeozoic rocks where metals were leached, and the resultant brine was focused in an updraught zone to the site of ore deposition. The intake zone where the seawater initially entered the system is suggested to have an approximate radius of 40km around the present deposit (Russell, 1978). The implications are that: firstly, if the dolomitic horizons are only developed in the mine vicinity then the 40km radius of the intake zone would allow seawater containing bacteriogenic sulphide to permeate down into the carbonates. Secondly, some of this seawater could have migrated laterally through permeable carbonate lithologies instead of continuing down into the underlying Lower Palaeozoic rocks and therefore provided the bacteriogenic sulphide for ore deposition. However, there must have been a driving mechanism behind this lateral movement of bacteriogenic sulphide-bearing seawater. Anderson (1983) postulated a mechanism for MVT deposits involving local temperature gradients established near a hydrothermal conduit where the upward movement of fluids at temperatures of 80-150°C, may have

resulted in the lateral migration of bacteriogenic sulphides generated some distance from the deposit to the site of ore deposition. He states however, that considerable work is needed to establish the exact mechanisms involved. Recently, Kucha (1988) has proposed a model to explain the mineralization at Moyvoughly, which incorporated bacteriogenic sulphide. The model consists of two convective cells separated by an impermeable layer, the Mixed Beds (equivalent to the Laminated Beds at Navan). High heat flow initiated the lower convective cell which generated the metals in a fractured basement. An upper convective cell which provided a continual supply of bacteriogenic sulphide was initiated where the impermeable layer was cut by a fault thereby allowing a heat source into the Pale Beds. The idea of an upper convective cell provides one mechanism for drawing bacteriogenic sulphide to the site of mineralization.

The faults observed in the mine area post-date the mineralization, however it is postulated that precursors to these faults existed at the time of the mineralization (Chapter 5). The implication is that any faults which cut and offset the dolomitic horizons in the vicinity of the mine area, could have provided permeable access routes for the migration of bacteriogenically-derived  $H_2S$  (Fig. 7.2). This would provide a mechanism to overcome the inferred impermeability of the dolomites in relation to the supply of bacteriogenic sulphide. A large vein swarm

in 2-5 Lens which formed in the later stages in the evolution of the orebody, is dominated by bacteriogenic sulphide (Section 6.6.5). The size, morphology and abundance of the veins indicates significant extension occurred at the time of their formation. The presence of both bacteriogenic sulphide and barite with seawater sulphate values may indicate that late-stage, large scale fracturing allowed seawater sulphate and bacteriogenic sulphide directly down into the Pale Beds in the central mine area, where it encountered ascending metal-bearing solutions.

2) Reduction of sulphate in seawater within laterally equivalent stratigraphic horizons to those hosting the mineralization, rich in organic material, eg argillaceous limestones, with subsequent lateral migration of the sulphur to the site of ore deposition (Fig. 7.2). This could provide quantities of bacteriogenic  $H_2S$  and also overcome the problem of the impermeable dolomite horizons (Fig. 7.2). Boast et al. (1981) proposed a bacteriogenic origin for the sulphur in the main stage of the mineralization in Waulsortian mudbanks in the Tynagh deposit, with the sulphur generated within argillaceous, organic-rich, off-bank facies which then migrated into the Waulsortian mudbank. There are no obvious argillaceous, organic-rich sequences present stratigraphically equivalent to the Pale Beds in the Navan area. However, the presence of thick micrites around the Navan area (up to 100m in drillhole EP28 west

of the deposit) containing numerous birdseye structures, may reflect the generation of H<sub>2</sub>S during diagenesis. It is interesting to note that accumulations of H<sub>2</sub>S are common in modern-day intertidal environments similar to that inferred for the micrites at Navan (Shinn, 1983). Bacteriogenic sulphur may therefore have been generated in the thick micrites and subsequently migrated to the site of ore deposition as the result of a gentle gradient induced by faulting in the area (Fig. 7.2).

#### 7.5 A COMPARISON WITH SEDEX AND MVT DEPOSITS AND STYLES OF MINERALIZATION

This study began with a simplified classification/description of the SEDEX and MVT Zn+Pb deposits in relation to Lower Carboniferous base metal mineralization in Ireland. The Navan deposit illustrates styles of mineralization which are observed in both SEDEX and MVT deposits.

Sulphide textures and relationships with host rocks indicative of open space growth are features common to MVT and generally absent from the SEDEX deposits. It is instructive to examine the features at Navan which are similar to those from some MVT deposits. An obvious feature at Navan, and one that is characteristic of MVT deposits, is the presence of a limestone/dolomite host rock. Although MVT deposits are generally stratabound and discordant mineralization is common, concordant or

stratiform mineralization does occur, for example in the tabular orebodies at Pine Point (Rhodes et al., 1984). A subtle comparison may be made between Pine Point and Navan in that at Pine Point the tabular karstic networks developed at the base of the Presqu'île dolomite and sulphides were subsequently deposited within the open spaces. The Presqu'île dolomite is regarded as having formed diagenetically by mixing of saline Mg-rich fluids with meteoric waters (Rhodes et al., 1984). It is also interesting that the principal karstic networks at Pine Point occur in two trends which are coincident with the maximum development of the dolomite, and in plan these two trends form linear strips on either side of an undolomitized central area (Rhodes et al., 1984). At Navan, sulphides also accumulated as open space growths below early, diagenetic dolomite horizons, although it is not proposed that the mechanism for open space formation or sulphide deposition was the same at Pine Point and Navan. However, similarities exist in the styles of mineralization and perhaps the role of early dolomitization.

Many MVT deposits are characterized by coarse sphalerite and galena crystals cementing breccia fragments, for example the Tri-state, zinc-lead district in south-west Missouri. However internal sulphide sediments are observed in some deposits, eg Pine Point (Rhodes et al., 1984) and the Alpine deposits (Klau and Mostler, 1983) and well-developed skeletal galena and collomorphic

sphalerite growths are characteristic of many MVT deposits (Roedder, 1968). These latter styles are observed at Navan. Stalactitic pyrite growths similar to those at Navan have been observed in the sulphides deposited in palaeo-karst networks at Nanisivik (Olson, 1984) and sphalerite stalactites are present in the Alpine deposits (Klau and Mostler, 1983).

However, a striking difference between MVT mineralization and the sulphides at Navan is the abundance of fine-grained sulphide at Navan (ie, internal sediments, skeletal and dendritic growths and rhythmically banded textures) and the absence of the coarse sphalerite crystal growths so common in many MVT deposits. This is a consequence of the rapid sulphide precipitation at Navan, in a zone of mixing of hydrothermal fluid with fluid carrying bacteriogenically-derived  $H_2S$ , thus precipitating fine-grained sulphides.

One of the major differences between the open space growths at Navan when compared to MVT deposits is the relative lack of brecciation so common in most MVT deposits associated with the mineralization (Ohle, 1985). The lack of brecciation associated with open space formation at Navan may be due to the fact that much of the open space was formed during the mineralizing process and therefore large spaces were not present at any one time to allow gravity-induced collapse and brecciation.

The stratiform nature of some of the ore and the presence

of tabular ore lenses at Navan is a feature characteristic of SEDEX deposits (Large, 1980, 1983), however the fine-grained sulphide layers and laminations interbedded with barren host rock observed in so many SEDEX deposits, eg McArthur River (Williams, 1978) and Sullivan (Hamilton et al., 1983) are absent in the Pale Beds mineralization at Navan. In contrast, Navan is characterized by high-grade, massive sulphides surrounded by essentially barren host carbonate, a feature more akin to many MVT deposits (eg, Pine Point). The framboidal pyrite layers in the CGO are very similar to hand specimens seen from Mt Isa, and the interpretation of pyrite in the CGO as sedimentary-early diagenetic mineralization is consistent with the SEDEX-type model of deposition.

Bedded barite is a feature indicative of seafloor exhalation eg, Silvermines, (Taylor and Andrew, 1978). Barite at Navan was precipitated as carbonate replacement and late-stage, coarse infill of remaining porosity after the Zn/Pb mineralization, and not in stratiform horizons. This is consistent with the absence of sedimentary exhalative mineralization in the Pale Beds.

SEDEX deposits are generally hosted in carbonaceous shales and siltstones (usually dolomitic), sandstones and cherts, eg McArthur River (Muir, 1983), Sullivan (Hamilton et al., 1983) and Red Dog (Lange et al., 1985). By contrast, the Navan deposit is hosted by clean oolitic and bioclastic limestones.

At Silvermines the sulphides occur in a carbonate sequence, however the exhalative mineralization overlies very argillaceous limestones (Taylor and Andrew, 1978; Boyce et al., 1983), and it is significant that where well-developed oolitic grainstones similar to those at Navan were originally present, they have been dolomitized and host the lower epigenetic ores (Andrew, 1986b).

Metal zoning patterns are a feature common in many SEDEX deposits (Large, 1980, 1983), but generally absent from MVT deposits. At Navan the most pronounced zonation occurs vertically with an overall increase in the Zn/Pb ratio and in the Fe content representing a change in the deposited sulphide assemblages with time (Andrew and Ashton, 1985). Large scale lateral zonation is only now becoming apparent. The vertical zonation clearly implies that although the mineralization process occurred below the sea floor, the internal sulphide deposition and replacement process migrated upward through the stratigraphic section with time, rather than continual deposition throughout the succession over a particular time-span, as suggested for many MVT deposits. The presence of significant amounts of Fe-sulphides (in the stratigraphically highest mineralization) at Navan is more characteristic of SEDEX rather than MVT deposits (Gustafson and Williams, 1981).

In summary, the Navan deposit exhibits characteristic features and similarities to both SEDEX and MVT deposits, but in its own way is substantially different from both

MVT and SEDEX and should not be fitted into one of these two "endmember" classifications. The gross stratiform nature of the deposit, with sulphide lenses, and the metal zonation are features suggestive of a SEDEX origin, however many of the textures and mechanisms of sulphide deposition are akin to those proposed for MVT deposits. It is proposed that the late-stage Fe-rich mineralization in the Pale Beds was synchronous with the deposition of pyrite in the Boulder Conglomerate/ Conglomerate Group Ore. Assuming that a "normal" thickness of Upper Pale Beds (60m), Shaley Pales (100m) and ABC (250m?) has been removed by the submarine erosion/slumping, then the mineralization would have formed at depths of at least 400m at this time, which is within the depth range as indicated by stratigraphic evidence in MVT deposits - a few hundred to around 1000m (Anderson and Maqueen, 1982). However, the implications of basinal brine expulsion and the "epigenetic" connotation frequently attached to the origin of MVT deposits are inconsistent with the mineralization at Navan and hence an MVT model for the mineralization at Navan is rejected.

The near surface mixing in a diagenetic environment at Navan, of a hydrothermal fluid and Lower Carboniferous seawater containing sulphate and bacteriogenically-derived  $H_2S$  is possibly closer in a gross sense to a SEDEX model, although it is stressed that Navan exhibits so many features that are uncharacteristic of the SEDEX deposits that it should not be classified as SEDEX.

These features are attributed to the fact that the ore fluids precipitated the sulphides in a sub-seafloor, diagenetic environment within a limestone-dominated succession. It is possible that if the host lithologies had been say siliclastic shales and siltstones, more typical sedimentary exhalative mineralization could have occurred.

#### 7.6 THE MODEL (Figs. 7.3-7.4)

During the Lower Carboniferous, shallow marine carbonate deposition of the Pale Beds succession exhibited strong facies variations from east to west in the Navan mine area. Calcite cementation was accompanied by an early episode of dolomitization of probable diagenetic origin, consisting of a fine-grained replacement of the original carbonate grains and cement which occurred preferentially in bedding-parallel, silt-rich horizons in the mine area. The result of this dolomitizing event was an increase in the competency and a decrease in the permeability of the rock and was critical in the later accumulation and formation of ore.

Metal-bearing brines entered the Pale Beds during diagenesis. The metal zoning patterns and local accumulation of sulphides suggest that a structural control on the mineralization was NE to ENE-trending fractures, some of which acted as precursors to faults presently observed in the mine.

The metals were derived from the underlying Lower Palaeozoic succession, involving open system hydrothermal metamorphism by modified convecting seawater (Russell, 1978, 1983, 1986; Russell et al., 1981). Two sources of sulphur were involved in the genesis of the bulk of the deposit: hydrothermal sulphur (transported with the metals) and a dominant component of bacteriogenically-derived sulphur. The bacteriogenic sulphur was derived from the reduction of contemporaneous Lower Carboniferous seawater sulphate and could have been generated either in the Lower Carboniferous sea and top few metres of the sediment column, above the mineralizing zone, or else laterally in stratigraphically equivalent lithologies to the Pale Beds, rich in organic matter. In either case, the bacteriogenically-derived sulphide subsequently migrated to the site of ore deposition.

The origin of the hydrothermal sulphur is uncertain. However, the two most plausible explanations are leaching of diagenetic pyrite in the Lower Palaeozoic pile and thermochemical reduction of convected Lower Carboniferous seawater sulphate. The former is supported by the discovery of Lower Palaeozoic diagenetic pyrite with extraordinarily heavy  $\delta^{34}\text{S}$  values.

Constraints on the timing of the mineralization and the actual styles of sulphide deposition imply that the ore was deposited sub-seafloor, syn-diagenetically in semi-lithified or semi-consolidated carbonates. The ore horizons formed by a variety of processes generally

reflecting the host rock geology as well as the availability and nature of the hydrogen sulphide.

Spaces were created by diagenetic processes below the rigid dolomitized or partially dolomitized lithologies during compaction of the limestone-dominated succession. These spaces enhanced the permeability directly below the dolomite and facilitated the flow of the ore fluids which migrated laterally along the base of the dolomitic horizons. At the same time, the dolomitic horizons also acted as barriers to the ascending fluids. High-grade sulphides formed by infill and replacement around these small cavities (eg, 2-2 Lens), but more commonly the permeability was enhanced during the mineralization and all the sulphides precipitated as open-space growths. The limestone host rock was semi-consolidated at the time of mineralization. In the micrites episodic extension created an anastomosing network of fractures which were enlarged by dissolution and infilled with sulphides. Fracturing and brecciation were also associated with sulphide deposition in the central 2-5 Lens.

In massive sulphides characterized by coarse galena growths (eg, 2-5 and 2-2 Lenses) initial mineralization from a pulse of ore fluid was lead-rich and dominated by hydrothermal, relative to bacteriogenic, sulphur. As the lead and sulphur were used up during galena deposition, so the ratio of hydrothermal/bacteriogenic sulphur decreased as the bacteriogenic sulphide was continually supplied, and the ore fluids, which were now zinc-

enriched, precipitated sphalerite dominated by bacteriogenically-derived sulphur. In places these zinc-enriched/sulphur-depleted fluids migrated to more distal locations where they encountered bacteriogenic sulphide and precipitated sphalerite as bedding-parallel replacements. The sphalerite replacement style is best developed in the upper lenses and is consistent with the upward migration of the Zn-rich solutions after deposition of the lead. This type of mineralization preserved the original allochems in the limestone.

Where dissolution and possibly slumping enlarged the diagenetic spaces below the dolomites, open-space growth sulphide precipitation was characterized by internal sulphide sediments, stalactitic, dendritic and colloform growths, all often disrupted into a complex assemblage of clasts. These textures formed by rapid precipitation and growth as a result of mixing of two chemically contrasting solutions, interpreted as the metal-bearing, hydrothermal solution and a bacteriogenic sulphide-rich solution. The sulphur isotope results suggest that a small component of hydrothermal sulphur was present, but it was swamped by mixing with a plentiful supply of bacteriogenic  $H_2S$  below the dolomitic horizons.

During periods of increased extension probably associated with higher fluid pressures, the fluids were able to break through the confining dolomite barriers and form local breccia styles of mineralization. The unconfined mineralizing fluids were able to migrate upwards and

continue the ore depositional processes at higher levels.

Fe-rich mineralization occurred in the later (waning) stages in the genesis of the Pale Beds-hosted ore, at which time the hydrothermal system was unroofed by submarine erosion/slumping. The late-stage Fe-rich mineralizing fluids debouched on to the seafloor and deposited as the Conglomerate Group Ore (CGO). The CGO is regarded as being cogenetic with Fe-rich mineralization in the 2-1 Lens and this is supported by the sulphur isotopic composition of pyrite. Both incorporated bacteriogenically-derived sulphide. However, the deep water (>500m?) carbonate depositional environment at this time was drastically different to that at the time of Zn/Pb mineralization in the Pale Beds, and this environmental change caused a greater isotopic fractionation in the bacteriogenic sulphide. The initiating T Fault may have acted as a pathway for some of these Fe-rich fluids.

## REFERENCES

- ANDERSON, G.M., and MacQUEEN, R.W., 1982. Ore deposit models 6. Mississippi Valley-type lead-zinc deposits: Geoscience Canada, vol.9, no.2, pp. 108-117.
- ANDERSON, G.M., 1973. The hydrothermal transport and deposition of galena and sphalerite near 100°C: Econ. Geol., v.68, pp. 480-492.
- ANDERSON, G.M., 1975. Precipitation of Mississippi Valley-type ores: Econ. Geol., v.70, pp. 937-942.
- ANDERSON, G.M., 1983. Some geochemical aspects of sulphide precipitation in carbonate rocks. In: International Conference on Mississippi Valley-type Lead-Zinc Deposits. Proceedings Volume (Kisvarsanyi, G., Grant, S.K., Pratt, W.P., and Koenig, J.W., eds). Rolla, University of Missouri-Rolla Press, pp. 61-76.
- ANDERTON, R., BRIDGES, P.H., LEEDER, M.R., and SELLWOOD, B.W., 1979. A Dynamic Stratigraphy of the British Isles - A study in crustal evolution. London, George Allen and Unwin, 301pp.
- ANDERTON, R., 1986. Personal communication.
- ANDREW, C.J., 1986a. Sedimentation, tectonism and mineralization in the Irish Orefield. In: The Genesis of Stratiform Sediment-hosted Lead and Zinc Deposits: Conference Proceedings (Turner, R.J.W., and Enaudi, M.T., eds). Stanford University Publications, California, pp. 44-56.
- ANDREW, C.J., 1986b. Tectono-stratigraphic controls at Silvermines. In: Geology and Genesis of Mineral Deposits in Ireland, I.A.E.G., Dublin (Andrew, C.J., Crowe, R.W.A., Finlay, S., Pennell, W.M., and Pyne, J.F., eds). pp. 377-417.
- ANDREW, C.J., 1986c. A diagrammatic representation of the Courcayan stratigraphy of the Irish Midlands. In: Geology and Genesis of Mineral Deposits in Ireland, I.A.E.G., Dublin (Andrew, C.J., Crowe, R.W.A., Finlay, S., Pennell, W.M., and Pyne, J.F., eds). pp. 239-241.

ANDREW, C.J., and ASHTON, J.H., 1982. Mineral textures, metal zoning and ore environment of the Navan orebody, Co. Meath, Ireland. In: Mineral exploration in Ireland: progress and developments 1971-81/ Wexford Conference 1981, I.A.E.G., Dublin (Brown, A.G., and Pyne, J.F., eds). pp. 35-46.

ANDREW, C.J., and ASHTON, J.H., 1985. Regional setting, geology and metal distribution patterns of Navan orebody, Ireland: Trans. Inst. Min. Metall. (Sect.B: Appl. earth Sci.), v.94, pp. 66-93.

ANDREW, C.J., and POUSTIE, A., 1986. Syndiagenetic or epigenetic mineralization - the evidence from the Tatestown zinc-lead prospect, Co. Meath. In: Geology and Genesis of Mineral Deposits in Ireland, I.A.E.G., Dublin (Andrew, C.J., Crowe, R.W.A., Finlay, S., Pennell, W.M., and Pyne, J.F., eds). pp. 281-296.

ASHTON, J.H., DOWNING, D.T., and FINLAY, S., 1986. The geology of the Navan Zn-Pb orebody. In: Geology and Genesis of Mineral Deposits in Ireland, I.A.E.G., Dublin (Andrew, C.J., Crowe, R.W.A., Finlay, S., Pennell, W.M., and Pyne, J.F., eds). pp. 243-280.

BACHINSKI, D.J., 1969. Bond strength and sulfur isotopic fractionation in coexisting sulfides: Econ. Geol., v.64, pp. 56-65.

BADHAM, J.P.N., 1981. Shale-hosted Pb-Zn deposits: Products of exhalation of formation waters?: Trans. Inst. Min. Metall. (Sect.B: Appl. earth sci.), v.90, pp. 70-76.

BADIOZAMI, K., 1973. The dorag dolomitization model - Application to the Middle Ordovician of Wisconsin: J. sediment. petrol., v.43, pp. 965-984.

BAKER, P.A., and KASTNER, M., 1981. Constraints on the formation of sedimentary dolomite: Science, v.213, pp. 214-216.

BANKS, D.A., 1986. Hydrothermal chimneys and fossil worms from the Tynagh Pb-Zn deposit, Ireland. In: Geology and Genesis of Mineral Deposits in Ireland, I.A.E.G., Dublin (Andrew, C.J., Crowe, R.W.A., Finlay, S., Pennell, W.M., and Pyne, J.F., eds). pp. 441-447.

- BARNES, H.L., 1979. Solubilities of ore minerals. In: Geochemistry of Hydrothermal Ore Deposits, 2nd Ed, Chap.8 (Barnes, H.L., ed). Wiley-Interscience, New York, pp. 405-461.
- BARRETT, T.J., and ANDERSON, G.M., 1982. The solubility of sphalerite and galena in NaCl brines: Econ. Geol., v.77, pp. 1923-1933.
- BATHURST, R.G.C., 1975. Carbonate Sediments and Their Diagenesis, Elsevier, Amsterdam, 658pp.
- BATHURST, R.G.C., 1982. The genesis of stromatactis cavities between submarine crusts in Palaeozoic carbonate mud buildups: J. geol. Soc. London, v.139, pp. 165-181.
- BEALES, F.W., 1975. Precipitation mechanisms for Mississippi Valley-type ore deposits: Econ. Geol., v.70, pp. 943-948.
- BEALES, F.W., and HARDY, J.W., 1980. Criteria for the recognition of diverse dolomite types with an emphasis on studies of host rocks for Mississippi Valley-type ore deposits. In: Concepts and Models of Dolomitization, S.E.P.M., Spec. Publ. No.28 (Zenger, D.H., Dunham, J.B., and Ethington, R.L., eds). pp. 197-213.
- BEALES, F.W., and JACKSON, S.A., 1966. Precipitation of lead-zinc ores in carbonate resevoirs as illustrated by Pine Point orefield, Canada: Trans. Can. Inst. Min. Metall., v.75 (Sect.B), pp. 278-285.
- BENTHKE, C.M., 1986. Hydrologic constraints on the genesis of the Upper Mississippi Valley mineral district from Illinois Basin brines: Econ. Geol., v.81, pp. 233-249.
- BISCHOFF, J.L., RADTKE, A.S., and ROSENBAUER, R.J., 1981. Hydrothermal alteration of greywacke by brine and seawater: roles of alteration and chloride complexing on metal solubilization at 200 and 350°C: Econ. Geol., v.76, pp. 659-676.

- BISCHOFF, J.L., ROSENBAUER, R.J., ARUSCAVAGE, P.J., BAEDECKER, P.A., and CROCK, J.G., 1983. Seafloor massive sulphide deposits from 21°N, East Pacific Rise, Juan de Fuca Ridge, and Galapagos Rift; Bulk chemical composition and economic implications: Econ. Geol., v.78, pp. 1711-1720.
- BLACK, A.P., 1988. Personal communication.
- BOAST, A.M., 1978. A textural and isotopic study of Irish base metal mineralization of Lower Carboniferous age, with specific reference to the Tynagh deposit: Unpubl. Ph.D. thesis, Imperial College of Science and Technology, London.
- BOAST, A.M., COLEMAN, M.L., and HALLS, C., 1981. Textural and stable isotopic evidence for the genesis of the Tynagh base metal deposit, Ireland: Econ. Geol., v.76, pp. 27-55.
- BOYCE, A.J., 1986. Personal communication.
- BOYCE, A.J., ANDERTON, R., and RUSSELL, M.J., 1983. Rapid subsidence and early Carboniferous base-metal mineralization in Ireland: Trans. Inst. Min. Metall. (Sect.B: Appl. earth sci.), v.92, pp. 55-67.
- BOYCE, A.J., COLEMAN, M.L., and RUSSELL, M.J., 1984. Formation of fossil hydrothermal chimneys and mounds from Silvermines, Ireland: Nature, v.306, no.5943, pp. 545-550.
- BRINDLEY, J., 1973. The structural setting of the Leinster granite, Ireland - A review: Scientific Proc. Roy. Dublin Soc. Sect. A, v.5, pp. 27-33.
- BROWN, C., and WILLIAMS, B., 1985. A gravity and magnetic interpretation of the structure of the Irish Midlands and its relation to ore genesis: J. geol. Soc. London, v.142, pp. 1059-1076.
- BURNS, S.J., and BAKER, P.A., 1987. A geochemical study of dolomite in the Monterey Formation, California: J. sediment. petrol., v.57, no.1, pp. 128-139.

- BUTLER, G.P., 1969. Modern evaporite deposition and geochemistry of co-existing brines, the sabkha, Trucial Coast, Arabian Gulf: J. sediment. petrol., v.39, pp. 70-89.
- CARVALHO, P., 1988. An introduction to the Neves Corvo copper mine, Portugal. In: Society for Geology Applied to Mineral Deposits. Iberian Field Conference Guide (Laboratorio De Geologia Institutio Superior Tecnico Lisboa). pp. 83-99.
- CATHLES, L.M., and SMITH, A.T., 1983. Thermal constraints on the formation of Mississippi Valley-type lead-zinc deposits and their implications for episodic basin dewatering and deposit genesis: Econ. Geol., v.78, pp. 983-1002.
- CAULFIELD, J.B.D., LEHURRAY, A.P., and RYE, D.M., 1986. A review of lead and sulphur isotope investigations of Irish sediment-hosted base metal deposits with new data from the Keel, Ballinalack, Moyvoughly and Tatestown deposits. In: Geology and Genesis of Mineral Deposits in Ireland, I.A.E.G., Dublin (Andrew, C.J., Crowe, R.W.A., Finlay, S., Pennell, W.M., and Pyne, J.F., eds). pp. 591-615.
- CHOWNS, T.M., and ELKINS, J.E., 1974. The origin of quartz geodes and cauliflower cherts through the silicification of anhydrite nodules: J. sediment. petrol., v.44, no.3, pp. 885-903.
- CLAYPOOL, C.E., HOLSER, W.T., SAKI, I.R., and ZAK, I., 1980. The age curves for sulfur and oxygen isotopes in marine sulfate and their mutual interpretation: Chem. Geol., v.28, pp. 199-260.
- CLIFFORD, J.A., RYAN, P., and KUCHA, H., 1986. A review of the geological setting of the Tynagh orebody, Co. Galway. In: Geology and Genesis of Mineral Deposits in Ireland, I.A.E.G., Dublin (Andrew, C.J., Crowe, R.W.A., Finlay, S., Pennell, W.M., and Pyne, J.F., eds). pp. 419-440.
- COLLER, D.W., 1984. Variscan structures in the Upper Palaeozoic rocks of west Ireland. In: Variscan tectonics of the North Atlantic region. Geol. Soc. Spec. Publ. No.14 (Hutton, D.H.W., and Sanderson, D.J., eds). Blackwell Scientific Publications, Oxford, pp. 185-194.

- COOMER, P.G., and ROBINSON, B.W., 1976. Sulphur and sulphate-oxygen isotopes and the origin of the Silvermines deposits, Ireland: Mineralium Deposita., v.11, pp. 155-169.
- COOPER, M.A., COLLINS, D., FORD, M., MURPHY, F.X., and TRAYNER, P.M., 1984. Structural style, shortening estimates and the thrust front of the Irish Variscides. In: Variscan tectonics of the North Atlantic region. Geol. Soc. Spec. Publ. No.14 (Hutton, D.H.W., and Sanderson, D.J., eds). Blackwell Scientific Publications, Oxford, pp: 167-176.
- CRAIG, H., 1957. Isotopic standards for carbon and oxygen and correction factors for mass-spectrometric analysis of carbon dioxide: Geochimica et Cosmochimica Acta, v.12, pp. 133-149.
- DANIELLI, C., 1983. Deposition, diagenesis and mineralization in the Moyvoughly prospect, Ireland: Getty Research Center, Houston, Research Report No.83-138, 28pp.
- DATE, J., WATANABE, Y., and SAEKI, Y., 1983. Zonal alteration around the Fukazawa Kuroko deposits, Akita Prefecture, Northern Japan. In: Economic Geology Monograph 5, "The Kuroko and related volcanogenic massive sulphide deposits" (Ohmoto, H., and Skinner, B.J., eds). pp. 365-386.
- DUNHAM, R.J., 1962. Classification of carbonate rocks according to depositional texture. In: Classification on Carbonate Rocks. A.A.P.G., Tulsa, Oklahoma (Ham, W.E., ed). pp. 108-121.
- EITHER, V.G., and CAMPBELL, F.F., 1977. Tourmaline concentrations in Proterozoic sediments of the Southern Cordillera of Canada and their economic significance: Can. J. Earth Sci., v.14, pp. 2348-2363.
- ELDRIDGE, C.S., COMPSTON, W., WILLIAMS, I.S., BOTH, R.A., WALSHE, J.L., and OHMOTO, H., 1988. Sulfur isotope variability in sediment-hosted massive sulphide deposits as determined using the ion microprobe SHRIMP: I. An example from the Rammelsberg orebody: Econ. Geol., v.83, pp. 443-449.

- ELDRIDGE, C.S., COMPSTON, W., WILLIAMS, I.S., PATTERSON, D.J., OHMOTO, H., WALSHE, J.L., and BOTH, R.A., 1986. Shrimp ion microprobe determination of sulfur isotopic ratios in some sediment hosted massive sulphide ores: variability in their timing and formation: Terra cognita, vol. 6, Abstracts, pp. 134.
- EMO, G.T., 1986. Some considerations regarding the styles of mineralization at Harberton Bridge, Co. Kildare. In: Geology and enesis of Mineral Deposits in Ireland. I.A.E.G., Dublin (Andrew, C.J., Crowe, R.W.A., Finlay, S., Pennell, W.M., and Pyne, J.F., eds). pp. 461-470.
- FINLAY, S., ROMER, D.M., and CAZALET, P.C.D., 1984. Lithogeochemical studies around the Navan zinc-lead orebody in County Meath, Ireland. In: Prospecting in areas of glaciated terrain: Proceedings Volume, Strathclyde Symposium. I.M.M., London, pp. 35-36.
- FINLOW-BATES, T., 1980. The chemical and physical controls on the genesis of submarine exhalative orebodies and their implications for forming exploration concepts. A review: Geol. Jb., v.40, pp. 131-168.
- FORD, D.C., 1986. Genesis of palaeokarst and strata-bound zinc-lead sulfide deposits in a Proterozoic dolostone, northern Baffin Island - A discussion: Econ. Geol., v.81, pp. 1562-1566.
- FRANK, J.R., CARPENTER, A.B., and OGLESBY, T.W., 1982. Cathodoluminescence and composition of calcite cement in the Taum Sauk Limestone (Upper Cambrian), southeast Missouri: J. sediment. petrol., v.30, pp. 631-638.
- FRANKLIN, J.M., 1986. Volcanic-associated massive sulphide deposits - an update. In: Geology and Genesis of Mineral Deposits in Ireland. I.A.E.G., Dublin (Andrew, C.J., Crowe, R.W.A., Finlay, S., Pennell, W.M., and Pyne, J.F., eds). pp. 49-70.
- FANKLIN, J.M., LYDON, J.W., and SANGSTER, D.F., 1981. Volcanic-associated massive sulphide deposits. In: Economic Geology 75<sup>th</sup> Anniversary Volume (Skinner, B.J., and Simms, P.K., eds). pp. 485-627.

- GARDINER, P.R.R., 1974. The Duncannon Group: an Upper Ordovician unit in south-west County Wexford: Geol. Surv. Ireland Bull., v.1, No.4, pp. 429-446.
- GARDINER, P.R.R., 1975a. Tectonic controls of Devonian and Lower Carboniferous sedimentation in the south of Ireland. In: 9<sup>th</sup> International Congress of Sedimentology, Nice, Vol.4, pp. 141-146.
- GARDINER, P.R.R., 1978. The Duncannon District: Cambro-Ordovician flysh and Ordovician volcanic sequences: Field guide to the Caledonian and Pre-Caledonian rocks of south-east Ireland: Geol. Surv. Ireland, Guide Series No.2, pp. 25-40.
- GARDINER, P.R.R., and MacCARTHY, I.A.J., 1981. The late Palaeozoic evolution of southern Ireland in the context of tectonic basins and their transatlantic significance. In: Geology of the North Atlantic borderlands. Can. Soc. Petrol. Geol. Memoir 7 (Kerr, J.W., and Fergusson, A.J., eds). pp. 683-725.
- GAWTHORPE, R.L., 1986. Sedimentation during carbonate ramp-to-slope evolution in a tectonically active area: Bowland Basin (Dinantian), northern England: Sedimentology, v.33, pp. 185-206.
- GEORGE, M.T., and VAIDYAN, V.K., 1981. A new electrode method to grow silver dendrites and single crystals in gel: J. Crystal Growth, v.53, pp. 300-304.
- GILL, W.D., 1962. The Variscan fold belt in Ireland. In: Some aspects of the Variscan fold belt (Coe, K., ed). Manchester University Press, pp. 49-64.
- GOLDHABER, M.B., and KAPLAN, I.R., 1975. Controls and consequences of sulphate reduction rates in recent marine sediments: Soil Science, v.119, no.1, pp. 42-55.
- GOODFELLOW, W.D., and JONASSON, I.R., 1984. Ocean stagnation and ventilation defined by  $\delta^{34}\text{S}$  secular trends in pyrite and barite, Selwyn Basin, Yukon: Geology, v.12, pp. 583-586.

- GOODELLOW, W.D., and JONASSON, I.R., 1986. Geology and geochemistry of the Howard's Pass Zn-Pb Deposits: Constraints on metal source, migration and concentration. In: The Genesis of Stratiform Sediment-hosted Lead and Zinc Deposits: Conference Proceedings (Turner, R.J.W., and Einaudi, M.T., eds). Stanford University Publications, California, pp. 22-32.
- GRAY, G.J., and RUSSELL, M.J., 1984. Regional Mn-Fe litho geochemistry of the Lower Carboniferous Waulsortian "Reef" Limestone in Ireland. In: Prospecting in areas of glaciated terrain, 1984. Institution of Mining and Metallurgy, pp. 57-68.
- GREIG, J.A., BAADSGAARD, H., CUMMING, G.L., FOLINSBEE, R.E., KROUSE, H.R., OHMOTO, H., SASAKI, A., and SMEJKAL, V., 1971. Lead and sulfur isotopes of the Irish base metal mines in Carboniferous carbonate host rocks: Soc. Mining Geol. Japan, Spec. Issue 2, pp. 84-92.
- GUSTAFSON, L.B., and WILLIAMS, N., 1981. Sediment-hosted stratiform deposits of copper, lead, and zinc. In: Economic Geology 75<sup>th</sup> Anniversary Volume (Skinner, B.J., and Simms, P.K., eds). pp. 139-178.
- GWOSDZ, W., and KREBBS, W., 1977. Manganese halo surrounding Meggen ore deposit: Trans. Inst. Min. Metall. (Sect. B: Appl. earth sci.), v.86, pp. 73-77.
- HALLBERG, R.O., 1984. Computer simulation of sulfur isotope fractionation in a closed sulfuretum: Geomicrobiol. J., v.4, no. 2, pp. 131-152.
- HALLBERG, R.O., and BAGANDER, L.E., 1985. Fractionation of stable sulphur isotopes in a closed sulfuretum. In: The Sixth International Symposium on Environmental Biochemistry (Caldwell, D.E, Brierly, J.A., and Brierly, C.L., eds). pp. 85-296.
- HALLEY, R.B., HARRIS, P.M., and HINE, A.C., 1983. Bank margin environment. In: Carbonate Depositional Environments. A.A.P.G. Memoir 33, Tulsa, Oklahoma (Scholle, P.A., Bebour, D.G., and Moore, C.H., eds). pp. 463-506.

- HAMILTON, J.M., DELANEY, G.D., HAUSER, R.L., and RANSOM, P.W., 1983. Geology of the Sullivan deposit, Kimberley, B.C, Canada. In: Mineralogical Association of Canada, Short Course Handbook vol. 8, Sediment-hosted stratiform lead-zinc deposits (Sangster, D.F., ed). pp. 31-83.
- HARDIE, L.A., 1987. Dolomitization: A critical view of some current views: J. sediment. petrol., v.57, no.1, pp. 166-183.
- HARRISON, A.G., and THODE, H.G., 1957. Mechanism of bacterial reduction of sulphate from isotope fractionation studies: Faraday Soc. Trans., v.54, pp. 84-92.
- HARTMANN, M., and NIELSON, H., 1969.  $\delta^{34}\text{S}$  Werte in rezenten Meeressedimenten und ihre Deutung am Beispiel einiger Sedimentprofile aus der westlichen Ostsee: Geol. Rundschau, v.58, pp. 621-655.
- HEYL, V.A., 1983. Geologic characteristics of three major Mississippi Valley districts. In: International Conference on Mississippi Valley-type lead-zinc deposits. Proceedings volume (Kisvarsanyi, G., Grant, S.K., Pratt, W.P., and Koenig, J.W., eds). Rolla, Univ. of Missouri-Rolla Press, pp. 27-60.
- HIRD, K., TUCKER, M.E., and WATERS, R.A., 1987. Petrography, geochemistry and origin of Dinantian dolomites from south-east Wales. In: European Dinantian Environments (Miller, J., Adams, A.E., and Wright, V.P., eds). pp. 359-377.
- HONJO, H., and SAWADA, Y., 1982. Quantitative measurements on the morphology of a  $\text{NH}_4\text{Br}$  dendritic crystal growth in a capillary: J. Crystal Growth, v.58, pp. 297-303.
- HUTTON, D.H.W., and MURPHY, F.C., 1987. The Silurian of the Southern Uplands of Scotland and Ireland as a successor basin to the end-Ordovician back-arc basin: J. geol. Soc. London, v.144, pp. 765-772.
- JANNASCH, H.W., TRUPER, H.G., and TUTTLE, J.H., 1974. Microbial sulfur cycle in Black Sea. In: The Black Sea - Geology, Chemistry and Biology. A.A.P.G. Tulsa, Oklahoma (Degens, E.T., and Ross, D.A., eds). pp. 419-425.

- JONES, B., and KAHLE, C.F., 1986. Dendritic calcite crystals formed by calcification of algal filaments in a vadose environment: J. sediment. petrol., v.56, no.2, pp. 217-227.
- JONES, G.V., and BRAND, S.F., 1986. The setting, styles of mineralization and mode of origin of the Ballinalack Zn-Pb deposit. In: Geology and Genesis of Mineral Deposits in Ireland. I.A.E.G., Dublin (Andrew, C.J., Crowe, R.W.A., Finlay, S., Pennell, W.M., and Pyne, J.F., eds). pp. 355-376.
- KAPLAN, I.R., and RITTENBERG, S.C., 1964. Microbiological fractionation of sulfur isotopes: J. Gen. Microbiol., v.34, pp. 195-212.
- KEEGAN, J.R., 1981. Stratigraphic palynology of the early Carboniferous sediments in two borehole cores from Moate, Co. Westmeath, Ireland: Unpubl. M.Sc. thesis, University of Dublin.
- KEMP, A.L.W., and THODE, H.G., 1968. The mechanism of the bacterial reduction of sulfate and of sulfite from isotopic fractionation studies: Geochim. et Cosmochim. Acta, v.32, pp. 71-91.
- KIYOSU, Y., 1980. Chemical reduction and sulfur-isotope effects of sulfate by organic matter under hydrothermal conditions: Chem. Geol., v.30, pp. 47-56.
- KLAU, W., and MOSTLER, H., 1983. Alpine Middle and Upper Triassic Pb-Zn deposits. In: International Conference on Mississippi Valley-type lead-zinc deposits. Proceedings volume (Kisvarsanyi, G., Grant, S.K., Pratt, W.P., and Koenig, J.W., eds). Rolla, Univ. of Missouri-Rolla Press, pp. 113-128.
- KLAU, W., and MOSTLER, H., 1986. On the formation of Alpine Middle and Upper Triassic Pb-Zn deposits, with some remarks on Irish carbonate-hosted base metal deposits. In: Geology and Genesis of Mineral Deposits in Ireland. I.A.E.G., Dublin (Andrew, C.J., Crowe, R.W.A., Finlay, S., Pennell, W.M., and Pyne, J.F., eds). pp. 663-676.

- KROUSE, H.R., VIAU, C.A., ELIUK, L.S., UEDA, A., and HALAS, S., 1988. Chemical and isotopic evidence of thermochemical sulphate reduction by light hydrocarbon gases in deep carbonate resevoirs: Nature, v.333, pp. 415-419.
- KUCHA, H., 1988. Zn-Pb sulphides as rim cements, filling cements and replacements of carbonate cements, Moyvoughly, Ireland - a product of two convective cells: Trans. Inst. Min. Metall. (Sect.B: Appl. earth sci.), v.97, pp. 64-76.
- LANGE, I.M., NOKLEBERG, W.J., PLAHUTA, J.T., KROUSE, H.R., and DOE, B.R., 1985. Geologic setting, petrology and geochemistry of stratiform sphalerite-galena-barite deposits, Red Dog Creek and Drenchwater Creek areas, northwestern Brookes Range, Alaska: Econ. Geol., v.80, pp. 1896-1926.
- LARGE, D.E., 1980. Geological parameters associated with sediment-hosted, submarine exhalative Pb-Zn deposits: an empirical model for mineral exploration. Geol. Jb., v.40, pp. 59-129.
- LARGE, D.E., 1981a. Sediment-hosted, submarine exhalative lead-zinc deposits - A review of their geological characteristics and genesis. In: Handbook of strata-bound and stratiform ore deposits, vol.9 (Wolf, K.H., ed). Elsevier, Amsterdam. pp. 469-507.
- LARGE, D.E., 1983. Sediment-hosted massive sulphide lead-zinc deposits: an empirical model. In: Mineralogical Association of Canada, Short Course Handbook vol.8, Sediment-hosted stratiform lead-zinc deposits (Sangster, D.F., ed). pp. 1-29.
- LARGE, D.E., 1986. A Palaeotectonic setting of Rammelsberg and Meggen, Germany: A Basin Analysis Study. In: The Genesis of Stratiform Sediment-hosted Lead and Zinc Deposits: Conference Proceedings (Turner, R.J.W., and Enaudi, M.T., eds). Stanford University Publications, California, pp. 109-112.
- LEES, A., 1961. The Waulsortian "Reefs" of Eire: a carbonate mudbank complex of Lower Carboniferous age: J. Geol., v.69, pp. 101-109.

- LEES, A., and MILLER, J., 1985. Facies variation in Waulsortian buildups II. Mid-Dinantian buildups from Europe and North America: Geol. J., v.20, pp. 159-180.
- LEHURRAY, A.P., CAULFIELD, J.B.D., RYE, D.M., and DIXON, P.R., 1987. Basement controls on sediment-hosted Zn-Pb deposits: A Pb isotope study of Carboniferous mineralization in central Ireland: Econ. Geol., v.82, pp. 1695-1709.
- LIBBY, D.J., DOWNING, D.T., ASHTON, J.H., OAM, R.A., O'MURCHU, D., DALLAS, W.G., and MAYBURY, M., 1985. The Tara Mines story: Trans. Inst. Min. Metall. (Sect.A: Mining Industry), v.94, pp. 1-41.
- LONG, J.V.P., and AGRELL, S.O., 1965. The cathodoluminescence of minerals in thin section: Mineralog. Mag. London, v.34, pp. 318-326.
- LONGACRE, S.A., and STOUDET, E.L., 1982. Carbonate facies seminar manual. Getty Oil Company Research Center, Houston, Texas.
- LYDON, J.W., 1983. Chemical parameters controlling the origin and deposition of sediment-hosted stratiform lead-zinc deposits. In: Mineralogical Association of Canada, Short Course Handbook vol. 8, Sediment-hosted stratiform lead-zinc deposits (Sangster, D.F., ed). pp. 172-250.
- LYDON, J.W., 1984(a). Ore Deposit Models - 8. Volcanogenic sulphide deposits, Part 1: A descriptive model: Geoscience Canada, v.11, no.4, pp. 195-202.
- LYDON, J.W., 1986. Models for the generation of metalliferous hydrothermal systems within sedimentary rocks and their applicability to the Irish Zn-Pb deposits. In: Geology and Genesis of Mineral Deposits in Ireland. I.A.E.G., Dublin (Andrew, C.J., Crowe, R.W.A., Finlay, S., Pennell, W.M., and Pyne, J.F., eds). pp. 555-557.
- MacDERMOT, C.V., and SEVASTOPULO, G.D., 1982. Upper Devonian and Lower Carboniferous stratigraphical setting of Irish mineralization: Geol. Surv. Ireland Bull., No.1, pp. 267-280.

- MACHEL, H.G., 1987. Saddle dolomite as a by-product of chemical compaction and thermochemical sulphate reduction: Geology, v.15, pp. 936-940.
- MacQUEEN, R.M., 1986. Application of organic geochemistry to the ore genesis of Mississippi Valley-type deposits. In: The Genesis of Stratiform Sediment-hosted Lead and Zinc Deposits: Conference Proceedings (Turner, R.J.W., and Enaudi, M.T., eds). Stanford University Publications, California, pp. 188-192.
- MacQUEEN, R.M., and POWELL, T.G., 1983. Organic geochemistry of the Pine Point lead-zinc ore field and region, Northwest Territories, Canada: Econ. Geol. v.78, pp. 1-25.
- MASON, J.T., VERHOEVEN, J.D., and TRIVEDI, R., 1982. Primary dendrite spacing I. Experimental studies: J. Crystal Growth, v.59, pp. 516-524.
- MATTES, B.W., and MOUNTJOY, F.W., 1980. Burial dolomitization of the Upper Devonian Miette buildup, Jasper National Park, Alberta. In: Concepts and Models of Dolomitization, S.E.P.M., Spec. Publ. No.28 (Zenger, D.H., Dunham, J.B., and Ethington, R.L., eds). pp. 259-297.
- MAX, M.D., and DHONAU, N.B., 1974. The Cullenstown Formation: late Pre-Cambrian sediments in south-east Ireland: Geol. Surv. Ireland Bull., v.1, no.4, pp. 447-458.
- McILREATH, I.A., and JAMES, N.P., 1984. Carbonate slopes. In: Facies Models (second edition), Geoscience Can., Reprint Series 1 (Walker, R.G., ed). pp. 245-258.
- MILLER, J., 1985. Introduction to Cathodoluminescence Microscopy, workshop notes, University of Edinburgh.
- MILLER, J., 1986. Facies relationships and diagenesis in Waulsortian mudmounds from the Lower Carboniferous of Ireland and N. England. In: Reef Diagenesis (Schroeder, J.H., and Pursrer, B.H., eds). Springer-Verlag Berlin Heidelberg, pp. 311-335.
- MILLER, J., 1986. Personal communication.

- MILLS, H., HALLIDAY, A.N., ASHTON, J.H., ANDERSON, I.K., and RUSSELL, M.J., 1987. Origin of a giant orebody at Navan, Ireland: Nature, v.327, pp. 223-225.
- MORRIS, J.H., 1983. The stratigraphy of the Lower Palaeozoic rocks in the western end of the Longford-Down inlier, Ireland: J. Earth Sci. R. Dubl. Soc., v.5, pp. 201-218.
- MORRIS, J.H., 1987. The Northern Belt of the Longford-Down inlier, Ireland and Southern Uplands, Scotland: J. geol. Soc. London, v.144, pp. 773-786.
- MUIR, M.D., 1983. Depositional environments of host rocks to Northern Australian lead-zinc deposits, with special reference to McArthur River. In: Mineralogical Association of Canada, Short Course Handbook vol. 8, Sediment-hosted stratiform lead-zinc deposits (Sangster, D.F., ed). pp. 141-174.
- NEUDART, M.K., 1986. Sedimentological constraints on the timing of Mount Isa lead-zinc ore genesis. In: Sediments Down Under, 12<sup>th</sup> International Sedimentological Congress, Canberra, Australia (Abstracts). pp. 228-229.
- NEUDART, M.K., and RUSSELL, R.E., 1982. Shallow water and hypersaline features from the Middle Proterozoic Mount Isa Sequence, northern Australia: Nature, v.293, pp. 284-288.
- O'BRIEN, M.V., and ROMER, D.M., 1971. Tara geologists describe Navan discovery: World Min., v.24, pp. 38-39.
- O'CONNOR, P.J., and BRUCK, P.M., 1978. Age and origin of the Leinster granite: J. Earth Sci. R. Dubl. Soc., v.1, pp. 105-113.
- OHLE, E.L., 1980. Some considerations in determining the origin of ore deposits of the Mississippi Valley-type - Part II: Econ. Geol., v.75, pp. 161-172.
- OHLE, E.L., 1985. Breccias in Mississippi Valley-type deposits: Econ. Geol., v.80, pp. 1736-1752.

- OHMOTO, H., 1972. Systematics of sulfur and carbon isotopes in hydrothermal ore deposits: Econ. Geol., v.67, pp. 551-578.
- OHMOTO, H., and LASAGA, A.C., 1982. Kinetics of reactions between aqueous sulfates and sulfides in hydrothermal systems: Geochim. et Cosmochim. Acta, v.46, pp. 1727-1746.
- OHMOTO, H., and SKINNER, B.J., 1983. The Kuroko and related volcanogenic massive sulphide deposits: introduction and summary of new findings. In: Economic Geology Monograph 5, "The Kuroko and related volcanogenic massive sulphide deposits" (Ohmoto, H., and Skinner, B.J., eds). pp. 1-8.
- OLIVER, G.J.H., 1978. Prehnite-pumpellyite facies metamorphism in County Cavan, Ireland: Nature, v.274, pp. 242-243.
- OLSON, R.A., 1984. Genesis of palaeokarst and strat-bound zinc-lead sulfide deposits in a Proterozoic dolostone, northern Baffin Island, Canada: Econ. Geol., v.79, pp. 1056-1103.
- PHILCOX, M.E., 1980. Unpublished reports for Tara Mines Ltd.
- PHILCOX, M.E., 1984. Lower Carboniferous Lithostratigraphy of the Irish Midlands: Irish Association for Economic Geology, Spec. Publ., Dublin. 89pp.
- PHILCOX, M.E., 1989. The mid-Dinantian unconformity at Navan. In: The role of tectonics in Devonian and Carboniferous sedimentation in the British Isles. Occasional Publ. No.6, Yorks. Geol. Soc., Bradford (Arthurton, R.S., Gutteridge, P., and Nolan, S.C., eds.). pp. 67-81.
- PHILLIPS W.E.A., and SEVASTOPULO, G.D., 1986. The stratigraphic and structural setting of Irish mineral deposits. In: Geology and Genesis of Mineral Deposits in Ireland. I.A.E.G., Dublin (Andrew, C.J., Crowe, R.W.A., Finlay, S., Pennell, W.M., and Pyne, J.F., eds). pp. 1-30.

- PHILLIPS, W.E.A., STILLMAN, C.J., and MURPHY, T.A., 1976. A Caledonian plate tectonic model: J. geol. Soc. London, v.132, pp. 579-609.
- PINE, R.J., and BATCHELOR, A.S., 1982. Downward migration of shearing in jointed rock during hydraulic injections: Int. J. Rock. Mech. Min. Sci. and Geomech. Abstr., v.21, pp. 249-263.
- POSTGATE, J.R., 1984. The sulphate-reducing bacteria. Cambridge University Press, Cambridge. Second edition. 208pp
- POTTORF, R.J., and BARNES, H.L., 1983. Mineralogy, geochemistry and ore genesis of hydrothermal sediments from the Atlantis II Deep, Red Sea. In: Economic geology monograph 5, "The Kuroko and related volcanogenic massive sulphide deposits" (Ohmoto, H., and Skinner, B.J., eds). pp. 198-223.
- POWELL, T.G., and MacQUEEN, R.W., 1984. Precipitation of sulphide ores and organic matter: Sulphate reactions at Pine Point, Canada: Science, v.224, pp. 63-66.
- PROBERT, K., 1983. Fluid inclusion data from carbonate-hosted Irish base metal deposits. In: Mineral Deposits Studies Group, Program with Abstracts, University of Manchester, pp. B4.
- RADKE, B.M., and MATHIS, R.L., 1980. On the formation and occurrence of saddle dolomite: J. sediment. petrol., v.50, pp. 1149-1168.
- RHODES, D., LANTOS, E.A., LANTOS, J.A., WEBB, R.J., and OWENS, D.C., 1984. Pine Point orebodies and their relationship to stratigraphy, structure, dolomitization, and karstification of the Middle Devonian barrier complex: Econ. Geol., v.79, pp. 991-1055.
- ROBINSON, B.W., and KUSABE, M., 1975. Quantitative preparation of SO<sub>2</sub> for <sup>34</sup>S/<sup>32</sup>S analysis from sulphides by combustion with cuprous oxide: Analytical Chemistry, v.47, pp. 1179-1181.
- ROEDDER, E., 1968a. The non-colloidal origin of "colloform" textures in sphalerite ores: Econ. Geol., v.63, pp. 451-471.

- ROEDDER, E., 1968b. Temperature, salinity and origin of the ore-forming fluids at Pine Point, Northwest Territories, Canada, from fluid inclusion studies: Econ. Geol., v.63, pp. 439-450.
- ROMANO, M., 1980. The stratigraphy of the Ordovician rocks between Slane (County Meath) and Collon (County Louth), eastern Ireland: J. Earth Sci. R. Dubl. Soc., v.3, pp. 53-79.
- ROSEN, M.R., and HOLDREN, G.R., 1986. Origin of dolomite cement in Chesapeake Group (Miocene) siliclastic sediments: an alternative model to burial dolomitization: J. Sed. Pet., v.56, no.6, pp.788-798.
- RUSSELL, M.J., 1975. Lithochemical environment of the Tynagh base metal deposit, Ireland, and its bearing on ore deposition: Trans. Inst. Min. Metall. (Sect.B: Appl. earth sci.), v.84, pp. 128-133.
- RUSSELL, M.J., 1978. Downward-excavating hydrothermal cells and Irish-type ore deposits: importance of an underlying thick Caledonian prism: Trans. Inst. Min. Metall. (Sect.B: Appl. earth sci.), v.87, pp. 168-171.
- RUSSELL, M.J., 1983. Major sediment-hosted exhalative zinc + lead deposits: formation from hydrothermal convection cells that deepen during crustal extension. In: Mineralogical Association of Canada, Short Course Handbook vol. 8, Sediment-hosted stratiform lead-zinc deposits (Sangster, D.F., ed). pp. 251-282.
- RUSSELL, M.J., 1986. Extension and convection: a genetic model for the Irish Carboniferous base metal and barite deposits. In: Geology and Genesis of Mineral Deposits in Ireland. I.A.E.G., Dublin (Andrew, C.J., Crowe, R.W.A., Finlay, S., Pennell, W.M., and Pyne, J.F., eds.). pp. 545-554.
- RUSSELL, M.J., 1986. Personal communication.
- RUSSELL, M.J., in press
- RUSSELL, M.J., SOLOMON, M., and WALSH, J.L., 1981. The genesis of sediment-hosted exhalative zinc-lead deposits: Mineralium Deposita., v.16, pp. 113-127.

- RYE, D.M., and WILLIAMS, N., 1981. Studies of base metal sulphide deposits at McArthur River, Northern Territory, Australia: III. The Stable Isotope Geochemistry of the H.Y.C., Ridge, and Cooley Deposits: Econ. Geol., v.76, pp. 1-26.
- RYE, R.O., HALL, W.E., and OHMOTO, H., 1974. Carbon, hydrogen oxygen, and sulfur isotope study of the Darwin lead-silver-zinc deposit, southern California: Econ. Geol., v.69, pp. 468-481.
- RYE, R.O., and OHMOTO, H., 1974. Sulfur and carbon isotopes and ore genesis: A review: Econ. Geol., v.69, pp. 826-842.
- SAMSON, I.M., and RUSSELL, M.J., 1983. Fluid inclusion data from Silvermines base metal - baryte deposits, Ireland: Trans. Inst. Min. Metall. (Sect.B: Appl. earth sci.), v.92, pp. 67-71.
- SAMSON, I.M., and RUSSELL, M.J., 1987. Genesis of the Silvermines zinc-lead-barite deposit, Ireland: Fluid inclusion and stable isotopic evidence: Econ. Geol., v.82, pp. 371-394.
- SANDERSON, D.J., 1984. structural variations across the northern margin of the Variscides in NW Europe. In: Variscan tectonics of the North Atlantic region. Geol. Soc. Spec. Publ. No.14 (Hutton, D.H.W., and Sanderson, D.J., eds). Blackwell Scientific Publications, Oxford, pp. 149-168.
- SANGSTER, D.F., 1983. Mississippi Valley-type deposits: a geological melange. In: International conference on Mississippi Valley-type lead-zinc deposits. Proceedings volume: Rolla, Univ. of Missouri-Rolla Press (Kisvarsanyi, G., Grant, S.K., Pratt, W.P., and Koenig, J.W., eds). pp. 7-19.
- SASAKI, A., and KROUSE, H.R., 1969. Sulfur isotopes and the Pine Point lead-zinc mineralization: Econ. Geol., v.64, pp. 718-730.

- SASS-GUSTKIEWICZ, M., 1983. Zinc-lead ore structures from Upper Silesian Region in the light of solution transfer. In: International Conference on Mississippi Valley-type lead-zinc deposits. Proceedings volume: Rolla, Univ. of Missouri-Rolla Press (Kisvarsanyi, G., Grant, S.K., Pratt, W.P., and Koenig, J.W., eds). pp. 20-26.
- SASS-GUSTKIEWICZ, M., DZULYNSKI, S., and RIDGE, J.D., 1982. The emplacement of zinc-lead sulphide ores in the Upper Silesian district - A contribution to the understanding of Mississippi Valley-type deposits: Econ. Geol., v.77, pp. 392-412.
- SAWKINS, F.J., 1984. Ore genesis by episodic dewatering of sedimentary basins: Application to giant Proterozoic lead-zinc deposits: Geology, v.12, pp. 451-454.
- SCHWARCZ, H.P., and BURNIE, S.W., 1973. Influence of sedimentary environments on sulfur isotope ratios in clastic rocks: a review: Mineralium Deposita., v.8, pp. 264-177.
- SECCOMBE, P.K., SPRY, P.G., BOTH, R.A., JONES, M.T., and SCHILLER, J.C., 1985. Base metal mineralization in the Kanmantoo Group, South Australia: A regional sulfur isotope study: Econ. Geol., v.80, pp. 1824-1841.
- SEVASTOPULO, G.D., 1979. The stratigraphic setting of base metal deposits in Ireland. In: Prospecting in areas of glaciated terrain, 1979. Institution of Mining and Metallurgy, London. pp. 8-15.
- SEVASTOPULO, G.D., 1981. Lower Carboniferous. In: A Geology of Ireland (Holland, C.H., ed). Scottish Academic Press, Edinburgh, pp. 147-171.
- SHAW, D.R., and HODGSON, C.J., 1986. Wall-rock alteration at the Sullivan Mine, Kimberley, B.C. In: The Genesis of Stratiform Sediment-hosted Lead and Zinc Deposits: Conference Proceedings (Turner, R.J.W., and Enaudi, M.T., eds). Stanford University Publications, California, pp. 13-21.

- SHERIDAN, D.J.R., 1972a. The stratigraphy of the Trim No. 1 well, Co. Meath and its relationship to Lower Carboniferous outcrop in east-central Ireland: Geol. Surv. Ireland Bull., vol.1, pp. 311-334.
- SHINN, E.A., 1983. Tidal flat environment. In: Carbonate Depositional Environments. A.A.P.G. Memoir 33, Tulsa, Oklahoma (Scholle, P.A., Bebout, D.G., and Moore, C.H., eds). pp. 171-210.
- SIBSON, R.H., MOORE, J.M., and RANKIN, A.H., 1975. Seismic pumping - a hydrothermal fluid transport mechanism: J. geol. Soc. London, v.130, pp. 163-177.
- SIMONEIT, B.R.T., 1986. Organic metamorphism and transport of hydrocarbons - Guaymas Basin geothermal system. In: The Genesis of Stratiform Lead and Zinc Deposits: Conference Proceedings (Turner, R.J.W., and Enaudi, M.T., eds). Stanford University Publications, California, pp. 145-150.
- SOMMER, S.E., 1972. Cathodoluminescence of carbonates, I. Characterization of cathodoluminescence from carbonate solid solutions: Chem. Geol., v.9, pp. 257-273.
- STILLMAN, C.J., 1978. South-east County Waterford and South Tipperary: Ordovician volcanic and sedimentary rocks and Silurian turbidites: Field guide to the Caledonian and Pre-Caledonian rocks of south-east Ireland. Geol. Surv. Ireland, Guide Series No. 2, pp. 41-60.
- STILLMAN, C.J., and WILLIAMS, C.J., 1979. Geochemistry and tectonic setting of some Upper Ordovician volcanic rocks in east and south-east Ireland: Earth. planet. Sci. Lett., v.42, pp. 288-310.
- STONE, P., FLOYD, J.D., BARNES, R.P., and LINTERN, B.C., 1987. A sequential back-arc and foreland basin thrust duplex model for the Southern Uplands of Scotland: J. geol. Soc. London, v.144, pp. 753-764.
- STROGEN, P., 1973. The volcanic rocks of the Carrigunnel area, Co. Limerick: R. Dubl. Soc., Scientific Proceedings, Ser.A, no.5, pp. 1-26.

- STROGEN, P., 1977. The evolution of the Carboniferous volcanic complex of southeast Limerick, Ireland: J. geol. Soc. London, v.133, pp. 409-410.
- TANIMURA, S., DATE, J., TAKAHASHI, T., and OHMOTO, H., 1983. Kuroko deposits geological setting - Part II. In: Economic Geology Monograph 5, "The Kuroko and related volcanogenic massive sulphide deposits" (Ohmoto, H., and Skinner, B.J., eds). pp. 24-54.
- TAYLOR, S., and ANDREW, C.J., 1978. Silvermines Orebodies, Co. Tipperary, Ireland: Trans. Inst. Min. Metall. (Sect.B: Appl. earth sci.). v.87, pp. 111-124.
- THODE, H.G., and MONSTER, J., 1965. Sulfur-isotope geochemistry of petroleum, evaporites and ancient seas. In: Fluids in Subsurface Environments. A.A.P.G. Memoir 4 (Young, A., and Galley, J.E., eds). pp. 367-377.
- TRUDINGER, P.A., CHALMERS, L.A., and SMITH, J.W., 1985. Low-temperature sulphate reduction: biological versus abiological: Can. J. Earth Sci., v.22, pp. 1910-1918.
- VARKER, W.J., and SEVASTOPULO, G.D., 1985. The Carboniferous System: Part 1 - Conodonts of the Dinantian Subsystem from Great Britain and Ireland. In: A Stratigraphical Index of Conodonts. The British Micropalaentological Society/ Ellis Horwood Ltd., Chichester (Higgins, A.C., and Austin, R.L., eds). pp. 167-209.
- VINOGRADOV, A.P., GRINENKO, V.A., and USTINOV, V.I., 1962. Isotopic composition of sulfur compounds in the Black Sea: Geokhimiya, v.10, pp. 973-997.
- WALKDEN, G.M., and BERRY, J.R., 1984. Natural calcite in cathodoluminescence: crystal growth during diagenesis: Nature, v.308, no.5959, pp. 525-527.
- WALLACE, M.W., 1987. The role of internal erosion and sedimentation in the formation of stromatactis mudstones and associated lithologies: J. sediment. petrol., v.57, no.4, pp. 695-700.

WILLIAMS, B., and BROWN, C., 1986. A model for the genesis of Zn-Pb deposits in Ireland. In: Geology and Genesis of Mineral Deposits in Ireland. I.A.E.G., Dublin (Andrew, C.J., Crowe, R.W.A., Finlay, S., Pennell, W.M., and Pyne, J.F., eds). pp. 579-590.

WILLIAMS, N., 1978a. Studies of the base metal sulphide deposits at McArthur River, Northern Territory, Australia I. The Cooley and Ridge deposits: Econ. Geol., v.73, pp. 1005-1035.

WILLIAMS, N., and LOGAN, R.G., 1986. Geology and evolution of the H.Y.C stratiform Pb-Zn orebodies, Australia. In: The Genesis of Stratiform Lead and Zinc Deposits: Conference Proceedings (Turner, R.J.W., and Enaudi, M.T., eds). Stanford University Publications, California, pp. 57-64.

WILLIAMS, N., and RYE, D.M., 1974. Alternative interpretation of sulphur isotope ratios in the McArthur lead-zinc-silver deposit: Nature, v.247, no.5442, pp. 535-537.

APPENDIX I STAINING TECHNIQUE AND  
CATHODOLUMINESCENCE

1) Staining technique

Uncovered thin sections prepared from carbonate lithologies were carefully etched in dilute HCL (5%) for 60-90 seconds (2-3 minutes for dolomites) and then placed in a mixed solution of Potassium ferricyanide and Alizarin red for a period of 3-5 minutes. The slides were then removed from the solution and gently flushed with deionized water. After drying, the slides were then covered with a thin coverslip to protect the stain.

2) Cathodoluminescence

Cathodoluminescence is the emission of light (luminescence) resulting from the bombardment of a phosphor by electrons or cathode rays (Sommer, 1972). In calcite and dolomite, this phosphor or "activator" is generally believed to be manganese, however "quenching" of luminescence results from the presence of  $Fe^{2+}$  (Sommer, 1972; Frank et al., 1981; Fairchild, 1983). Cathodoluminescent light in calcite and dolomite is controlled by the Fe/Mn ratio and not by the absolute concentrations of each cation (Frank et al., 1981).

Cathodoluminescence was carried out on uncovered, polished thin sections using a Tecnosyn cold cathode 8200

Mark II Luminoscope at 0.06 Torr at voltages between 12 and 20 kV and beam currents of between 400 and 250 microamps. Photographs were taken with 200 ASA Fujicolour print film.

## APPENDIX II    SULPHUR ISOTOPIC ANALYSES

Two hundred and fifty two sulphur isotope analyses were carried out on sulphides and sulphates throughout the deposit collected from underground headings and diamond drill core.

Sulphides were extracted using a fine-tipped dental drill or by crushing and recovery with heavy liquid separation. Where necessary X-ray diffraction was used to check the purity of the phases. The  $\text{SO}_2$  gas was produced by combustion of the sulphides or sulphates at 1070 and 1120°C respectively with an excess of  $\text{Cu}_2\text{O}$  (after Robinson and Kusabe, 1975). The prepared gas was then analyzed on a 12cm radius model double collector mass spectrometer (Isospec 44 modified for  $\text{SO}_2$ ). The ion beams monitored are  $m/z$  66 and 64, with standard correction factors applied to the raw  $\delta^{34}\text{S}$  ratios (after Craig, 1957). The entire instrument is operated at 110°C. Within run precision is typically  $+0.08\text{‰}$  ( $2\sigma$ ) or better, with a long term reproducibility of  $+0.27\text{‰}$ , based on 20 replicate analyses (including combustion) of an internal laboratory standard. All  $\delta^{34}\text{S}$  results are reported as ‰ (per mil) variations relative to the Canon Diablo troilite (CDT).

The reproducibility of the analyses run on the mass spectrometer was continually checked using three International Standards, with a standard gas prepared and run on a routine basis for every six samples put through.

The International Standards used were:

- a) CP1 - chalcopyrite (BGS, London)  $\delta^{34}\text{S} = -4.1\text{‰}$
- b) NBS-123 - sphalerite (I.A.E.A., Vienna)  $\delta^{34}\text{S} = +17.1\text{‰}$
- c) NZ-1 - silver sulphide (I.A.E.A., Vienna)  $\delta^{34}\text{S} = -0.1\text{‰}$

To also test reproducibility, a sample of honeyblende sphalerite from Navan was crushed and homogenized and three gases were prepared and run on the mass spectrometer, giving  $\delta^{34}\text{S}$  values of -15.56, -15.68 and -15.48‰ respectively. This gave a mean value of -15.57‰ with  $\sigma^{n-1} = 0.10\text{‰}$ .

APPENDIX III      ABBREVIATIONS FOR THE STYLES OF MINERALIZATION

AND A LIST OF SULPHUR ISOTOPE RESULTS

ALL - Allochem replacement by sphalerite  
COL = Colloform pyrite/marcasite in bedding-parallel cavities  
in 2-1 Lens  
FRA = Framboidal pyrite in the BC/CGO  
LAT = Barite laths and rosettes  
GYP = Gypsum crystals  
DGN = Diagenetic pyrite clots and concretions in the Lower  
Palaeozoics  
VNT = Small veinlets in the Lower Palaeozoics

Styles of mineralization within coarse  
galena/sphalerite horizons

BVN = Coarse bladed galena within the massive sulphides  
ZON = Coarse, poorly zoned sphalerite  
MAS = Zoned sphalerite crystals replacing host carbonate  
RHY = Rhythmically banded to crustiform sphalerite including  
small, coeval geopetal sphalerite sediments  
MSA = Massive sphalerite in 2-5 Lens west  
CBU = Cubic/layered/dendritic galena in 2-5 Lens west  
CLO = Colloform pyrite overgrowth on galena in 1-5 Lens  
BRN = Late-stage bournonite crystals

Styles of mineralization within massive  
sulphide horizons deposited in  
continually developing open spaces

LAM = Layered, internal sphalerite sediment  
LAY = Layers of galena within the sphalerite sediment  
DPC = Dendritic, skeletal and platelet galena growths  
CUB = Coarse cubic galena  
STL = "Stalactitic" growths  
RYH = Rhythmically banded or colloform sphalerite  
HYB = Honeyblende sphalerite

Styles of mineralization within  
cross-cutting veins

VNB = Coarse bladed galena and marcasite in veins  
YRH = Rhythmically banded to crustiform sphalerite in veins  
YHR = Rhythmically banded sphalerite in the 2-5 Lens vein swarm  
DCP = Skeletal to cubic galena in the 2-5 Lens vein swarm  
HBY = Honeyblende sphalerite in the 2-5 Lens vein swarm

RESULTS

| <u>Extraction</u><br><u>No.</u> | <u>Sample No.</u> | <u>Lens</u> | <u>Mineral</u> | <u>Style</u> | $\delta^{34}\text{S}$<br>(‰) |
|---------------------------------|-------------------|-------------|----------------|--------------|------------------------------|
| S1004                           | NAV G135          | 1-2         | sphalerite     | HYB          | -13.7                        |
| S0685                           | NAV G007          | 1-2         | sphalerite     | ALL          | -23.0                        |
| S0678                           | NAV G001          | 1-2         | sphalerite     | ALL          | -20.9                        |
| S0679                           | NAV G002          | 1-3         | sphalerite     | ALL          | -21.6                        |
| S0680                           | NAV G003          | 1-3         | sphalerite     | LAM          | -22.2                        |
| S0681                           | NAV G004          | 1-3         | sphalerite     | ALL          | -20.3                        |
| S0683                           | NAV G005          | 1-3         | sphalerite     | ALL          | -21.4                        |
| S0684                           | NAV G006          | 1-3         | sphalerite     | ALL          | -21.3                        |
| S0686                           | NAV G008          | 1-3         | sphalerite     | ALL          | -22.6                        |
| S0688                           | NAV G009          | 1-4         | sphalerite     | ALL          | -22.5                        |
| S0432                           | NAV 081           | 1-5         | sphalerite     | HYB          | -10.8                        |
| S0433                           | NAV 082           | 1-5         | sphalerite     | HYB          | -10.1                        |
| S0499                           | NAV 083           | 1-5         | barite         | LAT          | +21.6                        |
| S0498                           | NAV 084           | 1-5         | barite         | LAT          | +23.6                        |
| S0437                           | NAV 085           | 1-5         | sphalerite     | HYB          | -8.7                         |
| S0497                           | NAV 086           | 1-5         | barite         | LAT          | +24.4                        |
| S0435                           | NAV 087           | 1-5         | galena         | DPC          | -6.9                         |
| S0512                           | NAV 088           | 1-5         | sphalerite     | LAM          | -6.6                         |
| S0513                           | NAV 089           | 1-5         | sphalerite     | LAM          | -10.2                        |
| S0514                           | NAV 090           | 1-5         | sphalerite     | LAM          | -9.4                         |
| S0407                           | NAV 091           | 1-5         | galena         | DPC          | -6.1                         |
| S0439                           | NAV 092           | 1-5         | sphalerite     | RYH          | -10.2                        |
| S0490                           | NAV 100           | 1-5         | galena         | BVN          | +8.5                         |
| S0487                           | NAV 101           | 1-5         | galena         | BVN          | +8.2                         |
| S0489                           | NAV 102           | 1-5         | galena         | BVN          | +8.5                         |
| S0488                           | NAV 103           | 1-5         | galena         | BVN          | +9.8                         |
| S0492                           | NAV 104           | 1-5         | galena         | BVN          | +11.8                        |
| S0500                           | NAV 107           | 1-5         | barite         | LAT          | +17.7                        |
| S0533                           | NAV 112           | 1-5         | sphalerite     | LAM          | -21.1                        |
| S0534                           | NAV 114           | 1-5         | sphalerite     | LAM          | -7.7                         |
| S0553                           | NAV 116           | 1-5         | sphalerite     | LAM          | -8.6                         |
| S0552                           | NAV 117           | 1-5         | sphalerite     | LAM          | -9.4                         |
| S0535                           | NAV 118           | 1-5         | sphalerite     | LAM          | -10.7                        |
| S0536                           | NAV 121           | 1-5         | sphalerite     | LAM          | -6.0                         |
| S0551                           | NAV 122           | 1-5         | sphalerite     | LAM          | -3.4                         |
| S0708                           | NAV G014          | 1-5         | barite         | LAT          | +27.9                        |
| S0701                           | NAV G018          | 1-5         | galena         | DPC          | -11.1                        |
| S0703                           | NAV G022          | 1-5         | sphalerite     | HYB          | -9.3                         |
| S0707                           | NAV G026          | 1-5         | galena         | DPC          | -6.5                         |
| S0854                           | NAV G085          | 1-5         | galena         | VNB          | +12.3                        |
| S0924                           | NAV G088          | 1-5         | barite         | LAT          | +19.4                        |
| S0940                           | NAV G112          | 1-5         | pyrite         | CLO          | -26.6                        |
| S0725                           | NAV G012          | 1-5         | sphalerite     | LAM          | -12.5                        |
| S0691                           | NAV G013          | 1-5         | galena         | LAY          | -17.2                        |
| S0178                           | NAV 022           | 1-5         | pyrite         | STL          | -19.3                        |
| S0748                           | NAV G030          | 2-1         | sphalerite     | LAM          | -18.2                        |
| S0749                           | NAV G031          | 2-1         | sphalerite     | LAM          | -15.3                        |

| <u>Extraction</u><br><u>No.</u> | <u>Sample No.</u> | <u>Lens</u> | <u>Mineral</u> | <u>Style</u> | $\delta^{34}\text{S}$<br>(‰/‰) |
|---------------------------------|-------------------|-------------|----------------|--------------|--------------------------------|
| S0750                           | NAV G032          | 2-1         | sphalerite     | LAM          | -9.7                           |
| S0751                           | NAV G033          | 2-1         | galena         | BVN          | +13.5                          |
| S0752                           | NAV G034          | 2-1         | galena         | BVN          | +9.7                           |
| S0844                           | NAV G040          | 2-1         | galena         | CUB          | +1.2                           |
| S0918                           | NAV G095          | 2-1         | barite         | LAT          | +19.5                          |
| S0919                           | NAV G096          | 2-1         | barite         | LAT          | +19.3                          |
| S0925                           | NAV G101          | 2-1         | barite         | LAT          | +17.9                          |
| S0922                           | NAV G099          | 2-1         | barite         | LAT          | +20.1                          |
| S0926                           | NAV G102          | 2-1         | barite         | LAT          | +17.9                          |
| S0932                           | NAV G108          | 2-1         | sphalerite     | HYB          | -15.3                          |
| S0933                           | NAV G109          | 2-1         | sphalerite     | HYB          | -15.3                          |
| S0943                           | NAV G115          | 2-1         | marcasite      | COL          | -32.3                          |
| S0961                           | NAV G128          | 2-1         | marcasite      | COL          | -37.3                          |
| S0962                           | NAV G129          | 2-1         | marcasite      | COL          | -28.2                          |
| S0964                           | NAV G131          | 2-1         | marcasite      | COL          | -32.3                          |
| S0965                           | NAV G132          | 2-1         | sphalerite     | HYB          | -16.6                          |
| S0966                           | NAV G133          | 2-1         | marcasite      | COL          | -30.1                          |
| S0755                           | NAV G036          | 2-1         | galena         | VNB          | +7.3                           |
| S0756                           | NAV G037          | 2-1         | sphalerite     | MAS          | +7.2                           |
| S0186                           | NAV 019           | 2-1         | pyrite         | COL          | -28.9                          |
| S0182                           | NAV 023           | 2-1         | pyrite         | COL          | -32.9                          |
| S1151                           | NAV G-A           | 2-1         | galena         | BVN          | +4.8                           |
| S1173                           | NAV G-B           | 2-1         | galena         | BVN          | +5.8                           |
| S1154                           | NAV G-C           | 2-1         | galena         | BVN          | +0.7                           |
| S1174                           | NAV G-D           | 2-1         | galena         | BVN          | +7.6                           |
| S1175                           | NAV G-E           | 2-1         | galena         | BVN          | +9.9                           |
| S1152                           | NAV G-F           | 2-1         | galena         | BVN          | +8.8                           |
| S1155                           | NAV G-G           | 2-1         | galena         | BVN          | +10.7                          |
| S1156                           | NAV G-H           | 2-1         | galena         | BVN          | +9.8                           |
| S1176                           | NAV G-I           | 2-1         | galena         | BVN          | +11.0                          |
| S1153                           | NAV G-J           | 2-1         | galena         | BVN          | +6.5                           |
| S1240                           | NAV G-K           | 2-1         | galena         | BVN          | +4.7                           |
| S1241                           | NAV G-L           | 2-1         | galena         | BVN          | +0.7                           |
| S1242                           | NAV G-M           | 2-1         | sphalerite     | RHY          | -9.3                           |
| S0149                           | NAV 001           | 2-2         | sphalerite     | ALL          | -15.0                          |
| S0150                           | NAV 002           | 2-2         | sphalerite     | ALL          | -14.5                          |
| S0151                           | NAV 003           | 2-2         | sphalerite     | ALL          | -14.8                          |
| S0153                           | NAV 005           | 2-2         | galena         | BVN          | +7.0                           |
| S0152                           | NAV 004           | 2-2         | galena         | BVN          | +1.5                           |
| S0154                           | NAV 006           | 2-2         | galena         | BVN          | -0.4                           |
| S0155                           | NAV 007           | 2-2         | galena         | BVN          | +1.7                           |
| S0156                           | NAV 009           | 2-2         | sphalerite     | RHY          | +2.1                           |
| S0160                           | NAV 010           | 2-2         | galena         | BVN          | +3.7                           |
| S0161                           | NAV 011           | 2-2         | galena         | BVN          | -1.1                           |
| S0190                           | NAV 012           | 2-2         | barite         | LAT          | +19.5                          |
| S0157                           | NAV 013           | 2-2         | sphalerite     | LAM          | -19.5                          |
| S0158                           | NAV 014           | 2-2         | sphalerite     | LAM          | -17.5                          |
| S0159                           | NAV 015           | 2-2         | galena         | BVN          | +5.8                           |
| S0189                           | NAV 016           | 2-2         | barite         | LAT          | +19.3                          |
| S0170                           | NAV 017           | 2-2         | galena         | BVN          | +2.1                           |
| S0171                           | NAV 018           | 2-2         | galena         | BVN          | +2.6                           |
| S0168                           | NAV 024           | 2-2         | sphalerite     | LAM          | -16.2                          |

| <u>Extraction</u><br><u>No.</u> | <u>Sample No.</u> | <u>Lens</u> | <u>Mineral</u> | <u>Style</u> | $\delta^{34}\text{S}$<br>(‰) |
|---------------------------------|-------------------|-------------|----------------|--------------|------------------------------|
| S0167                           | NAV 026           | 2-2         | sphalerite     | ALL          | -20.2                        |
| S0176                           | NAV 033           | 2-2         | galena         | BVN          | +6.2                         |
| S0177                           | NAV 034           | 2-2         | galena         | BVN          | +0.3                         |
| S0226                           | NAV 035           | 2-2         | galena         | BVN          | +9.3                         |
| S0227                           | NAV 036           | 2-2         | galena         | BVN          | +10.8                        |
| S0235                           | NAV 037           | 2-2         | sphalerite     | RHY          | +11.3                        |
| S0237                           | NAV 039           | 2-2         | galena         | BVN          | +14.1                        |
| S0236                           | NAV 041           | 2-2         | galena         | BVN          | +10.5                        |
| S0229                           | NAV 051           | 2-2         | galena         | BVN          | +5.9                         |
| S0230                           | NAV 052           | 2-2         | galena         | BVN          | +10.0                        |
| S0231                           | NAV 053           | 2-2         | galena         | BVN          | +6.0                         |
| S0238                           | NAV 055           | 2-2         | galena         | BVN          | +6.1                         |
| S0246                           | NAV 062           | 2-2         | sphalerite     | ALL          | -20.0                        |
| S0242                           | NAV 063           | 2-2         | sphalerite     | ALL          | -22.3                        |
| S0251                           | NAV 064           | 2-2         | sphalerite     | RHY          | +4.0                         |
| S0314                           | NAV 067           | 2-2         | barite         | LAT          | +22.5                        |
| S0316                           | NAV 069           | 2-2         | barite         | LAT          | +21.6                        |
| S0331                           | NAV 073           | 2-2         | galena         | BVN          | +9.9                         |
| S0332                           | NAV 074           | 2-2         | galena         | BVN          | +9.8                         |
| S0406                           | NAV 075           | 2-2         | galena         | BVN          | +6.5                         |
| S0429                           | NAV 076           | 2-2         | galena         | BVN          | +7.6                         |
| S0430                           | NAV 077           | 2-2         | galena         | BVN          | +7.5                         |
| S0333                           | NAV 078           | 2-2         | sphalerite     | MAS          | +3.8                         |
| S0431                           | NAV 079           | 2-2         | sphalerite     | MAS          | +3.3                         |
| S0436                           | NAV 080           | 2-2         | galena         | BVN          | +1.9                         |
| S0529                           | NAV 126           | 2-2         | sphalerite     | ALL          | -21.1                        |
| S0530                           | NAV 127           | 2-2         | sphalerite     | ALL          | -14.9                        |
| S0528                           | NAV 128           | 2-2         | sphalerite     | MAS          | -0.1                         |
| S0531                           | NAV 129           | 2-2         | galena         | BVN          | +3.4                         |
| S0548                           | NAV 130           | 2-2         | sphalerite     | ALL          | -19.2                        |
| S0843                           | NAV G039          | 2-2         | galena         | VNB          | +10.2                        |
| S1007                           | NAV G138          | 2-2         | sphalerite     | HYB          | -11.8                        |
| S1067                           | NAV G042          | 2-2         | galena         | LAY          | -24.8                        |
| S0689                           | NAV G011          | 2-2         | galena         | LAY          | -20.6                        |
| S0720                           | NAV G019          | 2-2         | barite         | LAT          | +20.8                        |
| S1278                           | NAV G150          | 2-2         | bournonite     | BRN          | -4.2                         |
| S1068                           | NAV G143          | 2-3         | galena         | CUB          | -9.5                         |
| S1009                           | NAV G140          | 2-3         | sphalerite     | HYB          | -11.5                        |
| S1006                           | NAV G137          | 2-3         | sphalerite     | ZON          | +3.7                         |
| S0699                           | NAV G016          | 2-3         | sphalerite     | LAM          | -5.7                         |
| S0700                           | NAV G017          | 2-3         | sphalerite     | LAM          | -8.9                         |
| S0702                           | NAV G021          | 2-3         | sphalerite     | HYB          | -16.8                        |
| S0705                           | NAV G024          | 2-3         | galena         | CUB          | -12.0                        |
| S0706                           | NAV G025          | 2-3         | galena         | CUB          | -11.1                        |
| S0960                           | NAV G127          | 2-3         | sphalerite     | HYB          | -10.2                        |
| S0929                           | NAV G105          | 2-3         | barite         | LAT          | +23.2                        |
| S0932                           | NAV G108          | 2-3         | barite         | LAT          | +21.0                        |
| S0934                           | NAV G110          | 2-3         | sphalerite     | HYB          | -9.7                         |
| S0721                           | NAV-CEL           | 2-3         | celestite      | LAT          | +39.1                        |
| S0714                           | NAV G020          | 2-3         | barite         | LAT          | +35.0                        |
| S0248                           | NAV 048           | 2-4         | galena         | BVN          | +2.2                         |
| S0233                           | NAV 054           | 2-4         | sphalerite     | LAM          | -20.3                        |

| <u>Extraction</u><br><u>No.</u> | <u>Sample No.</u> | <u>Lens</u> | <u>Mineral</u> | <u>Style</u> | $\delta^{34}\text{S}$<br>( $\text{‰}$ ) |
|---------------------------------|-------------------|-------------|----------------|--------------|---|
| S0537                           | NAV 125           | 2-4         | galena         | LAY          | -15.6                                   |
| S0240                           | NAV 049           | 2-4         | galena         | LAY          | -18.7                                   |
| S0234                           | NAV 057           | 2-4         | sphalerite     | LAM          | -22.0                                   |
| S0241                           | NAV 058           | 2-4         | sphalerite     | HYB          | -17.4                                   |
| S0244                           | NAV 059           | 2-4         | galena         | CUB          | -6.1                                    |
| S0243                           | NAV 060           | 2-4         | galena         | CUB          | -7.4                                    |
| S0245                           | NAV 061           | 2-4         | sphalerite     | LAM          | -19.5                                   |
| S0253                           | NAV 065           | 2-4         | sphalerite     | RHY          | +7.8                                    |
| S0464                           | NAV 095           | 2-4         | galena         | DPC          | -20.8                                   |
| S0465                           | NAV 096           | 2-4         | galena         | DPC          | -20.8                                   |
| S0467                           | NAV 097           | 2-4         | galena         | STL          | -16.0                                   |
| S0482                           | NAV 098           | 2-4         | galena         | STL          | -16.8                                   |
| S0483                           | NAV 099           | 2-4         | pyrite         | STL          | -14.0                                   |
| S0463                           | NAV 110           | 2-4         | galena         | BVN          | +13.3                                   |
| S0484                           | NAV 111           | 2-4         | sphalerite     | LAM          | -11.0                                   |
| S0550                           | NAV 124           | 2-4         | sphalerite     | LAM          | -15.0                                   |
| S1073                           | NAV G145          | 2-4         | sphalerite     | LAM          | -19.3                                   |
| S0549                           | NAV 123           | 2-4         | sphalerite     | LAM          | -16.0                                   |
| S0941                           | NAV G113          | 2-4         | pyrite         | STL          | -12.9                                   |
| S0942                           | NAV G114          | 2-4         | pyrite         | STL          | -32.6                                   |
| S0949                           | NAV G116          | 2-4         | sphalerite     | LAM          | -12.0                                   |
| S0950                           | NAV G117          | 2-4         | sphalerite     | LAM          | -15.6                                   |
| S0951                           | NAV G118          | 2-4         | sphalerite     | LAM          | -17.5                                   |
| S0952                           | NAV G119          | 2-4         | sphalerite     | LAM          | -13.7                                   |
| S0955                           | NAV G122          | 2-4         | galena         | DPC          | -8.2                                    |
| S0956                           | NAV G123          | 2-4         | galena         | DPC          | -8.4                                    |
| S0954                           | NAV G121          | 2-4         | sphalerite     | LAM          | -23.5                                   |
| S0973                           | NAV G134          | 2-4         | barite         | LAT          | +21.7                                   |
| S0971                           | NAV G072          | 2-4         | galena         | DPC          | -19.7                                   |
| S0969                           | NAV G073          | 2-4         | sphalerite     | RYH          | -18.3                                   |
| S0967                           | NAV G074          | 2-4         | sphalerite     | HYB          | -18.2                                   |
| S0923                           | NAV G100          | 2-4         | barite         | LAT          | +22.1                                   |
| S1005                           | NAV G136          | 2-4         | sphalerite     | HYB          | -3.6                                    |
| S1014                           | NAV G142          | 2-5         | sphalerite     | ZON          | +12.3                                   |
| S1069                           | NAV G144          | 2-5         | sphalerite     | RHY          | -11.6                                   |
| S0959                           | NAV G126          | 2-5         | sphalerite     | ZON          | +8.8                                    |
| S0704                           | NAV G023          | 2-5         | marcasite      | VNB          | +10.9                                   |
| S0856                           | NAV G046          | 2-5         | galena         | BVN          | +10.3                                   |
| S0862                           | NAV G047          | 2-5         | sphalerite     | RHY          | -1.5                                    |
| S0857                           | NAV G048          | 2-5         | galena         | BVN          | +7.8                                    |
| S0863                           | NAV G049          | 2-5         | sphalerite     | ZON          | +8.0                                    |
| S0893                           | NAV G050          | 2-5         | sphalerite     | ZON          | +7.1                                    |
| S0896                           | NAV G051          | 2-5         | sphalerite     | ZON          | +8.4                                    |
| S0897                           | NAV G053          | 2-5         | sphalerite     | RHY          | -15.6                                   |
| S0895                           | NAV G055          | 2-5         | galena         | BVN          | +8.8                                    |
| S0898                           | NAV G057          | 2-5         | sphalerite     | RHY          | +3.0                                    |
| S0899                           | NAV G058          | 2-5         | sphalerite     | RHY          | -0.9                                    |
| S1070                           | NAV G059          | 2-5         | galena         | BVN          | +10.8                                   |
| S0894                           | NAV G060          | 2-5         | sphalerite     | ZON          | +10.5                                   |
| S0905                           | NAV G061          | 2-5         | galena         | BVN          | +9.4                                    |
| S0903                           | NAV G063          | 2-5         | sphalerite     | ZON          | +8.8                                    |
| S0904                           | NAV G067          | 2-5         | sphalerite     | ZON          | +10.8                                   |

| <u>Extraction No.</u> | <u>Sample No.</u> | <u>Lens</u> | <u>Mineral</u> | <u>Style</u> | $\delta^{34}\text{S}$<br>(‰/‰) |
|-----------------------|-------------------|-------------|----------------|--------------|--------------------------------|
| S0858                 | NAV G061          | 2-5         | galena         | BVN          | +11.0                          |
| S0860                 | NAV G066          | 2-5         | galena         | BVN          | +7.7                           |
| S0859                 | NAV G068          | 2-5         | galena         | BVN          | +10.2                          |
| S1071                 | NAV G069          | 2-5         | sphalerite     | RHY          | -2.8                           |
| S1072                 | NAV G070          | 2-5         | sphalerite     | RHY          | -14.5                          |
| S0972                 | NAV G076          | 2-5         | galena         | DCP          | -6.8                           |
| S1011                 | NAV G080          | 2-5         | sphalerite     | YHR          | -14.6                          |
| S0970                 | NAV G077          | 2-5         | sphalerite     | YHR          | -17.0                          |
| S0968                 | NAV G078          | 2-5         | sphalerite     | HBV          | -14.4                          |
| S1010                 | NAV G079          | 2-5         | galena         | DCP          | -10.3                          |
| S0900                 | NAV G086          | 2-5         | marcasite      | VNB          | +14.9                          |
| S1177                 | NAV G089          | 2-5         | sphalerite     | YRH          | +9.0                           |
| S0861                 | NAV G091          | 2-5         | galena         | VNB          | +0.2                           |
| S0901                 | NAV G087          | 2-5         | sphalerite     | YRH          | +9.3                           |
| S0855                 | NAV G094          | 2-5         | galena         | VNB          | +8.5                           |
| S0920                 | NAV G097          | 2-5         | barite         | LAT          | +24.4                          |
| S0921                 | NAV G098          | 2-5         | barite         | LAT          | +22.7                          |
| S0927                 | NAV G103          | 2-5         | barite         | LAT          | +22.5                          |
| S0928                 | NAV G104          | 2-5         | barite         | LAT          | +29.4                          |
| S0930                 | NAV G106          | 2-5         | barite         | LAT          | +21.6                          |
| S0935                 | NAV G111          | 2-5         | sphalerite     | ZON          | +9.3                           |
| S1008                 | NAV G139          | 2-5         | sphalerite     | ZON          | +7.2                           |
| S1244                 | NAV G200          | 2-5         | galena         | CBU          | -19.9                          |
| S1251                 | NAV G201          | 2-5         | sphalerite     | MSA          | -15.7                          |
| S1254                 | NAV G202          | 2-5         | galena         | CBU          | -20.3                          |
| S1276                 | NAV G203          | 2-5         | bournonite     | BRN          | -14.9                          |
| S1277                 | NAV G204          | 2-5         | bournonite     | BRN          | -17.2                          |
| S0851                 | NAV G045          | 3-5         | galena         | VNB          | +5.9                           |

Pyrite in the Conglomerate Group Ore

|       |         |     |        |     |       |
|-------|---------|-----|--------|-----|-------|
| S0181 | NAV 021 | 1-0 | pyrite | FRA | -30.8 |
| S0179 | NAV 025 | 1-0 | pyrite | FRA | -32.0 |
| S0187 | NAV 020 | 1-0 | pyrite | FRA | -30.2 |

Gypsum from the Laminated Beds and F26 Fault

|       |                      |     |        |     |       |
|-------|----------------------|-----|--------|-----|-------|
| S1760 | GY-Laminated Beds(1) |     | gypsum | GYP | +22.5 |
| S0330 | GY-Laminated Beds(2) |     | gypsum | GYP | +24.9 |
| S1759 | GY-F26               | 1-5 | gypsum | GYP | +21.0 |

| <u>Extraction No.</u> | <u>Sample No.</u> | <u>Lens</u> | <u>Mineral</u> | <u>Style</u> | $\delta^{34}\text{S}$<br>(‰/∞) |
|-----------------------|-------------------|-------------|----------------|--------------|--------------------------------|
|-----------------------|-------------------|-------------|----------------|--------------|--------------------------------|

Diagenetic pyrite in the Lower Palaeozoics

|       |                   |  |        |     |       |
|-------|-------------------|--|--------|-----|-------|
| S0841 | NAV-LP2           |  | pyrite | DGN | +15.5 |
| S0842 | NAV-LP3           |  | pyrite | DGN | +18.8 |
| S0850 | NAV-LP1+3         |  | pyrite | DGN | +19.2 |
| S0869 | NAV U80-45m       |  | pyrite | DGN | +61.1 |
| S0872 | Repeat            |  | pyrite | DGN | +61.7 |
| S0878 | NAV U80-54m       |  | pyrite | DGN | +31.4 |
| S1106 | NAV U80-55m       |  | pyrite | DGN | +7.2  |
| S1111 | NAV U80-88.6m     |  | pyrite | DGN | +7.1  |
| S0885 | NAV U80-96.1m     |  | pyrite | DGN | +52.7 |
| S0888 | Repeat            |  | pyrite | DGN | +52.7 |
| S0993 | NAV N168-1(60m)   |  | pyrite | DGN | +24.1 |
| S0995 | NAV N168-2(63.1m) |  | pyrite | DGN | +6.0  |

Minor sulphides in fractures in the Lower Palaeozoics

|       |      |  |              |     |      |
|-------|------|--|--------------|-----|------|
| S1312 | LP/1 |  | sphalerite   | VNT | +3.6 |
| S1313 | LP/2 |  | sphalerite   | VNT | +3.5 |
| S1314 | LP/3 |  | chalcopyrite | VNT | +4.5 |
| S1315 | LP/4 |  | galena       | VNT | +1.2 |